2021

Determination of extreme flood events in the Black Creek, Julington Creek, Dubin Creek, Big Davis Creek, Ortega River, and Pablo Creek sub-basins of the lower St. Johns River basin, Florida, USA

Samantha Kovalenko
University of North Florida, n00945365@unf.edu

DETERMINATION OF EXTREME FLOOD EVENTS IN THE BLACK CREEK, JULINGTON CREEK, DUBIN CREEK, BIG DAVIS CREEK, ORTEGA RIVER, AND PABLO CREEK SUB-BASINS OF THE LOWER ST. JOHNS RIVER BASIN, FLORIDA, USA

by

Samantha K. Kovalenko

A thesis submitted to the School of Engineering in conformity

with the requirements for the degree of

Master of Science in Civil Engineering

UNIVERSITY OF NORTH FLORIDA

COLLEGE OF COMPUTING, ENGINEERING, AND CONSTRUCTION

2020

The thesis “Determination of Extreme Flood Events in the Black Creek, Julington Creek, Durbin Creek, Big Davis Creek, Ortega River, and Pablo Creek Sub-Basins of the Lower St. Johns River of the St. Johns River Basin, Florida, USA” submitted by Samantha K. Kovalenko in fulfillment of the requirements for the degree of Master of Science in Civil Engineering has been

Approved by the thesis committee: (Date)

_____ _____

Christopher J. Brown, Ph.D., P.E.
Thesis Advisor and Committee Chairperson

_____ _____

Alexandra Schönning, Ph.D., Committee Member

_____ _____

Çiğdem Akan, Ph.D., Committee Member

Accepted for the School of Engineering:

_____ _____

Osama Jadaan, Ph.D.
Director of the School of Engineering

Accepted for the College of Computing, Engineering, and Construction:

_____ _____

William Klostermeyer, Ph.D.
Dean of the College of Computing, Engineering, and Construction

ACKNOWLEDGEMENTS

I would like to extend my deepest gratitude to those who encouraged and helped me in the completion of this research and thesis. Your support means the world to me.

I would like to thank my advisor, Dr. Christopher Brown, for the incredible support he has provided me in completing this research. Considering the current pandemic and restrictions involving remote work, Dr. Brown provided much appreciated direction and consistent communication. His experience and knowledge were a valuable resource and I am incredibly thankful for his willingness to guide me in this research. It was also an honor to work with him once more as I have fond memories of the Guatemala Water Distribution Project that he guided myself and my team members on when we were undergraduate seniors in 2018. I am also deeply thankful for my thesis committee, Dr. Akan and Dr. Schonning. They have helped me build a solid foundation as an engineer and to believe in myself as a female engineer in a male dominant career. I would also like to thank the engineers and hydrologists at the St. Johns River Water Management District in their guidance as well as my supervisor and co-workers at the USACE for their support as I balanced work and school.

To my fiancé, Vince, thank you for being my constant. I could not have completed this thesis without your endless love and support. I know I can accomplish any challenge with you by my side. I am looking forward to a lifetime of adventures with you. Finally, I would like to extend my deepest thanks to my family. To my parents, Ben and Marina, you are my constant inspiration and I am forever thankful for your love and the abundant life you have given me. To my sister, Paulina, I am so thankful for our eternal bond and your encouragement over the course of our lifetime.

TABLE OF CONTENTS

LIST OF TABLES

LIST OF FIGURES

ABSTRACT

Extreme flood estimation is a continuously developing field of research. Economic and community well-being are dependent on flood risk preventative planning, which can only be successfully implemented through sound flood estimating methods. Without the execution of proper flood prevention measures, many communities remain at risk. In addition to a new extreme flood estimation methodology, this research presents a new approach to establish flood estimates. Traditionally, more than one flood estimate per return frequency storm does not exist. This research produced a set of 10-, 25-, 50-, and 100-year flood estimates for the Black Creek, Julington Creek, Durbin Creek, Big Davis Creek, Ortega River, and Pablo Creek sub-basins in northeastern Florida. The flood estimates for each recurrence interval were developed using HSPF hydrologic modeling, statistical computations involving the use of the Log-Pearson Type III and Power Law distribution, and analysis of existing Federal Emergency Management Agency (FEMA) Flood Insurance Study (FIS) estimates. Sensitivity of parameters such as land-use change, precipitation frequency values (median versus 90th percentile), and rainfall distribution (uniform versus Synthetic Type II Modified) were assessed in the resulting extreme flows determined from the HSPF Model. The hydrologic modeling component presented in this research utilizes the St. John's River Water Management District's (SJRWMD) powerful Hydrologic Simulation Program – FORTRAN (HSPF) model. This is a new methodology as the SJRWMD's HSPF model has previously never been used to estimate extreme flood flows. This methodology has the capability of being implemented in any sub-basin along the St. Johns River in Florida.

Chapter 1 INTRODUCTION

Research on flood frequency and magnitude is crucial in a world where urbanization, sea level rise, and climate change are prevalent. Accurate flood estimation methods are a powerful tool in securing economical and community wellbeing. This thesis presents several methods of flood estimation for six sub-basins of the St. Johns River in Jacksonville, Florida. These methods include model simulations, statistical estimates, and comparison of existing flood estimates. A new methodology for flood estimation has also been established in this research using existing numerical models. The new methodology can be implemented to other sub-basins along the St. Johns River. The existing model includes hydrodynamic and hydrologic components. The hydrodynamic component of the model simulates water levels during low periods and during flood events including hurricane storm surge. Ocean tides, rainfall-driven flows, evapotranspiration, sea level rise, and urbanization effects may also be simulated. The hydrologic component of the water resource model is the focus of this research. Numerous hydrologic models have been developed. These models provide flow, salinity, and water-quality inputs to the main stems of the St. John's River.

This research includes the assessment of six critical sub-basins of the St. Johns River, which are Black Creek, Julington Creek, Durbin Creek, Big Davis Creek, Ortega River, and Pablo Creek. The 10-, 25-, 50-, and 100-year return frequency storms have been assessed. The assessment provides details of the river flows associated with the respective 10%, 4%, 2%, and 1% annual probability of storm occurrence, respectively. The three primary outcomes of this research are: (i) development of the 10-, 25-, 50-, and 100-year return frequency flood flows in the six critical sub-basins (Black Creek, Julington Creek, Big Davis, Durbin Creek, Ortega River, and Pablo Creek) (ii) document a new approach to estimate extreme flood flows by developing a range of reasonable

flood estimates using multiple methods to account for inevitable uncertainties (iii) the development of a new methodology involving the modification of existing HSPF models which are capable of producing flood estimates in any sub-basin of the St. Johns River.

This thesis has been organized into eight chapters. Chapter 1 encompasses an introduction to the research conducted. Chapter 2 discusses a detailed literature review of relevant work. Chapter 3 introduces a project background including the project location and existing model background. Chapter 4 explains the model development process, inputs, and output processing. Chapter 5 describes the statistically derived flood estimation protocol. Chapter 6 presents the results of this research. Chapter 7 presents a comparison of all developed results. Chapter 8 summarizes the conclusions of this research and provides recommendations for future research.

Chapter 2 LITERATURE REVIEW

Existing literature was evaluated relative to (1) model simulated flood estimation, (2) statistically obtained flood estimates, and (3) existing documentation of flood estimates.

2.1 Model Simulated Estimates

Model simulation is a common and reliable methodology for flood estimation. Considering this research focuses on sub-basins of the St. Johns River, a starting point for this research involved the understanding of the St. John's River Water Management District's Water Supply Impact Study. In 2012, the St. Johns River Water Management District (SJRWMD) published the St. Johns River Water Supply Impact Study (WSIS). The SJRWMD, the South Florida Water Management District (SFWMD), and the Southwest Florida Water Management District (SWFWMD) recognized the potential harm to water resources in central Florida associated with continued reliance on groundwater to meet the growing need of human water consumption (SJRWMD, 2012). Extensive sets of data on hydrology, water quality, and biology were used to develop predictive computer models. These models were used to simulate the effects of withdrawing water from the St. Johns River and the Ocklawaha River. The ultimate finding of the WSIS state that "under the most likely scenario of surface water withdrawals, an appreciable quantity of surface water may be safely withdrawn from the St. Johns River with minimal to negligible environmental effects" (SJRWMD, 2012). The Hydrologic Simulation Program – FORTRAN (HSPF) and Better Assessment Science Integrating Point and Nonpoint Sources (BASINS) were the SJRWMD's models of choice. One of the reasons for selecting HSPF and BASINS is due to the Environmental Protection Agency's (EPA) sponsorship and use of these models for many years (SJRWMD, 2012). Surface flows and surficial groundwater flows to the

streams and rivers of the St. Johns River watershed are represented in the models. Although this model is originally aimed at determining safe water withdrawal conditions and not flood estimates, there are other documented instance of the use of HSPF for flood estimation.

Research conducted by Gebremariam et al. (2014) depicts the advantages of using HSPF over other models. Their research is centered around evaluating the Maumee River Basin in the Great Lakes region of North America. Their goal was to assess the watershed flow regimes to better understand the nutrient runoff into downstream environments. Gebremariam et al. (2014) evaluated the SWAT (version 528.0), DLBRM (version 2004), and the HSPF (version 12.0) models in terms of (1) daily and monthly flow, (2) flood and low-flow pulse frequency, magnitude and duration, and (3) watershed response to extreme weather events. Gebremariam et al. (2014) discovered that the HSPF model slightly over-predicts the slope in their analysis of the least-squared regression line between simulated and observed flow data. They determined that the HSPF model is better at predicting high flows rather than low flows. Gebremariam et al. (2014) observed that source-code modification for the HSPF model was challenging primarily because of lack of documentation related to code structure and subroutines. Gebremariam et al. (2014) observed that the HSPF model outperformed applications found in previous studies related to their research in terms of more accurate goodness-of-fit parameters. They also uncovered that the HSPF model was better at simulating extreme wet conditions than extreme dry conditions in the Maumee River Basin. Their conclusion was that the HSPF model was able to simulate average daily and monthly Maumee River flows with acceptable accuracy. Lastly, out of all three models assessed by Gebremariam et al. (2014), the HSPF model was best at simulating extreme wet events. The findings of Gebremariam et al. (2014) support this proposed research and the decision of

implementing the HSPF model to simulate extreme rainfall and flood events in the Lower St. Johns River Basin.

In 2019, Yadzi et al. conducted similar research to Gebramariam et al. (2014). They conducted a comparative assessment of the HSPF and SWMM models in simulating the hydrology of Stroubles Creek in Montgomery County, Virginia. Yadzi et al. (2019) assessed the capabilities of HSPF and SWMM "in terms of (1) most sensitive hydrologic parameters in the watershed, (2) simulation of daily and monthly stream flows in comparison with observed data, (3) simulation of peak flows, baseflows and their respective durations, and (4) predicted runoff coefficients during storm events with set return periods". Their statistical analysis results of both models showed good agreement between simulated and observed streamflow. Like Gebramariam et al. (2014), Yadzi et al. (2019) discovered HSPF predicts streamflow in wet periods better than the other investigated models. They observed "somewhat similar" peak flows of the SWMM and HSPF 24-hour storm distribution for the 100-year recurrence interval. Overall, their statistical analysis indicated that both HSPF and SWMM models simulate streamflow adequately although they both tended to underestimate stream flow. HSPF was also determined to produce a higher runoff coefficient for recurrence intervals that are greater than 10-years compared to SWMM (Yadzi et al., 2019). Although Yadzi et al. (2019) determined that HSPF tends to underestimate streamflow, both the findings of Yadzi et al. (2019) and Gerbramarian et al. (2014) suggest that HSPF predicts streamflow best in wet periods, which further encourages the implementation of HSPF in this research.

2.2 Statistical Flood Estimation

There are numerous approaches available to conduct statistical flood frequency and magnitude analysis. Research by Kidson and Richards (2005) goes as far as to claim that there is a "confusing

range of models available". They outline the flood frequency analysis (FFA) procedure in three steps: (1) data choice, (2) model choice, and (3) parameter estimation procedure. Their research claims that the current method of FFA is dominated by a single particular approach to modeling which includes the use of a range of "skewed, relatively complex, and often theoretically unjustified probability distributions". Kidson and Richards (2005) go on to acknowledge the large body of research concerning the Log-Pearson Type III (LP3), which has been the United States of America's official model since 1967. However, they offer sound evidence regarding the use of a simpler alternative – the Power Law (PL). Kidson and Richards (2005) explain that where there exists less than 100 years of discharge data, a degree of extrapolation is necessary, which in turn requires curve-fitting to existing data. Therefore, all methods of FFA are methods of extrapolation (Kidson and Richards, 2005). They bring forth an apparent limitation of FFA. An assumption must be made about the underlying distribution generating flood events. They go on to explain that this information is unknown for hydrological events beyond observed record. Despite these conditions, in order to make predictions, models must be fitted. Kidson and Richards (2005) outline three tools for extending instrumented gauging record. The first tool involves rainfall-runoff modeling in continuous simulation. The second tool involves combining data from several regional gauges. The third tool involves incorporating historical and palaeoflood information into the instrumented record. The three main steps of model fitting are data choice, model choice, and parameter estimation procedure according to Kidson and Richards (2005). Regarding data choice, they explain that the FFA is classically performed on annual maximum discharge values. However, they also note that the peaks over threshold (POT) method, which includes every event over a given threshold, has become a cornerstone technique in FFA. Their study focuses on the variety of model choice in FFA. Kidson and Richards (2005) highlight simple two-parameter function

models such as the log normal and Gumbel extreme value, which can be fitted analytically. The two parameters represent location and shape (Kidson and Richards, 2005). They classify the Log-Pearson Type III (LP3) and generalized extreme value (GEV) as three-parameter models which cannot be fitted analytically. Ultimately, the two-parameter functions have the advantage of being simpler and easier to fit than three-parameter parameter models. However, the three parameter models can fit a larger number of records due to its flexibility according to Kidson and Richards (2005). Table 1 depicts several of the common models used to fit data. Kidson and Richard (2005) go on to explain the parameter estimation process, which is the final step of the model fitting process. They highlight several methods of parameter estimation including the method of moments (MOM), the L-moment method, and the maximum likelihood (ML) method. A major component of Kidson and Richard's (2005) research is the encouraged use of the Power Law (PL) model as an alternative in the model selection process of FFA. They argue that the PL is a simple alternative to the more complex probability models seen in Table 1. Reference Kidson and Richards 2005 publication*, Flood Frequency Analysis: Assumptions and Alternatives,* for information regarding the variables of each equation. They demonstrate supporting evidence involving the use of the PL distribution in extreme natural events as well as in the field of hydrology.

Table 1. Statistical probability models (Kidson and Richards, 2005)

Data Fitting Model	**Equation**
Normal	$f(x) = \frac{1}{\sqrt{2\pi{\sigma_x}^2}} \exp\left[-\frac{1}{2}\left(\frac{x-\mu_x}{\sigma_x}\right)^2\right]$
Log Normal (2-Parameter) LN2	$f(x) = \frac{1}{x\sqrt{2\pi{\sigma_y}^2}} \exp\left[-\frac{1}{2}\left(\frac{\ln(x)-\mu_y}{\sigma_y}\right)^2\right]$ $y = \ln(x)$

Pearson Type III	$f(x) = \lvert\beta\rvert[\beta(x-\epsilon)]^{\alpha-1}\frac{exp[-\beta(x-\epsilon)]}{\Gamma(\alpha)}$
Log Pearson Type III (LP3)	$f(x) = \lvert\beta\rvert\{\beta[\ln(x)-\epsilon]\}^{\alpha-1}\frac{exp\{-\beta[\ln(x)-\epsilon]\}}{x\Gamma(\alpha)}$
Exponential	$f(x) = \beta exp[-\beta(x-\epsilon)]\ pdf$ $F(x) = 1 - exp\{-\beta(x-\epsilon)\}\ cdf$
Gumble EVI	$f(x) = \frac{1}{\alpha}\left[-\frac{x-\epsilon}{\alpha} - exp\left(-\frac{x-\epsilon}{\alpha}\right)\right] pdf$ $F(x) = exp\left[-\exp\left(-\left(\frac{x-\epsilon}{\alpha}\right)\right]\right. cdf$
Generalized Extreme Value (GEV)	$F(x) = exp\left\{-\left[1-\frac{k(x-\epsilon)}{\alpha}\right]^{1/k}\right\} cdf$
Weibull	$f(x) = \left(\frac{k}{\alpha}\right)\left(\frac{x}{\alpha}\right)^{k-1} exp\left[-\left(\frac{x}{\alpha}\right)^{k}\right] pdf$ $F(x) = 1 - exp\left[-\left(\frac{x}{\alpha}\right)^{k}\right] cdf$
Generalized Pareto (GP)	$f(x) = \left(\frac{1}{\alpha}\right)\left[1-k\frac{(x-\epsilon)}{\alpha}\right]^{1/k-1} pdf$ $F(x) = 1 - \left[1-k\frac{(x-\epsilon)}{\alpha}\right]^{1/k} cdf$
Generalized Logistic (GL)	$f(x) = \frac{1}{\alpha}\left[1-k\left(\frac{x-\epsilon}{\alpha}\right)\right]^{\left(\frac{1}{k}-1\right)}\left[1+\left\{1-k\left(\frac{x-\epsilon}{\alpha}\right)\right\}^{\frac{1}{k}}\right]^{-2} pdf$ $F(x) = \left[1+\left\{1-k\left(\frac{x-\epsilon}{\alpha}\right)\right\}^{\frac{1}{k}}\right]^{-1} cdf$
Power Law (PL)	$f(x) = Cx^{-\propto}$

Kidson and Richards (2005) conclude that the PL may be more applicable for extreme events but not for events around the mean annual flood. However, it is noted that the PL may be more effective for long records (e.g.,100 years) because the PL behavior may be visible in the gauged record and thus a regression relation using the data would be permitted.

The United States Army Corps of Engineers (USACE) has developed an extensive manual on flood-runoff analysis (1994). This manual encompasses extensive information regarding problem definition, methodology selection, hydrologic analysis, methods for flood runoff analysis, and engineering applications (USACE, 1994). The USACE (1994) manual describes the data requirements for statistical models of streamflow frequency which include (1) homogeneous data, (2) spatially consistent data, and (3) a continuous time series. Regarding the distribution selection and parameter estimation procedure, a frequency distribution is selected based on its ability to model the observed data and the parameters are selected to optimize the fit of the data (USACE, 1994). According to the manual (USACE, 1994), the steps of the numerical techniques, which will be implemented in this research, are as follows: (1) select the candidate frequency model, (2) obtain a sample, (3) use the sample to estimate the parameters of the model, (4) use the model and the parameters to estimate quantiles to construct the frequency curve that represents the population. This procedure is analogous with the procedure described by Kidson and Richards (2005). The USACE (1994) identifies the normal distribution, the log- normal distribution, and the Log-Pearson Type III distribution as the three most common distributions used for the analysis of hydrometeorological data.

Documentation regarding the successful implementation of the Log-Pearson Type III Distribution is available. Kumar (2019) conducted a flood frequency analysis in the Rapti River Basin, which encompasses areas of India and Nepal. The LP3 method and Gumbel Extreme Value 1 (Gumbel

EV1) were used to develop the discharge results of return periods ranging from 1.05 to 1,000 years (Kumar, 2019). The comparison between LP3 and Gumbel EV1 is of interest because the LP3 method is one of the proposed methods for the proposed research while the Gumbel EV1 is one of the other viable methods mentioned by Kidson and Richards (2005) for flood frequency analysis. In Kumar's (2019) research, the implementation of the LP3 method resulted in higher discharge values than those computed using the Gumbel EV1 method at the 50-, 100-, 200-, 500-, and 1,000-year return period at one location of interest, while the Gumbel EV1 method produced higher discharge values at the second location of interest. The Kolmogorov-Smirnov (K-S) and Anderson-Darling (A-D) methods were used to assess the goodness-of-fit of the discharge data. Based on the goodness-of fit tests' results, Kumar's (2019) research revealed that the LP3 method is more appropriate and reliable than the Gumbel EV1 method for the Rapti River Basin. Another instance of LP3 superiority was observed in the research conducted by Saf, Dikbaş, and Yaşar (2007). Saf, Dikbaş, and Yaşar (2007) compared the Gumbel, Pareto, Log logistic, Pearson Type III, Log-Pearson Type III (LP3), Log-normal with two (LN2) and three (LN3) parameters, and the Generalized Extreme Value distributions. Their objective was to apply and evaluate those probability distribution functions of the annual maximum stream-flows measured in the West Mediterranean river basins in Turkey. They implemented the method of moments (MOM) and probability weighted moments (PWM) for parameter estimation. Lastly, they applied the chi-square and Kolmogorov-Smirnov method to assess the goodness-of-fit of their parameter estimation (Saf, Dikbaş, and Yaşar, 2007). After narrowing down their list to the top three best performing distributions, they assessed return periods ranging from 2 to 1,000,000 years using the LP3, LN3, and Gumbel distributions accompanied with the MOM and PWN methods. Their results unveiled that the LP3 distribution might be most appropriate for the West Mediterranean River

based on the accuracy and consistency of the goodness-of-fit tests (Saf, Dikbaş, and Yaşar, 2007). Considering that LP3 is the official method of the United States (Kidson and Richards, 2005) and the positive results of Kumar's (2019) and Saf, Dikbaş, and Yaşar's (2007) research regarding LP3, it is further evident that the LP3 method should be implemented in this research.

Circling back to the Power Law, it is arguably one of the simplest probability distributions (Richard and Kidson, 2005). Alipour, Rezakhani, and Shamsai (2016) explain that the power law behaviors can be explained by the fractal concept. Andriani and McKelvey (2009) provide a simple example of the fractal concept: "A cauliflower is an obvious example. Cut off a branch; cut a smaller branch from the first branch; then an even smaller one; and then even another, etc. Now set them all on a table, in line. Each fractal subcomponent is smaller than the former; each has the same shape and structure. They exhibit a 'power law effect' because they shrink by a fixed ratio. Power laws underlie fractal geometry." Like Kidson and Richards (2005), Alipour, Rezakhani, and Shamsai (2016) explain that these fractals have already been successfully used to describe hazardous and critical evets. According to Malamud and Turcotte (2006), the annual duration or partial duration flood series may be applied to the power law distribution. However, a major problem with using the annual flood series is that several floods in a given water year may be larger than the annual flood in another water year (Malamud and Turcotte, 2006). Therefore, the partial duration flood series is a practical alternative for the process.

Kidson and Richards (2005) demonstrated success in the use of the power law in a study conducted in Northern Thailand. The area of interest included the caves in the Ob Luang gorge, through which the Mae Chaem river passes through. These caves contain trapped woody debris that has accumulated from extreme flood events predating instrumental records (Kidson and Richards, 2005). After assessing large gauged floods in recent years and identifying four palaeostage

indicators at the highest-level flood deposits in the cave, Kidson and Richards (2005) were ultimately able to predict a discharge of 2420 $m^3 s^{-1}$ for the implied water levels. A return period of 84 years was assigned to that event. Flood frequency analysis was conducted using the log Pearson type III, Gumbel EV1, two-parameter log normal distributions for the instrumental flood records (Kidson and Richards, 2005). The resulting 84-year discharge estimates were 1005, 1012, and 1040 m^3/s respectively (Kidson and Richards, 2005). The power law model was then applied to the gauged data using a reduced major axis (RMA) regression and the resulting 84-year discharge estimate was determined to be 2479 m^3/s, which is similar to the original prediction (Kidson and Richards, 2005). In addition to the research conducted by Kidson and Richards (2005), Alipour, Rezakhani, and Shamsai (2016) applied the power law distribution and analyzed 50 streamflow gauging stations within two regions of the United States. Alipour, Rezakhani, and Shamsai (2016) assessed region 3 (entire Florida, almost entire Alabama, Georgia, South Carolina, North Carolina, and part of Virginia and Mississippi) and region 8 (Mississippi, Louisiana, Arkansas, and Tennessee). The summer and winter months partial-duration flood series were analyzed separately in their research and meaningful differences between both power law fit slopes were observed. Their results indicate that incorporating seasonality can improve the magnitude of the flood estimates. Alipour, Rezakhani, and Shamsai (2016) applied the power law distribution to the partial-duration peak streamflow series based on supporting research by Malamud and Turcotte (2006). However, when the partial-duration and annual peak flood series at all hydrologic stations were plotted side by side, they discovered close agreement between the two (Alipour, Rezakhani, and Shamsai, 2016). Overall, Alipour, Rezakhani, and Shamsai (2016) observed that power law analysis proved to be a useful tool in characterizing flood frequency behavior. This

research demonstrates the appeal of implementing the Power Law for extreme flood frequency analysis.

2.3 Existing Flood Estimates

Federal Emergency Management Agency (FEMA) Flood Insurance Studies (FIS) are a reliable source of flood estimates across the United States. The purpose of a FIS is to develop flood-risk data that aids in the establishment of flood insurance rates for communities' efforts of sound floodplain management (FEMA, 2014). The National Flood Insurance Act of 1968 and the Flood Disaster Protection Act of 1973 are the authorities for the Flood Insurance Studies (FEMA, 2014). Typically, an initial Consultation Coordination Officer (CC) meetings is conducted with representatives of the communities, FEMA, and the study contractors to discuss the scope of work (FEMA, 2014). The scope of study establishes the geographic areas to be assessed, incorporated communities, and methods agreed upon.

The Clay County, Florida FIS implemented the Magnitude and Frequency of Flood Discharges in Northeast Florida (Technical Publication SJ-86-2) to conduct their hydrologic analyses and obtain their flood estimates. The methodology involves the determination of different return periods (T). Given an annual exceedance probability of a maximum event, the return period is defined as $T = 1/P$, where P is the annual exceedance probability of a maximum event (Rao, 1986). The technique consists of applying an appropriate probability distribution and fitting it to a sample data, where the sample data consists of observed annual peak flows (Rao, 1986). From there, probability distributions such as the two-parameter Gumbel distribution and the five-parameter Wakeby distribution were implemented (Rao, 1986). The Log-Pearson Type III distribution was also recognized and used as it was recommended by the United States Water Resource Council (Rao, 1986).

Contrarily, the St. Johns County Flood Insurance Study is a compilation of previously printed FIS reports (FEMA, 2011). The 2003 countywide analyses were conducted by the United States Army Corps of Engineers using the HEC-1 computer program. The methodology was deemed appropriate for the characteristic drainage basin conditions; however, it was determined that the limited history of stream gage records prevented effective statistical analysis (FEMA, 2011). The HEC-1 models incorporated the Natural Resources Conservation Service (NRCS) unit hydrograph and kinematic wave routing methods, sub-basin runoff curve numbers, lag times, stream cross sections, and Manning's "n" roughness factors (FEMA, 2011). United States Geological Survey topographic maps, field inspection, and aerial photos were utilized. Additionally, the modified SCS Type II rainfall distribution was implemented into the model. Overall, only Durbin Creek and Sixmile Creek were adequately calibrated due to lack of sufficient stream gage data.

Finally, another methodology that was utilized to conduct hydrologic analyses was the Environmental Protection Agency Stormwater Management Model (EPA SWMM5 versions 12 to 14 (FEMA, 2013). This methodology was implemented by Duval County, Florida. The model applied precipitation across hydrologic units and performed hydrologic calculations, which account for hydrologic unit geometry, land use, and soil characteristics. The computed surface runoff hydrographs were routed to the dynamic hydraulic model.

Chapter 3 PROJECT BACKGROUND

3.1 Study Location

The following sub-sections discuss the various counties contained within the study location. Appendix A contains an aerial depiction of the three counties encompassed in this research. A detailed description of the Lower St. Johns River Basin, which includes all the sub-basin of interest in this research, is also presented.

3.1.2 Clay County

Located in northeastern Florida on the St. Johns River, Clay County is bordered by Duval County, the City of Jacksonville, St. Johns County, Putnam County, Bradford County, and Baker County (FEMA, 2012). Clay County encompasses 644 square miles, including 43 square miles of water (FEMA, 2012). Overall, the climate is mild, subtropical with an average annual rainfall of approximately 52 inches (FEMA, 2012). The terrain is nearly level to gently sloping with well-drained to poorly drained sandy soils overlain by weakly cemented, poorly drained, sandy subsoils (FEMA, 2012). Period flooding is caused by stream and lake overflow in low-lying areas of Clay County (FEMA, 2012). Large amounts of rainfall infiltrate when the antecedent rainfall has been low due to sandy soils in the area and the most severe flooding occurs along streams as a result of hurricanes (FEMA, 2012). Some flood protection measures have been installed by homeowners on the St. Johns River such as shoreline reinforcements in front of their homes to prevent wind and wave action (FEMA, 2012). Additionally, deepening in the lower reach of Governors Creek, dike construction between Black Creek and Lake Asbury, and a pipe culvert extending through the dike above the elevation of the 0.2-percent-annual-chance flood on Black Creek are also flood protection measures (FEMA, 2012).

3.1.2 St. Johns County

Located in northeast Florida, St. Johns County is bordered by Duval County, Clay County, Putnam County, Flagler County, and the Atlantic Ocean shoreline (FEMA, 2011). The county comprises an area of 609 square miles with about 42 square miles of Atlantic Ocean shoreline (FEMA, 2011). Over 40% of the county's population resides in the residential development between the coastline and the Intracoastal Waterway (FEMA, 2011). The county experiences a subtropical maritime climate and the average annual precipitation is about 52 inches (FEMA, 2011). The terrain of St. Johns County is comprised of nearly level, poorly drained, sandy and loamy sediments (FEMA, 2011). The primary soil associations are Myakka-Immokalee-St. Johns, Pomona-Tocoi-Ona, and Riviera-Holopaw-Winder (FEMA, 2011). The main sources of flooding occur from erosion due to ocean hurricane storm surges and waves and inland areas become flooded when rainfall accumulates in low, flat areas (FEMA, 2011). Poorly drained soil, high water table, and flat terrain contribute significantly to flooding issues (FEMA, 2011). Small flood control canals, pump stations, limited oceanfront seawalls, revetments, and ongoing beach nourishment are some of the limited but effective flood protection measures implemented in St. Johns County (FEMA, 2011).

3.1.3 Duval County

Located in the northeastern coastal region of Florida, Duval County is comprised of five (5) cities and two (2) major military installations (FEMA, 2013). Duval County contains the City of Jacksonville, the Cities of Atlantic Beach, Neptune Beach, Jacksonville Beach, and the City of Baldwin (FEMA, 2013). It is bordered by Nassau County, Baker County, Clay County, St. Johns County, and the Atlantic Ocean and it consists of 918 square miles including 144 square miles of water area (FEMA, 2013). Rainfall runoff causing overflow of streams, ponding, and sheet flow are the main causes of flooding; while, hurricane storm surge causes extreme water levels in coastal

and tidal regions (FEMA, 2013). Because of the flat terrain, many inland areas experience shallow flooding and ponding after heavy rainfall (FEMA, 2013). Additionally, strong nor'easters and tropical storms frequently occur in Duval County (FEMA, 2013). The Cities of Atlantic Beach, Jacksonville Beach, and Neptune beach are partially protected by a seawall and sections of it can withstand a 1-percet-annual-chance event (FEMA, 2013). Additionally, flood protection measures in the form of mitigation activities, including relocation and elevation of structures, have been implemented as flood protection measures (FEMA, 2013).

3.1.4 The Lower St. Johns River Basin

As previously mentioned in the literature review, the St. Johns River Water Management District conducted a Water Supply Impact Study (WSIS) along the St. Johns River. Appendix B depicts the modeled water withdrawal locations. As seen in Appendix B, the models include the following basins: Lower St. Johns River, Middle St. Johns River, Upper St. Johns River, Ocklawaha River, and other district basins. The Lower St. Johns River Basin consists of several sub-basins. These sub-basins are depicted as watersheds in Appendix C. The sub-basins (watersheds) in Appendix C are labeled using a watershed unit number. Table 2 explains the sub-basin name associated with each watershed unit number. The Lower St. Johns River Basin contains the sub-basins of interest in this research (Black Creek, Julington Creek, Durbin Creek, Big Davis Creek, Ortega River, and Pablo Creek).

Table 2. Lower St. Johns River Basin Sub-Basin Names

Watershed Unit Number	Sub-basin Name	Model Area (acres)
3A	Crescent Lake	381,058
3B	Etonia Creek	228,426
3C	Black Creek	325,312
3D	Ortega River	66,927
3E	Trout River	61,361
3F	Deep Creek	88,378
3G	Sixmile Creek	81,774
3H	Julington Creek	62,324
3I	Intracoastal Waterway	66,153
3J	South Main Stem	246,438
3K	North Main Stem	155,771

The Lower St. Johns River Basin (LSJRB) represents 22% of the area within the SJRWMD and it extends from Lake George to the mouth of the river near Jacksonville, Florida (SJRWMD, 2012). According to WSIS (2012), the landscape features are low and flat with surface elevations ranging from 200 feet to seal level.

3.2 Hydrologic Model Background

A detailed description of the hydrologic processes modeled is available in Chapter 3 of the WSIS Report. Chapter 3 describes the HSPF model input parameters, model construction, and results. In general, the HSPF model input parameters are either physical or empirical (SJRWMD, 2012). The physical parameters are watershed areas, land use, precipitation, evaporation, slope, roughness, and system hydraulics (SJRWMD, 2012). Several of the critical empirical parameters include surface storage, upper and lower zone storage, infiltration, interception storage, various evaporation components and active groundwater recession (SJRWMD, 2012). When a model is correctly developed with the inclusion of these parameters, HSPF generates time series of runoff, stream flow, loading rates, and concentrations of several water quality elements (SJRWMD, 2012). The HSPF model was calibrated by implementing an iterative process of changing parameters,

running simulations, checking results, and repeating until the simulated and observed data resemble each other (SJRWMD, 2012). Additionally, the SJRWMD (2012) developed a "common logic" which describes reasonable parameter value ranges for all model runs included in the district as part of the calibration process.

The model was originally calibrated by the SJRWMD using specific streamflow gages per sub-basin. Table 3 presents which United States Geologic (USGS) streamflow gages were used to calibrate each sub-basin of interest. The Black Creek sub-basin was calibrated with the North Fork gage and South Fork gage. The calibration using the North Fork gage was described as overall very good and the calibration using the South Fork gage was described as overall good (SJRWMD, 2012). The 02246318 (Kirwin Rd.) Ortega River gage calibration was unsatisfactory, and 02246300 (103rd St.) Ortega River gage calibration was overall good (SJRWMD, 2012). The Big Davis Creek gage 02246150 calibration was adequate and lastly, the Pablo Creek gage 02246828 calibration was reasonable (SJRWMD, 2012). During the calibration process, the observed gage data was directly compared to created "synthetic" gage data produced from the model output.

Table 3. Model Calibration Gages

Sub-Basin	**Gage Name**	**Gage ID**	**Notes**
Black Creek	North Fork near Middleburg	02246000	
	South Fork Penney Farms	02245500	
Julington Creek	Big Davis Creek at Bayard	02246150	
Durbin Creek	Big Davis Creek at Bayard	02246150	
Big Davis Creek	Big Davis Creek at Bayard	02246150	
Ortega River	Ortega 103rd St. Bridge	02246300	Discontinued in 2003
	Ortega at Kirwin Rd.	02246318	Replacement gage
Pablo Creek	Pablo Creek	02246828	Discontinued in 2002

As previously mentioned, one of the key requirements of the HSPF model is the incorporation of existing meteorological data. The SJRWMD maintains point rain gauge and Doppler radar rainfall datasets (SJRWMD, 2012). According to the WSIS (2012), a contractor adjusted the Doppler total

rainfall over long periods to match the total rainfall from the 25 separate daily and hours point rain gauges throughout the St. Johns River watershed, which was acquired from the National Weather Service (NWS). The Doppler radar data set provided only 13 years of rainfall data, whereas the NWS stations provided data dating back to the early 1900s. Due to the need to run long term simulations, the NWS rain gauge data was selected for the WSIS model. The model scenario simulations run from 1975 through 2008 (SJRWMD, 2012). The SJRWMD implemented the use of a Theissen polygon network to establish the area of influence for the NWS rain gauges. Appendix D depicts the Theissen polygon network that was developed by the SJRWMD.

3.3 Model Locations

As previously established, the six sub-basins of interest in this research are Black Creek, Julington Creek, Durbin Creek, Big Davis Creek, Ortega River, and Pablo Creek. The HSPF models are constructed by including various reaches associated within a sub-basin. This section will discuss the specific HSPF model reach locations that correspond with the sub-basins of interest.

3.3.1 Black Creek

The Black Creek sub-basin has a total of 19 reaches incorporated in its HSPF model run. The HSPF model view of the reaches is depicted in Figure 1. Table 4 presents the associated description for each reach and model area in acres. To properly assess the Black Creek sub-basin, Reach 12, 6, and 3 were selected. Reach 12 (also referred to as Black Out in this research) is a prominent location because it is the outlet location of the entire sub-basin. Reach 6 (also referred to as North Fork) and Reach 3 (also referred to as South Fork) are also critical locations that have been assessed. North Fork and South Fork are two prominent creeks that flow directly into the main branch of Black Creek as depicted in Figure 2.

Table 4. Black Creek Sub-Basin Reaches

Description	Reach ID	Model Area (Acres)
Ates Creek	1	23,372
Greens Creek	2	25,665
South Fork	3	28,167
Middle Black Creek	4	13,208
Right Bull Creek	5	15,508
Down North Fork	6	3,820
Big Branch	7	5,580
Peters Creek	8	12,020
Little Black Creek	9	2,330
Yellow Water Creek	10	42,240
Long Branch	11	15,390
Down Black Creek	12	10,710
Upper Little Black	13	15,050
Left Bull Creek	14	13,410
Middle 2 North Fork	15	25,050
Middle 1 North Fork	16	10,890
Kingsley Lake	17	2,660
Dummy Doctors Lake Inlet	918	9,970

3.3.2 Julington Creek

The next sub-basin of interest is Julington Creek. Table 5 depict the reaches and model area (in acres) incorporated in the HSPF Julington Creek model. The HSPF model view of the reaches is depicted in Figure 3. As evident from the figure and table below, the HSPF Julington Creek model encompasses Dubin Creek (Reach 1) and Big Davis Creek (Reach 6), which are addressed in separate sections of this thesis. Therefore, the main assessment of Julington Creek is encompassed in the analysis of Reach 2 and Reach 5. Figure 4 is an aerial which depicts the relationship between Julington Creek, Durbin Creek, and Big Davis Creek.

Table 5. Julington Creek Sub-Basin Reaches

Description	Reach ID	Model Area (Acres)
Durbin Creek	1	25,781
Julington Creek	2	5,032
Big Davis Creek (UP)	3	5,379
Old Field Creek	4	4,176
Julington Creek	5	6,141
Big Davis Creek	6	1,025

3.3.3 Durbin Creek

As previously discussed in Section 3.3.2, Durbin Creek is modeled as Reach 1 of the Julington Creek HSPF model run. Please reference Figure 3 and Table 5 for more details on where Durbin Creek was incorporated into the Julington Creek model run. Refer to Figure 4 for an aerial depicting the relationship between Durbin Creek, Julington Creek, and Big Davis Creek.

3.3.4 Big Davis Creek

As previously discussed in Section 3.3.2, Big Davis Creek is modeled as Reach 6 of the Julington Creek HSPF model run. Please reference Figure 3 and Table 5 for more details on where Big Davis Creek was incorporated into the Julington Creek model run. Reference Figure 4 for an aerial depicting the relationship between Big Davis Creek, Julington Creek, and Durbin Creek.

3.3.5 Ortega River

The Ortega River sub-basin reaches and modeled area (in acres) are depicted in Table 6. The HSPF model view of the reaches in the Ortega River Sub-basin is depicted in Figure 5. The location of interest in the Ortega River sub-basin model run is Reach 3. Reach 3 represents the outlet location of the Ortega River, which encompasses flows from McGrits Creek and the upstream portion of Ortega River. Figure 6 depicts an aerial photo of the Ortega River.

Table 6. Ortega River Sub-Basin Reaches

Description	Reach ID	Model Area (Acres)
McGirtsCk 3d1	1	17,634
OrtegaRivUps 3d2	2	6,967
OrtegaRivDns 3d3	3	12,133
WillsBranch 3d4	4	5,530
WilliamsonCk 3d5	5	973
ButcherPenCk 3d6	6	839
FishingCk 3d7	7	3,376
CedarRivUps 3d8	8	6,628
CedarRivDnsm 3d9	9	653
BigFishweirCk 3d10	10	2,335

3.3.6 Pablo Creek

The last sub-basin of interest is Pablo Creek. The main location of interest for this sub-basin is Reach 8, which depicts the outlet location of the entire Pablo Creek sub-basin. The HSPF model view of the reaches in the Pablo Creek sub-basin is depicted in Figure 7. Table 7 depict the structure of the Pablo Creek sub-basin and modeled area (in acres) in the HSPF model run. Reference Figure 8 for an aerial depiction of Pablo Creek.

Table 7. Pablo Creek Sub-Basin Reaches

Description	Reach ID	Model Area (Acres)
BoxBranch	1	5,236
Second Puncheon	2	5,420
Pablo Creek Mid S	3	3,265
Mill Dam Branch	4	3,227
SawmillSlough (PU)	5	695
Ryals Swamp	6	1,134
Cedar Swamp Creek	7	2,947
Pablo Creek DownS	8	2,405

Chapter 4 MODEL DEVELOPMENT – HSPF MODEL

4.1 Procedure Overview

As previously mentioned, the SJRWMD's HSPF models from their Water Supply Impact Study were utilized for this research. In order to obtain the 10-, 25-, 50-, and 100-year flood flow estimates at the sub-basins of interest, the original HSPF models were modified to simulate the scenarios of interest. The general procedure associated with these modifications involved:

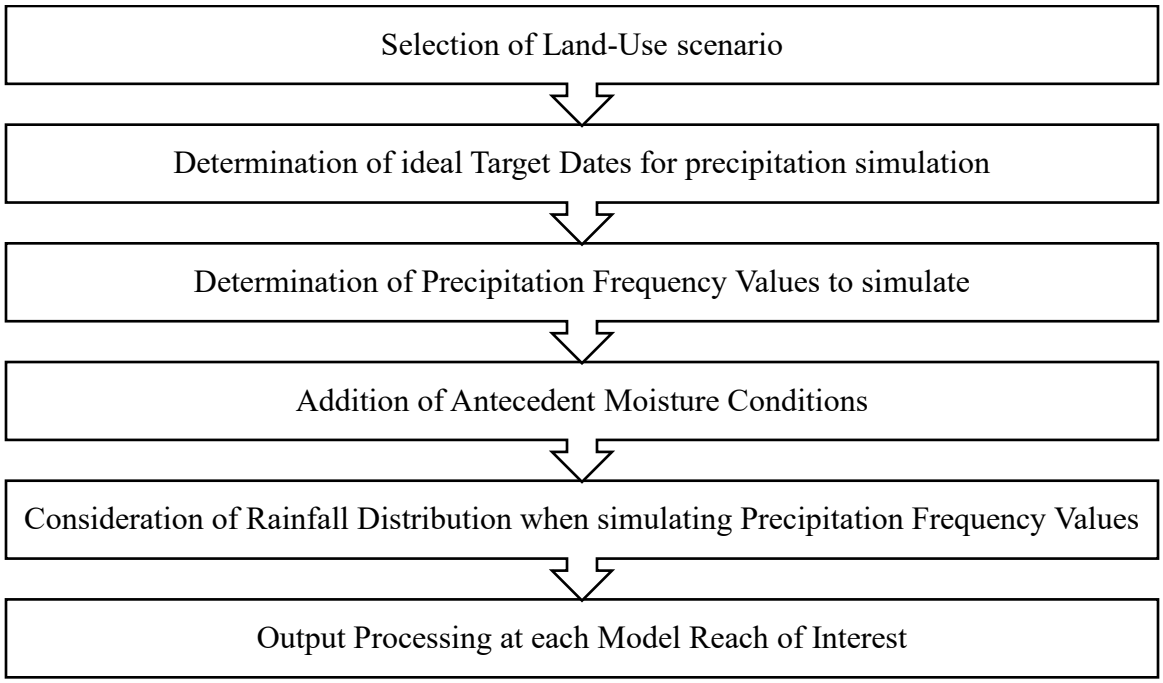

The following sub-sections discuss these components of the HSPF model development procedure. This research used the Windows operating system version of the HSPF and BASINS software. The original models were compiled in a custom Linux operating system. It is suspected that operating system differences may have resulted in some of the models repeatedly crashing (e.g. Black Creek).

4.2 Model Scenarios

Now that the relevant HSPF model reaches have been identified, a discussion of the model scenarios follows. Table 8 presents the six sub-basins and the criteria assessed for the various model scenarios. The primary goal of this research is to discover the 10-, 25-, 50-, and 100-year flood flows at the critical sub-basins (e.g. the 10%, 4%, 2%, and 1% annual exceedance probability). These flood flows were obtained by programming a specific rainfall event into the model. Therefore, the results that were obtained in this research were derived by varying the land-use, precipitation frequency values (median versus 90th percentile), varying rainfall distributions, and including the addition of antecedent moisture conditions. The following sections explain these model scenario components in more detail.

Table 8. HSPF Model Scenarios

Model Scenarios	Black Creek	Julington Creek	Durbin Creek	Big Davis Creek	Ortega River	Pablo Creek
10-year flood flow	X	X	X	X	X	X
25-year flood flow	X	X	X	X	X	X
50-year flood flow	X	X	X	X	X	X
100-year flood flow	X	X	X	X	X	X
1995 land-use condition	X	X	X	X	X	X
2030 land-use condition		X	X	X		
Synthetic Rainfall Distribution		X	X	X		
Uniform Rainfall Distribution	X	X	X	X	X	X
Antecedent moisture conditions	X	X	X	X	X	X

4.2.1 Data Sources

In addition to the varying model scenarios, this research incorporates various data sources. Real data and synthetic data sources were used in this research. Real data is classified as historic data. It is data that has occurred in real life. Real streamflow data was obtained from the United States Geological Survey (USGS, 2020) database. Figure 9 depicts the real gages that were used in this

research. The data sets obtained from these stream flow gages were used for the statistical analysis portion of this research.

Synthetic streamflow data is that which has been simulated. The synthetic streamflow data was obtained by running the original HSPF model runs before the precipitation data was altered. The synthetic data was obtained from the 1995 land-use conditions model runs. For each of the real streamflow gages discussed, the HSPF models incorporated the corresponding synthetic gage. The synthetic gage flow data was obtained prior to any model alterations. The synthetic gage flow data was used to conduct the statistical analysis. Table 9 outlines the gages that were used in this research. Again, real data was obtained from the USGS database at these gage locations and synthetic gage data was obtained from the HSPF models at those gages as well.

Table 9. Real USGS Gage Locations (USGS, 2020) and Corresponding HSPF Model Locations

Number	Real Gage ID	Name	Status	Synthetic HSPF Model Data Available?
1	02246000	North Fork near Middleburg	Active	No
2	02245500	South Fork Penney Farms	Active	No
3	02246150	Big Davis Creek at Bayard	Inactive	Yes
4	02246300	Ortega 103rd St. Bridge	Active	Yes
5	02246318	Ortega at Kirwin Rd.	Inactive	Yes
6	02246828	Pablo Creek	Inactive	No

4.3 Land-use

The SJRWMD's HSPF model was programmed to simulate land-use conditions from 1995 and those projected for 2030. The 1995 land-use condition is based on 1994 and 1995 color-infrared aerial photography of the entire SJRWMD and it has been used for many projects throughout the district (SJRWMD, 2012). The 2030 future condition is the SJRWMD's "planning horizon". The 2030 land use condition considers population growth, residential growth areas, and increased area for urban land use (SJRWMD, 2012). The WSIS (2012) provides an estimate that the 1995 urban

land use represented 16% of the total area of the LSJRB while the projected 2030 urban land use cover is about 40% of the basin or more than double the 1995 coverage.

The 1995 land-use condition was selected as the primary land-use for which each sub-basin was assessed at. The variation in land-use was assessed by performing the simulations at Julington Creek, Durbin Creek, and Big Davis Creek at both the 1995 and 2030 land-use condition. From there, a comparison of results provides insight into the effects that varying the land-use has on the resulting flood flows.

4.4 Target Date

To produce the 10-, 25-, 50-, and 100-year flood flows, a 10-, 25-, 50-, and 100-year frequency precipitation (24-hour duration) event was simulated. Thus, the simulated flood flows are rainfall driven. The process of simulating any given frequency precipitation event involves identifying the appropriate amount of rainfall to simulate on a specific date, referred to as a target date in this research. Before identifying the precipitation frequency values to simulate in the model, the target dates were determined.

The first step in selecting the appropriate target dates is to reference the output data generated from the original models. To do this, the original models obtained from the SJRWMD were simulated. The simulated flow data output values were obtained in graphical form. From there, it is simple to identify the 50th percentile flood from the flood frequency curve. The 50th percentile flood is a standard baseline for various flood frequency analysis procedures (Malamud and Turcotte, 2006). This process establishes the starting flow condition for each sub-basin for the new simulations. Figure 10 depicts an example of an original model flood frequency curve.

Next, an output list of the simulated flow data was obtained and organized in increasing order. From there, the dataset will be narrowed down to the dates on which the 50th percentile flood

occurred within a 15% range of accuracy. Finally, 10 target dates were selected. The 10 target dates were selected in varying months of the year to account for the varying rainfall conditions occurring throughout the seasons. This process was repeated for every sub-basin of interest. The simulated flow data was obtained from the outlet of each sub-basin. Therefore, 10 target dates were selected for each sub-basin. As previously explained, a specified amount of rainfall was simulated for each target date to represent the 10-, 25- 50-, and 100-year rainfall event. The simulated rainfall events produced the corresponding 10-, 25-, 50-, and 100-year flood events of interest.

4.5 Precipitation Data

Now that there is understanding on which specific dates the 10-, 25-, 50-, and 100-year rainfall event was simulated, a discussion on specifically how much rainfall to simulate follows. According to the WSIS (2012), the SJRWMD implemented rainfall data from one rainfall gauge per sub-basin based on the dominant polygon from the Theissen polygon network (refer to Appendix D) that was developed (SJRWMD, 2012). The SJRWMD's Theissen polygon network was used to determine each sub-basin's corresponding rainfall gage. Each sub-basin of interest was be assessed in terms of all associated polygons. From there, all rainfall gauges that fall within the boundary of the sub-basin were considered. With the use of National Oceanic Atmospheric Administration (NOAA) Atlas 14 (NOAA, 2017), each rainfall gauge of interest was investigated.

Since this research assessed the difference between varying precipitation frequency values and the resulting flood flows, the median and 90% percentile 24-hour 10-, 25-, 50-, and 100-year precipitation was recorded at each gage of interest (NOAA, 2005). Once the rainfall was recorded, the average of the rainfall per gauge was calculated in reference to the sub-basin of interest. The average was only determined in sub-basins which contained more than one rainfall gage. A deeper

explanation on the arrival of this conclusion is discussed in the results section. The median 24-hour precipitation values were simulated on the selected target dates in the Julington Creek, Durbin Creek, and Big Davis Creek sub-basins to provide data to compare to the simulated flows resulting from the 90th percentile rainfall events. Table 10 depicts the median and 90th percentile 24-hour 10-, 25-, 50-, and 100-year rainfall events at each sub-basins' corresponding rainfall gage.

Table 10. Precipitation Frequency Values (in inches)

Sub-basin	**Rainfall Gage**	**24-hour 90th Percentile Rainfall for each recurrence interval (years)**				**24-hour Median Rainfall for each recurrence interval (years)**			
		10	**25**	**50**	**100**	**10**	**25**	**50**	**100**
Black Creek	Jacksonville Airport	8.07	10.8	12.9	15.6	7.05	8.86	10.4	12.2
	Glen St. Mary	7.45	9.56	11.2	13.1	6.29	7.69	8.88	10.2
	Starke	7.12	9.12	10.6	12.5	5.83	7.13	8.27	9.52
	Federal Point	7.49	9.83	11.6	13.8	6.34	7.90	9.27	10.8
	Palatka	7.25	9.40	11.0	13.0	6.19	7.60	8.83	10.2
	Average	7.48	9.74	11.5	13.6	6.34	7.84	9.13	10.6
Julington Creek	Jacksonville Beach	8.74	11.6	13.8	16.4	7.34	9.23	10.8	12.6
	St. Augustine	8.18	11.2	13.4	16.2	6.98	8.90	10.6	12.4
	Average	8.46	11.4	13.6	16.3	7.16	9.07	10.7	12.5
Durbin Creek	Jacksonville Beach	8.74	11.6	13.8	16.4	7.34	9.23	10.8	12.6
	St. Augustine	8.18	11.2	13.4	16.2	6.98	8.90	10.6	12.4
	Average	8.46	11.4	13.6	16.3	7.16	9.07	10.7	12.5
Big Davis Creek	Jacksonville Beach	8.74	11.6	13.8	16.4	7.34	9.23	10.8	12.6
	St. Augustine	8.18	11.2	13.4	16.2	6.98	8.90	10.6	12.4
	Average	8.46	11.4	13.6	16.3	7.16	9.07	10.7	12.5
Ortega River	Jacksonville Airport	8.07	10.8	12.9	15.6	7.05	8.86	10.4	12.2
Pablo Creek	Jacksonville Beach	8.74	11.6	13.8	16.4	7.34	9.23	10.8	12.6

4.6 Antecedent Moisture Conditions

The SJRWMD defines the antecedent soil moisture conditions as an indicator of watershed wetness and availability of soil storage prior to a storm (SJRWMD, 1985). It is known that these conditions have a significant effect on runoff volume and runoff rate. Three levels of antecedent

moisture conditions (AMC) exist: AMC-I for dry, AMC-II for normal, AMC-III for wet conditions (SJRWMD, 1985). Table 11 depicts the seasonal rainfall limits for these three AMCs. According to Schiariti (n.d.), AMC II is considered for modeling purposes because it is essentially the average moisture condition. Table 11 is divided into a dormant and growing season. According to the SJRWMD's Technical Publication SJ90-3 (1990), the rainy season is in northeast Florida lasts from June to October and the dry seasons lasts from November to May (1990). It can be inferred that the growing season is synonymous with the rainy season and the dormant season is synonymous with the dry season.

The most straightforward method to simulate antecedent moisture conditions (AMC) was to simulate it as daily rainfall. As depicted in Table 11, the AMC was simulated over the course of five days. Additionally, it was discovered in the preliminary phase of the research that the models performed better with the incorporation of wet antecedent moisture conditions during the dormant and growing months. Therefore, to summarize the AMC, 2.1 inches of rainfall over the course of five days was simulated before each target date.

Table 11. Seasonal Rainfall Limits Antecedent Moisture Conditions (SJRWMD, 1985)

AMC	**Total 5-Day Dormant Season**	**Total 5-Day Growing Season**
I	Less than 0.5 inches	Less than 1.4 inches
II	0.5 to 1.1 inches	1.4 to 2.1 inches
III	More than 1.1 inches	More than 2.1 inches

4.7 Rainfall Distribution

When applied on an hourly basis, the rainfall data described above will represent a uniform distribution – each hour will receive the same amount of rainfall. For example, the average median 10-year 24-hour rainfall in Black Creek is 6.34 inches according to Table 10. Therefore, when incorporating this information in the model, the 6.34 inches of rainfall will be distributed evenly

over a 24-hour period on the selected target dates. However, in reality, rainfall occurs in varying temporal distributions. Therefore, an additional rainfall distribution was also applied in a separate scenario. According to Suphunvorranop (1985), the Soil Conservation Service (SCS) has developed four types of rainfall distributions – Types I, II, III (representative of different climates in the United States), and Type II Modified (representative of Florida specifically). These synthetic rainfall distributions occur over a 24-hour time period. The SCS Modified Type II rainfall distribution, obtained from the Suphunvorranop (1985) and located in Appendix E, was also modeled to determine the effects on the flood magnitude predictions when different rainfall distributions are applied. It was simulated in the Julington Creek, Durbin Creek, and Big Davis Creek sub-basins paired with the 1995 land-use conditions, 90th percentile precipitation, and AMC.

4.8 Output Processing

After the original HSPF model runs were modified to incorporate the required return frequency precipitation, antecedent moisture conditions, varying rainfall distributions, and land-use conditions, the simulated flow values at each location were assessed.

Initially, the HSPF model locations were identified based on the existing HSPF models depicted in Figures 1-8. The reaches of interested were established as shown in Table 12. Therefore, when accessing the simulated flow data through the BASINS interface, each of the relevant reaches were assessed per sub-basin. Once the simulated flow data was obtained, processing the data was simple.

The data was organized in two columns: date and flow. The HSPF model runs simulated flow data from January 1, 1975 to December 31, 2008. A spreadsheet was created for every reach and the output simulated flow data was imported. From there, it was a matter of identifying the initial

target dates and recording the resulting simulated peak flow. The resulting peak flow typically occurred exactly on the target date and up to two days after the target date.

Table 12. HSPF Model Reaches of Interest

Sub-basin	**HSPF Model Reach of Interest**
Black Creek	3, 6, 12
Julington Creek	2, 5
Durbin Creek	1
Big Davis Creek	6
Ortega River	3
Pablo Creek	8

Chapter 5 STATISTICAL ANALYSIS

5.1 Log-Pearson Type III

The statistical Log-Pearson Type III model fit was implemented for real data and synthetic data. Using the synthetic streamflow data is advantageous because a longer period of record was at times observed compared to the real gauged streamflow data. Synthetic streamflow data was collected from applicable modeled gages (if available) as well as the previously discussed reaches of interest for each sub-basin. The Log Pearson Type III (LP3) statistical calculations were executed with the use of Excel 2016. The information presented in this section has been obtained from Oregon State University's guidance regarding the Log-Pearson Type III Distribution (2005).

The following equation was used to calculate the LP3 distribution:

$$log\ x = \overline{log\ x} + K\sigma_{log\ x} \qquad (1)$$

where x is the flood discharge value of some specified probability

log x represents the discharge values

K is the frequency factor

And σ is the standard deviation of the log x values.

The frequency factor, K, is a function of the skewness coefficient and return period.

The first step of the LP3 analysis involved obtaining streamflow data from the appropriate gauges. The annual duration flood series was analyzed. The gages of interest are the gages that were used to calibrate the model, which are depicted in Table 3. Synthetic gage streamflow data was obtained from the HSPF model output, where the gage data was available. Output data from each modeled reach of interest was also obtained. The real gage streamflow data was obtained from the USGS database. The simulated gage flow data and the specified reach flow data was obtained from original and unaltered HSPF model runs.

As previously mentioned, LP3 computations were conducted using real streamflow data and synthetic streamflow data. Table 13 depicts the real gage data sources used for LP3 computations. Table 14 depicts the synthetic streamflow data sources used for LP3 computations. Note that for the Pablo Creek Gages, the synthetic period of record is longer than the correspond real gage record. For all other cases, the real gages have a longer period of record than the synthetic gage locations since the HSPF models were designed to run from 1975 to 2008.

Table 13. Real Gages used for Log-Pearson Type III Statistical Analysis

Gage Name	USGS Gage ID	Years of Record
North Fork USGS Gage	2246000	88
South Fork USGS Gage	2245500	79
Big Davis Creek Gage	2246150	37
Ortega 103rd Street Gage	2246300	37
Pablo Creek Gage	2246828	27

Table 14. Synthetic Data used for Log-Pearson Type III Statistical Analysis

Sub-basin	HSPF Model Location	Years of Record
Black Creek	Reach 3,6, and 12	34
Julington Creek	Reach 2 and 5	34
Durbin Creek	Reach 1	34
Big Davis Creek	Reach 6 and Big Davis Creek Gage 2246150	34

Ortega River	Reach 3, Ortega at 103rd Street 02246300, Ortega at Kirwin Road Gage 2246318	34-44
Pablo Creek	Reach 8	34

From there, the maximum flow (Q) for each water year was determined. This information was then ranked from the largest discharge value to the smallest discharge value and each streamflow value was ranked from 1 to n, which is the total number of values included in the dataset. Next, the log of each yearly peak streamflow was obtained and defined as log(Q). The average of every Q and the average of every log(Q) was computed. The following computations were conducted for every water year:

$$\log(Q) - average(\log(Q))^2 \qquad (2)$$

$$\log(Q) - average(\log(Q))^3 \qquad (3)$$

Next, the return period was calculated using the Weibull plotting position presented in Malamud and Turcotte's (2006) research. The Weibull plotting position provides the recurrence interval in years with the following equation:

$$T = \frac{N_{WY}+1}{N_C} \qquad (4)$$

where, Nc is the rank and NWY is the number of water years in the data set.

Next, the final calculation was completed by determining the exceedance probability of each discharge value with the formula:

$$Exceedence\ Probability = \frac{1}{T} \qquad (5)$$

The sum of the values computed for Eq. (2) was determined as well as the sum of the values computed for Eq. (3). From there, the parameter estimation step remains. The variance, standard deviation and skew coefficient were determined using the equations below:

$$\frac{\sum_i^n((logQ - avg(logQ))\text{^}2}{n-1} \qquad (6)$$

$$\sigma_{\log x} = \sqrt{\frac{\sum(logx - \overline{\log x})\text{^}2}{n-1}} \quad (7)$$

$$skew\ coeff. = \frac{n * \sum_1^n (\log(Q) - average(\log(Q)))\text{^}3}{(n-1)(n-2)(\sigma \log(Q))\text{^}3} \quad (8)$$

An appropriate frequency factor table (Haan, 1977) was used along with the calculated skew coefficient to find the k-values. The k-values are a constant, which determines the symmetry of the flood frequency diagram. The following equation was used to calculate the 10-, 25-, 50-, and 100-year discharges:

$$\log(Q(T) = avg(\log(Q)) + [K(T, C_S)] * \sigma \log(Q) \quad (9)$$

5.2 Power Law

The Power Law (PL) is the second selected statistical model for flood flow estimation in this research. As previously mentioned, it is a considerably simpler statistical distribution compared to the Log-Pearson Type III distribution. The PL distribution requires analytical fitting of two parameters whereas the Log-Pearson Type III distribution requires analytical fitting of three parameters. The first step in implementing the PL was to obtain the appropriate data. Like the Log-Pearson Type III method, real data and synthetic data was assessed. Real gage flow data was obtained from the USGS database. Synthetic gage streamflow data and specific reach location flow data was obtained from the original HSPF model runs. Table 13 and Table 14 depict the locations at which the PL distribution was applied to obtain the flood frequencies of interest.

Once the data was obtained, either a linear or nonlinear model was selected for analysis. The linear model involves a parameter estimation procedure based on the linear regression of the data set. To obtain the linear regression of the dataset, the maximum streamflow value (Q) for every given year of water data was sorted from largest to smallest. As mentioned by Malamus and Turcotte (2006), the partial duration flood series was deemed a better selection over the annual duration flood series.

The annual duration was selected for the data selection component of the PL analysis. Preliminary research results indicated that the data sets in this research respond better to the PL distribution when the annual duration flood series is assessed. More details regarding this are presented in Chapter 8. The data was assigned a ranking value, N_C, which was used to determine the Weibull plotting position return recurrence interval, T. N_C is ranked as 1, 2, 3, …, N_{WY} and T is defined as:

$$T = \frac{N_{WY}}{N_C} \qquad (10)$$

The log function was applied to all peak streamflow values and all T values. Then, a scatterplot of log(T) versus log(Q) was created. A linear regression trendline and R-squared value was projected for reference. This methodology was based on the literature review of the conducted by Malamud and Turcotte (2006). Figure 11 depicts an example of the log plot of T verus Q at Pablo Creek Reach 8.

Recall Malamud and Turcotte's (2006) generalized power law equation:

$$logQ[T] = \alpha \log(T) + \log(C) \qquad (11)$$

The trendline of the scatterplot provided the initial estimate for the α and C regression coefficients. The α coefficient was identified as the slope of the trendline equation. The C coefficient was identified as the y-intercept of the trendline equation. Once these coefficients were determined, the discharge value of the 10-, 25-, 50-, and 100-year flood was estimated. Therefore, this methodology considers a linear model where the regression coefficients are estimated from the linear regression of the dataset.

Additionally, a nonlinear model approach was analyzed for the PL distribution. The nonlinear model was assessed using the least squared method using the Solver (Microstoft Excel, 2016) plug-in. This method produced an estimate for the nonlinearly obtained regression coefficient parameters, which was eventually compared to the linearly obtained regression coefficients. The

least squared method was implemented by first assuming an initial guess where the α and C coefficient are greater than 0.01. Then, the modeled Q values were calculated using the estimated α and C coefficient using the general PL equation:

$$Q[T] = CT^{\alpha} \qquad (12)$$

From there, the sum of squared differences was obtained using:

$$sum\ of\ the\ squared\ differences = \left(sum(Q) - sum(Qmodeled)\right)^2$$

Then, the Solver (Microsoft Excel, 2016) plug-in was used to minimize the sum of the squared differences while iterating for the most ideal values of α and C. The Generalized Reduced Gradient (GRG) Nonlinear was the solution method selected. Therefore, the α and C regression coefficient parameters were obtained using two methods (1) linear model approach graphically from the log plot of T versus Q and (2) by optimizing the modeled Q values using the Microsoft Excel Solver plug-in. Table 15 depicts the two sets of α and C regression coefficients derived from the two methods described at Pablo Creek Reach 8. Assessing two different methods of obtaining the α and C regression coefficients of the Power Law distribution proved to be beneficial because the two methods produced varying regression coefficients in some instances. The results of this research depict the varying flood estimates obtained using the regression coefficients determined from the linear and nonlinear models of the Power Law distribution.

Table 15. Example of Power Law Regression Coefficients

Method	**C**	**α**
Linear Regression	1840	0.2293
Nonlinear Regression	549.7	0.558

Chapter 6 RESULTS

6.1 HSPF Model Results

This section presents the HSPF model results conducted in this research. Each sub-section presents results from the Black Creek, Julington Creek, Durbin Creek, Big Davis Creek, Ortega River, and Pablo Creek sub-basins. Each sub-section presented outlines the results from each applicable reach of the HSPF model as well as any simulated gages, if present. All results are presented in cubic feet per second (cfs).

6.1.1 Black Creek

Table 16 depicts the results at Black Creek Reach 3 (South Fork), Reach 6 (North Fork), and Reach 12 (Black Out). When assessing the 1995 land-use condition with added 90th percentile precipitation and antecedent moisture conditions (AMC), the Black Creek sub-basin could not compute flow data past the 10-year flood. When assessing the same model scenario except by modeling the median precipitation scenario versus 90th percentile, the model was able to produce results up through the 50-year flood. However, the model crashed during the 100-year flood simulation. Therefore, the model runs at the Black Creek sub-basin were somewhat unsuccessful. Chapter 8 provides a further explanation of the failed model runs in the Black Creek sub-basin.

Table 16. Black Creek HSPF Model Results (in cfs)

HSPF Model Location	**1995 Land-use, 90th Percentile Precipitation, and AMC**				**1995 Land-use, Median Precipitation, and AMC**			
	10-year	**25-year**	**50-year**	**100-year**	**10-year**	**25-year**	**50-year**	**100-year**
Reach 3	8237	Crashed	Crashed	Crashed	6151	8872	11,138	Crashed
Reach 6	8628	Crashed	Crashed	Crashed	6284	9349	11900	Crashed
Reach 12	18063	Crashed	Crashed	Crashed	12257	20240	26304	Crashed

6.1.2 Julington Creek

Table 17 depicts the HSPF model runs in the Julington Creek sub-basin. The two main reaches of the Julington Creek sub-basin were Reach 2 (the sub-basin outlet location) and Reach 5 (an upstream portion of Julington Creek). Four different model scenarios were assessed at Julington Creek. The model scenarios varied in precipitation, rainfall distribution, and land-use. Each model included antecedent moisture conditions. Overall, the HSPF model was successful in simulating each of the scenarios. The variety in results produced from the varying model scenarios provided valuable insight regarding the sensitivity of model parameter selection. This will be discussed in further detail in Chapter 7.

Table 17. Julington Creek HSPF Model Results (in cfs)

HSPF Model Location	**1995 Land-use, 90th Percentile Precipitation, and AMC**				**1995 Land-use, Median Precipitation, and AMC**			
	10-year	**25-year**	**50-year**	**100-year**	**10-year**	**25-year**	**50-year**	**100-year**
Reach 2	1541	2454	3367	4676	1195	1709	2206	2886
Reach 5	472	806	993	1441	340	541	734	905
HSPF Model Location	**1995 Land-use, 90th Percentile Precipitation, Type II Modified Distribution, AMC**				**2030 Land-use, 90th Percentile Precipitation, and AMC**			
	10-year	**25-year**	**50-year**	**100-year**	**10-year**	**25-year**	**50-year**	**100-year**
Reach 2	1721	2807	3752	4980	2396	3682	4785	6290
Reach 5	544	869	1154	1605	715	1026	1348	1761

6.1.3 Durbin Creek

Table 18 depicts the model simulations in the Durbin Creek sub-basin. As previously discussed, the Durbin Creek sub-basin was included in Julington Creek HSPF model. Durbin Creek was identified as Reach 1. The same model scenarios that were assessed in Julington Creek were also assessed in Durbin Creek. The model runs were successful. The variety in results produced from

the varying model scenarios provided valuable insight regarding the sensitivity of model parameter selection. This will be discussed in further detail in Chapter 7.

Table 18. Durbin Creek HSPF Model Results (in cfs)

HSPF Model Location	1995 Land-use, 90th Percentile Precipitation, and AMC				1995 Land-use, Median Precipitation, and AMC			
	10-year	25-year	50-year	100-year	10-year	25-year	50-year	100-year
Reach 1	1077	1540	2116	3053	835	1164	1407	1801
HSPF Model Location	1995 Land-use, 90th Percentile Precipitation, Type II Modified Distribution, AMC				2030 Land-use, 90th Percentile Precipitation, and AMC			
	10-year	25-year	50-year	100-year	10-year	25-year	50-year	100-year
Reach 1	1145	1829	2425	3426	1508	2251	2997	4056

6.1.4 Big Davis Creek

Table 19 depicts the HSPF model results at Big Davis Creek. As previously mentioned, Big Davis Creek was modeled within the Julington Creek HSPF model. Big Davis Creek was identified as Reach 6. As also previously mentioned, the Big Davis USGS gage was used to calibrate the Julington Creek model, which includes the Dubin Creek and Big Davis Creek sub-basins. The HSPF model also includes a Big Davis Creek gage location, which is referred to as a synthetic gage. This synthetic gage corresponds to the real Big Davis Creek gage; however, the flow data is synthetic since it is simulated. Even though the Big Davis Creek gage was used to calibrate multiple sub-basins, the Big Davis Creek synthetic gage results are depicted here in the Big Davis Creek model simulation results.

Table 19. Big Davis HSPF Model Results (in cfs)

HSPF Model Location	1995 Land-use, 90th Percentile Precipitation, and AMC				1995 Land-use, Median Precipitation, and AMC			
	10-year	25-year	50-year	100-year	10-year	25-year	50-year	100-year
Reach 6	389	691	879	1042	290	440	606	805
Big Davis Gage Synth	336	583	842	1098	256	378	510	715
HSPF Model Location	**1995 Land-use, 90th Percentile Precipitation, Type II Modified Distribution, AMC**				**2030 Land-use, 90th Percentile Precipitation, and AMC**			
	10-year	**25-year**	**50-year**	**100-year**	**10-year**	**25-year**	**50-year**	**100-year**
Reach 6	398	766	950	1116	796	1047	1207	1424
Big Davis Gage Synth	333	634	911	1164	620	1039	1261	1553

6.1.5 Ortega River

Table 20 depicts HSPF model simulations conducted in the Ortega River sub-basin. Reach 3 was identified as the downstream portion of the Ortega River which drains into the St. Johns River. As previously discussed, the 103rd Street USGS gage and the Kirwin Rd. USGS gage were used to calibrate the Ortega River sub-basin. Both gages were also simulated in the Ortega River sub-basin. Therefore, synthetic gage data was available in this sub-basin. The 1995 land-use, 90th percentile precipitation, and antecedent moisture conditions scenario was the only scenario assessed in the Ortega River sub-basin and quality results were produced.

Table 20. Ortega River HSPF Model Results (in cfs)

HSPF Model Location	1995 Land-use, 90th Percentile Precipitation, and AMC			
	10-year	25-year	50-year	100-year
Reach 3	3293	4756	5978	7485
103rd St. Gage Synthetic	2152	3107	3642	4285
Kirwin Rd. Gage Synthetic	3206	4654	5567	6693

6.1.6 Pablo Creek

Table 21 depicts the HSPF model results obtained at Reach 8. Reach 8 is the location of the Pablo Creek sub-basin outlet into the Jacksonville, Florida intracoastal waterway. The 1995 land-use, 90th percentile precipitation, and antecedent moisture condition scenario was simulated in this sub-basin. Quality results were produced in this model simulations.

Table 21. Pablo Creek HSPF Model Results (in cfs)

HSPF Model Location	**1995 Land-use, 90th Percentile Precipitation, and AMC**			
	10-year	**25-year**	**50-year**	**100-year**
Reach 8	2088	2685	3041	3479

6.2 Log-Pearson Type III Results

This section presents the results of the Log-Pearson Type III (LP3) distribution statistical computations. The following sub-sections present the results from the Black Creek, Julington Creek, Durbin Creek, Big Davis Creek, Ortega River, and Pablo Creek sub-basins. The LP3 results were obtained from computations using simulated HSPF reach location flow data, simulated USGS flow gage data, and real USGS gage flow data, if available.

6.2.1 Black Creek

Table 22 depicts the LP3 results in the Black Creek sub-basin. The results were obtained for Reach 3 (South Fork), Reach 6 (North Fork), Reach 12 (Black Out), and the two real USGS gages at South and North Fork. There were no synthetic gage locations in the HSPF model from which to extract synthetic gage data to conduct LP3 computations.

Table 22. Black Creek Log-Pearson Type III Results (in cfs)

Location	Log-Pearson Type III			
	10-year	25-year	50-year	100-year
Reach 3	6269	8258	9935	11778
South Fork Real Gage	6036	8370	10257	12239
Reach 6	8797	11580	13682	15779
North Fork Real Gage	8372	11495	13952	16476
Reach 12	12606	14313	15335	16180

6.2.2 Julington Creek

Table 23 depicts the LP3 computations conducted using synthetic reach location data obtained from the HSPF model. Reach 2 and 5 are the main reaches within the Julington Creek sub-basin, where reach 2 is the sub-basin outlet location into the St. Johns River and Reach 5 is an upstream location of Julington Creek.

Table 23. Julington Creek Log-Pearson Type III Results (in cfs)

Location	Log-Pearson Type III			
	10-year	25-year	50-year	100-year
Reach 2	1695	2225	2648	3091
Reach 5	652	937	1200	1511

6.2.3 Durbin Creek

Table 24 depicts the LP3 computation results conducted in the Dubrin Creek sub-basin.

Table 24. Durbin Creek Log-Pearson Type III Results (in cfs)

Location	Log-Pearson Type III			
	10-year	25-year	50-year	100-year
Reach 1	1061	1414	1689	1967

6.2.4 Big Davis Creek

Table 25 depicts the LP3 computation results conducted in the Big Davis Creek sub-basin. As previously mentioned, the Big Davis Creek sub-basin is included in the Julington Creek sub-basin HSPF model. The real Big Davis Creek USGS gage was used to calibrate the entire basin.

However, the gage results are presented here in the Big Davis Creek sub-basin results. LP3 computations were conducted at Reach 6, using real gage data obtained from the USGS database, and using the synthetic gage data extracted from the HSPF model.

Table 25. Big Davis Creek Log Pearson Type III Results (in cfs)

Location	Log-Pearson Type III			
	10-year	25-year	50-year	100-year
Reach 6	694	930	1120	1320
Big Davis Gage Real	441	596	718	842
Big Davis Gage Synth	656	917	1140	1388

6.2.5 Ortega River

Table 26 depicts the LP3 computation results in the Ortega River sub-basin. Results were obtained using flow data from Reach 3, which represents the outlet location of the Ortega River into the St. Johns River. As previously mentioned, the Ortega River sub-basin HSPF model was calibrated using the real 103rd St. Gage and Kirwin Rd. gage. The Kirwin Rd. gage has a short period of record, so the calibration was not successful, and the model calibration ultimately depended on the 103rd St. gage. Therefore, LP3 computations were conducted using real gage data at 103rd St. and not Kirwin Rd. gage. Synthetic gage data was available for 103rd St. and Kirwin Rd., so LP3 computations were conducted using that data as well.

Table 26. Ortega River Log-Pearson Type III Results (in cfs)

Location	Log-Pearson Type III			
	10-year	25-year	50-year	100-year
Reach 3	5766	6841	7628	8400
103rd St. Gage Real	2128	3173	4124	5239
103rd St. Gage Synth	1969	2468	2828	3174
Kirwin Rd. Gage Synth	2771	3558	4149	4736

6.2.6 Pablo Creek

Lastly, Table 27 depicts the LP3 computations conducted in the Pablo Creek sub-basin. The results shown were obtained using data from the HSPF model Reach 8, which represents the outlet location of the entire Pablo Creek sub-basin into the Jacksonville, Florida intracoastal waterway, and the real Pablo Creek gage that was originally used to calibrate the HSPF model.

Table 27. Pablo Creek Log-Pearson Type III Results (in cfs)

Location	**Log-Pearson Type III**			
	10-year	**25-year**	**50-year**	**100-year**
Reach 8	1973	2646	3200	3798
Pablo Creek Real Gage	1006	1300	1515	1725

6.3 Power Law Results

This section presents the results of the Power Law (PL) distribution statistical computations. The following sub-sections present the results from the Black Creek, Julington Creek, Durbin Creek, Big Davis Creek, Ortega River, and Pablo Creek sub-basins. The PL results were obtained from computations using simulated HSPF reach location flow data, simulated USGS flow gage data, and real USGS gage flow data, if available.

6.3.1 Black Creek

Table 28 depicts the PL results in the Black Creek sub-basin using the linear regression approach. Table 29 depicts the results using the Microsoft Excel Solver plug-in approach. The results were obtained for Reach 3 (South Fork), Reach 6 (North Fork), Reach 12 (Black Out), and the two real USGS gages at South and North Fork. There were no synthetic gage locations in the HSPF model from which to extract synthetic gage data to conduct PL computations.

Table 28. Black Creek Power Law (Linear Regression) Results (in cfs)

Location	Power Law – Linear Regression			
	10-year	25-year	50-year	100-year
Reach 3	6,907	11,589	17,143	25,357
South Fork Real Gage	6,247	12,865	22,218	38,371
Reach 6	9,817	19,549	32,917	55,424
North Fork Real Gage	9,750	20,523	36,039	63,285
Reach 12	13,658	21,192	29,545	41,191

Table 29. Black Creek Power Law (Nonlinear Regression) Results (in cfs)

Location	Power Law – Nonlinear Regression			
	10-year	25-year	50-year	100-year
Reach 3	6,312	9,619	13,229	18,194
South Fork Real Gage	5,185	8,113	11,382	15,970
Reach 6	7,935	12,144	16,755	23,118
North Fork Real Gage	7,206	11,441	16,231	23,026
Reach 12	12,260	16,982	21,728	27,801

6.3.2 Julington Creek

Table 30 depicts the PL results in the Julington Creek sub-basin using the linear regression approach. Table 31 depicts the PL results using the Microsoft Excel Solver plug-in approach. The PL computations were conducted using synthetic reach location data obtained from the HSPF model. Reach 2 and 5 are the main reaches within the Julington Creek sub-basin, where Reach 2 is the sub-basin outlet location into the St. Johns River and Reach 5 is an upstream location of Julington Creek.

Table 30. Julington Creek Power Law (Linear Regression) Results (in cfs)

Location	Power Law – Linear Regression			
	10-year	25-year	50-year	100-year
Reach 2	1,867	3,352	5,219	8,125
Reach 5	738	1,411	2,304	3,762

Table 31. Julington Creek Power Law (Nonlinear Regression) Results (in cfs)

Location	Power Law – Nonlinear Regression			
	10-year	25-year	50-year	100-year
Reach 2	1,759	2,932	4,317	6,355
Reach 5	661	1,104	1,627	2,398

6.3.3 Durbin Creek

Table 32 depicts the PL results in the Durbin Creek sub-basin using the linear regression approach.

Table 33 depicts the PL results using the Microsoft Excel Solver plug-in approach.

Table 32. Durbin Creek Power Law (Linear Regression) Results (in cfs)

Location	Power Law – Linear Regression			
	10-year	25-year	50-year	100-year
Reach 1	1,208	2,453	4,193	7,166

Table 33. Durbin Creek Power Law (Nonlinear Regression) Results (in cfs)

Location	Power Law – Nonlinear Regression			
	10-year	25-year	50-year	100-year
Reach 1	841	1,727	2,977	5,131

6.3.4 Big Davis Creek

Table 34 depicts the PL results in the Big Davis Creek sub-basin using the linear regression approach. Table 35 depicts the PL results using the Microsoft Excel Solver plug-in approach. As previously mentioned, the Big Davis Creek sub-basin is included in the Julington Creek sub-basin HSPF model. The real Big Davis Creek USGS gage was used to calibrate the entire basin. However, the gage results are presented here in the Big Davis Creek sub-basin results. PL computations were conducted at Reach 6, using real gage data obtained from the USGS database, and using the synthetic gage data extracted from the HSPF model.

Table 34. Big Davis Creek Power Law (Linear Regression) Results (in cfs)

Location	Power Law – Linear Regression			
	10-year	25-year	50-year	100-year
Reach 6	790	1,528	2,516	4,143
Big Davis Gage Real	495	1,031	1,795	3,127
Big Davis Gage Synth.	747	1,501	2,546	4,316

Table 35. Big Davis Creek Power Law (Nonlinear Regression) Results (in cfs)

Location	Power Law – Nonlinear Regression			
	10-year	25-year	50-year	100-year
Reach 6	674	1,079	1,541	2,199
Big Davis Gage Real	411	675	983	1,431
Big Davis Gage Synth.	642	1,067	1,568	2,304

6.3.5 Ortega River

Table 36 depicts the PL results in the Ortega River sub-basin using the linear regression approach. Table 37 depicts the PL results using the Microsoft Excel Solver plug-in approach. Results were obtained using flow data from Reach 3, which represents the outlet location of the Ortega River into the St. Johns River. As previously mentioned, the Ortega River sub-basin HSPF model was calibrated using the real 103rd St. Gage and Kirwin Rd. gage. The Kirwin Rd. gage has a short period of record, so the calibration was not successful, and the model calibration ultimately depended on the 103rd St. gage. Therefore, PL computations were conducted using real gage data at 103rd St. and not Kirwin Rd. gage. Synthetic gage data was available for 103rd St. and Kirwin Rd., so PL computations were conducted using that data as well.

Table 36. Ortega River Power Law (Linear Regression) Results (in cfs)

Location	Power Law – Linear Regression			
	10-year	25-year	50-year	100-year
Reach 3	6,148	8,940	11,868	15,754
103rd St. Gage Real	2,174	4,441	7,625	13,092
103rd St. Gage Synth	1,983	3,052	4,229	5,860
Kirwin Rd. Gage Synth	2,789	4,378	6,159	8,664

Table 37. Ortega River Power Law (Nonlinear Regression) Results (in cfs)

Location	Power Law – Nonlinear Regression			
	10-year	25-year	50-year	100-year
Reach 3	5,623	7,509	9,346	11,633
103rd St. Gage Real	1,897	3,223	4,812	7,184
103rd St. Gage Synth	1,838	2,755	3,740	5,079
Kirwin Rd. Gage Synth	2,563	3,877	5,301	7,249

6.3.6 Pablo Creek

Table 38 depicts the PL results in the Pablo Creek sub-basin using the linear regression approach. Table 39 depicts the PL results using the Microsoft Excel Solver plug-in approach. The results shown were obtained using data from the HSPF model Reach 8, which represents the outlet location of the entire Pablo Creek sub-basin into the Jacksonville, Florida intracoastal waterway, and the real Pablo Creek gage that was originally used to calibrate the HSPF model.

Table 38. Pablo Creek Power Law (Linear Regression) Results (in cfs)

Location	Power Law – Linear Regression			
	10-year	25-year	50-year	100-year
Reach 8	3,120	3,849	4,512	5,289
Pablo Creek Real Gage	1,183	2,391	4,071	6,931

Table 39. Pablo Creek Power Law (Nonlinear) Results (in cfs)

Location	Power Law – Nonlinear Regression			
	10-year	25-year	50-year	100-year
Reach 8	1,986	3,311	4,875	7,176
Pablo Creek Real Gage	1,002	1,669	2,456	3,614

6.4 Existing Flood Insurance Studies

This section outlines the results of the existing Flood Insurance Studies. FEMA Flood Insurance Studies (FIS) were obtained from each sub-basin. The FEMA FIS flood estimates were adjusted accordingly to represent the modeled drainage basin area. In short, the HSPF modeled drainage basin area did not match the FEMA FIS drainage basin area from which the results were obtained.

Therefore, a simple extrapolation was conducted to standardize the FEMA FIS estimates' drainage basin area to match the drainage basin area of the HSPF modeled locations. The original Black Creek FEMA FIS flood estimates were obtained from the Clay County FEMA FIS (2014). The original Julington Creek, Durbin Creek, and Big Davis Creek FEMA FIS flood estimates were obtained from the St. Johns County FEMA FIS (2011). The original FEMA FIS flood estimates at Ortega River and Pablo Creek were obtained from the Duval County FEMA FIS (2014).

6.4.1 Black Creek

Table 40 depicts the results of the adjusted FEMA FIS flow estimates. The results obtained from the FEMA FIS were based on a 137 square mile drainage area for Reach 3 and the South Fork gage and a 167 square mile square mile drainage basin for Reach 6 and the North Fork gage. Conversely, the modeled area of the Reach 3 in HSPF is 120.63 square miles and 156.35 square miles for Reach 6. The FEMA FIS estimates at Reach 3 and Reach 6 were reduced by a percentage which represents the modeled drainage area to the FIS drainage area. Therefore, since the modeled area of Reach 3 and Reach 6 was approximately 88% and 94% of the discharge area covered at those locations in the FEMA FIS, the FEMA FIS estimates were reduced by 88% and 94%, respectively. It was important to reduce the FEMA FIS estimates so that the comparison was based on the same drainage area between the modeled estimates and the FEMA FIS estimates. The FEMA FIS estimates for the gages were not actually adjusted since the drainage area of location of the modeled gages was not disclosed. Therefore, it was assumed that the drainage area at the location of the modeled gage matched the drainage area at the gage location in the FEMA FIS and no adjustment was made to the flood estimates.

Table 40. Black Creek Adjusted FEMA FIS Estimates (in cfs)

Location	Adjusted FEMA FIS Estimates			
	10-year	25-year	50-year	100-year
Reach 3	8,277	12,296	15,145	18,755
South Fork Real Gage	9,400	13,964	17,200	21,300
Reach 6	8,714	12,084	14,817	16,977
North Fork Real Gage	9,000	12,392	15,640	18,030
Reach 12	20,853	30,242	37,194	44,814

6.4.2 Julington Creek

Table 41 depicts the adjusted FEMA FIS flow estimates for Reach 2 and Reach 5 of the Julington Creek sub-basin. The St. Johns County FEMA FIS contained an estimate for what was determined to be Reach 2 and 5 which had a drainage area of 28 square miles and 10 square miles, respectively. The HSPF modeled locations for Reach 2 and 5 have a drainage area of 27.46 square miles and 9.60 square miles, respectively. The same approach for adjusting the FEMA FIS estimates was conducted as described for the Black Creek sub-basin.

Table 41. Julington Creek Adjusted FEMA FIS Estimates (in cfs)

Location	Adjusted FEMA FIS Estimates			
	10-year	25-year	50-year	100-year
Reach 2	2,547	3,284	3,828	4,429
Reach 5	2,210	2,552	3,101	3,409

6.4.3 Durbin Creek

Table 42 depicts the adjusted FEMA FIS flow estimates for Reach 1 of the Durbin sub-basin. The St. Johns County FEMA FIS presented an estimate for what was determined to be the real-life equivalent of the HSPF modeled Reach 1. That flood estimate was based on a 45 square mile drainage area. The HSPF modeled Reach 1 consists of a 40.28 square mile drainage area. The same approach for adjusting the FEMA FIS estimates was conducted as described for the Black Creek sub-basin.

Table 42. Durbin Creek Adjusted FEMA FIS Estimates (in cfs)

Location	Adjusted FEMA FIS Estimates			
	10-year	25-year	50-year	100-year
Reach 1	2,720	3,850	4,643	5,637

6.4.4 Big Davis Creek

Table 43 depicts the adjusted FEMA FIS flow estimates for Reach 6 and the real USGS gage of the Big Davis sub-basin. The St. Johns County FEMA FIS estimates at Reach 6 were based on a drainage area of 14 square miles. The HSPF modeled Reach 6 consists of 10.0 square miles. The same approach for adjusting the FEMA FIS estimates was conducted as described for the Black Creek sub-basin. The flood estimates for the real gage were not adjusted because they were obtained directly from the FEMA FIS and no comparison to modeled drainage area was applicable.

Table 43. Big Davis Creek Adjusted FEMA FIS Estimates (in cfs)

Location	Adjusted FEMA FIS Estimate			
	10-year	25-year	50-year	100-year
Reach 6	471	609	887	1,120
Big Davis Real Gage	1,120	1,548	1,870	2,210

6.4.5 Ortega River

Table 44 depicts the adjusted FEMA FIS flow estimates for Reach 3, real USGS 103rd St. gage, and synthetic Kirwin Rd. gage of the Ortega River sub-basin. The modeled Reach 3 area was 57.40 square miles compared to FEMA's drainage area of 57 square miles. The same approach for adjusting the FEMA FIS estimates was conducted as described for the Black Creek sub-basin. The flood estimates for the real gage were not adjusted because it was obtained directly from the FEMA FIS and no comparison to modeled drainage area were applicable. The FEMA FIS estimates for the synthetic gage were also not adjusted because it was assumed that the modeled drainage area was the same as the drainage area in the FIS estimate.

Table 44. Ortega River Adjusted FEMA FIS Estimates (in cfs)

Location	Adjusted FEMA FIS Estimate			
	10-year	25-year	50-year	100-year
Reach 3	2,773	4,116	5,105	6,190
103rd St. Gage Real	1,626	2,460	3,111	3,729
Kirwin Rd. Gage Synth	2,739	4,222	5,396	6,420

6.4.6 Pablo Creek

Table 45 depicts the adjusted FEMA FIS flow estimates for Reach 8 and the real USGS Pablo Creek gage of the Pablo Creek sub-basin. The modeled Reach 8 area was 38.01 square miles compared to FEMA's drainage area of 46 square miles. The same approach for adjusting the FEMA FIS estimates was conducted as described for the Black Creek sub-basin. The flood estimates for the real gage were not adjusted because they were obtained directly from the FEMA FIS and no comparison to modeled drainage area was applicable.

Table 45. Pablo Creek Adjust FEMA FIS Estimates (in cfs)

Location	Adjusted FEMA FIS Estimate			
	10-year	25-year	50-year	100-year
Reach 8	3,882	5,890	7,516	8,800
Pablo Creek Real Gage	3,830	4,905	6,032	7,059

Chapter 7 COMPARISON OF RESULTS

This section presents a comparison of the results obtained from the various flood estimation methods conducted in this research. HSPF modeling, statistically derived estimates using the Log-Pearson Type III (LP3) and Power Law (PL) distributions, and analysis of existing FEMA Flood Insurance Studies (FIS) were the three methods conducted. This discussion is based on the results presented in the previous section. Before there is a comparison of the results obtained from the different methods, a discussion of the comparison of specific HSPF model scenarios will be discussed. As previously portrayed in Table 8, different modeling scenarios in the Julington Creek, Durbin Creek, and Big Davis Creek sub-basin were simulated to assess the model performance when land-use, rainfall quantity, and rainfall distribution were varied.

The difference between rainfall quantity was assessed by running two versions of the 1995 HSPF model run. One version of the 1995 model run included the simulation of the median precipitation frequency estimate values based on the rainfall gages within the sub-basins. Another version of the 1995 model runs included the addition of the 90^{th} percentile precipitation frequency values based on the associated rainfall gages within the sub-basins. Both model scenarios included the antecedent moisture conditions. Table 46 depicts the percent difference between the flood estimates obtained including the 90^{th} percentile and median precipitation frequency values at Reach 1, 2, 5, 6, and the synthetic Big Davis gage. The percent difference between the two scenarios increases as the return frequency flood increases. From this information, it can be deduced that simulating 90^{th} percentile precipitation frequency values compared to the median precipitation frequency values results in significantly higher flood flow estimates, which are closer to the adjusted FEMA FIS estimates.

Table 46. Percent Difference between varying Precipitation Frequency Values

HSPF Model Location	Percent Difference between 1995 HSPF Median PREC and 1995 HSPF 90% PREC			
	10-year	25-year	50-year	100-year
Reach 1 (Durbin)	25	28	40	52
Reach 2 (Julington)	25	36	42	47
Reach 5 (Julington)	32	39	30	46
Reach 6 (Big Davis)	29	44	37	26
Big Davis Gage Synth	27	43	49	42
Average	28	38	40	43

The difference in flood flow results based on simulation of two different rainfall distributions was assessed in this research. First, the 1995 land-use condition paired with the addition of the 90th percentile precipitation frequency values representing a uniform rainfall distribution and antecedent moisture conditions were simulated. Then, the 1995 land-use condition paired with the addition of the 90th percentile precipitation frequency values representing a Synthetic Type II Modified for Florida rainfall distribution and antecedent moisture conditions were simulated. Table 47 depicts the percent difference between the resulting flood flows at Reach 1, 2, 5, 6, and the synthetic Big Davis Gage when the uniform distribution is applied to the precipitation frequency values versus the Synthetic Type II Modified distribution is applied. Overall, the average percent difference between the HSPF model locations does not increase significantly as the return interval of the flood increases. Compared to the percent differences obtained when varying the precipitation frequency values, the variation of rainfall distributions does not produce drastic differences in flood flow estimates.

Table 47. Percent Difference between varying Rainfall Distributions

HSPF Model Location	Percent Difference between 1995 HSPF 90% PREC Uniform and Synthetic Rainfall Distribution			
	10-year	25-year	50-year	100-year
Reach 1 (Durbin)	6	17	14	12
Reach 2 (Julington)	11	13	11	6
Reach 5 (Julington)	14	7	15	11
Reach 6 (Big Davis)	2	10	8	7
Big Davis Gage Synth	1	8	8	6
Average	7	11	11	8

Lastly, the variation of land-use was assessed in the Durbin Creek, Julington Creek, and Big Davis Creek sub-basins. The land-use variation was assessed by simulating the 1995 land-use condition versus the 2030 land-use condition with the inclusion of the 90th percentile precipitation frequency values and antecedent moisture conditions. Table 48 depicts the percent difference between the flood flows when the 1995 land-use is simulated versus the 2030 land-use. The average percent difference between all the model locations decreased as the return frequency flood increased from the 10-year to the 100-year flood. The difference between the simulation of the two land-use conditions caused a percent difference between the 10-year flood values of about 50%, which is highly significant. This information could be used to deduce that the simulation of the 2030 land-use condition would consistently produce higher flood flows across the watershed.

Table 48. Percent Difference between varying Land-Use Conditions

HSPF Model Location	Percent Difference between 1995 HSPF 90% PREC and 2030 HSPF 90% PREC			
	10-year	25-year	50-year	100-year
Reach 1 (Durbin)	33	38	34	28
Reach 2 (Julington)	43	40	35	29
Reach 5 (Julington)	41	24	30	20
Reach 6 (Big Davis)	69	41	31	31
Big Davis Gage Synth	59	56	40	34
Average	49	40	34	29

Finally, a comparison of each method was assessed. Each sub-basin was organized by reach location for an accurate comparison of results. The results in the Black Creek sub-basin were grouped by comparing all flood estimates at Reach 3 and the South Fork Gage grouped together, Reach 6 and the North Fork gage grouped together, and Reach 12 individually. The results in the Julington Creek sub-basin were assessed by comparing all the flood estimates at Reach 2 and 5 individually. The results in the Durbin Creek sub-basin were assessed by comparing all flood estimates in Reach 1. The results in the Big Davis Creek sub-basin were assessed by comparing all results in Reach 6 (Big Davis Creek). The real and synthetic Big Davis gage estimates were grouped together for comparison. The Big Davis Gage results were not combined with the Reach 6 results because Big Davis gage is not exclusive to Reach 6. As previously mentioned, the Big Davis gage was used to calibrate Julington Creek, Durbin Creek, and Big Davis Creek. Therefore, it is believed that the flood estimates obtained from the real and synthetic Big Davis gage should be compared separately of Reach 6. The results in the Ortega River sub-basin were assessed by comparing all flood estimates at Reach 3 individually, comparing the real and synthetic gage results at the 103rd St. Gage grouped together, and the synthetic Kirwin Rd. gage results separately. Lastly, the results in the Pablo Creek sub-basin were compared by grouping Reach 8 and the real gage together. Appendix F contains plots of each sub-basins' comparable reach location results mentioned above. As previously mentioned, there are instances where the years of record at the gaged location are higher than the years of record at the synthetic gaged and reach locations. The results were compared to each other regardless of the years of record. It is well established that the flood estimates are most accurate when a long period of record exists. However, considering the variation between the years of record for the data sets analyzed in this research, separating the results by years of record and comparing results based on that constraint would have resulted in

fewer comparable locations. Therefore, the results were compared to each other regardless of the years of record at the appropriate comparable locations. The comparison plots depict the 10-, 25-, 50-, and 100-year return frequency flood on the x-axis and the estimated discharge in cubic feet per second on the y-axis. Each plot contains a legend, which outlines each method presented on the graph.

After plotting the results of each method assessed in each sub-basin's critical locations, the normal distribution was applied to the results. The normal distribution is characterized by a bell-shaped curve, which is obtained by computing the mean and standard deviation of the data set (Smantary and Sahoo, 2020). The normal distribution bell curves portray how variable and dispersed the data sets are. Appendix G contains the normal distribution bell curves for each sub-basin. The bell curves were creating by obtaining the mean and standard deviation for each data set. Three standard deviations were added to and subtracted from the mean. They were assessed in 0.1 increments for a smoother curve. Therefore, the x-axis represents ± 3 standard deviations from the mean in 0.1 increments. The y-axis represents the probability that a number falls at or above a given value of the normal distribution (Kyd, 2006). The Microsoft Excel NORMDIST(x, mean, standard_dev, cumulative) function was used where "x" is the value of interest, "mean" is the average of the distribution, "standard_dev" is the standard deviation of the distribution, and a cumulate input of "FALSE" returns the probability that "x" will occur (Kyd, 2006). Because the standard deviation of the flood estimates was so large for several locations, when three standard deviations were subtracted from the mean a negative number was obtained. Negative flood flows are evidently not possible, therefore, a question of the practicality of the normal distribution arises. Overall, the normal distribution bell curves portray a strong presence of a normal distribution in the flood frequency estimates.

Chapter 8 CONCLUSIONS AND RECOMMENDATIONS

This thesis presents a multi-method approach to flood frequency estimation. The 10-, 25-, 50-, and 100-year flood estimates were developed in Black Creek, Julington Creek, Durbin Creek, Big Davis Creek, Ortega River, and Pablo Creek sub-basins. The flood estimates were developed by modifying the St. John's River Water Management District's (SJRWMD) HSPF model, conducting statistical Log-Pearson Type III and Power Law calculations, and by analyzing the Federal Emergency Management Agency's (FEMA) Flood Insurance Studies (FIS). The results obtained from these methods were then compared to each other and statistically fit to a normal distribution.

This research benefits the basins that are experiencing rapid development and for those that are lacking existing data. In recent research conducted by Brody et al. (2007), coastal communities in Florida have been identified as increasingly vulnerable as flooding risks are growing. Brody et al. (2007) estimated that Florida suffered $2.5 billion in losses from 1990 to 2003 and they determined that Florida is ranked as the state with the highest risk for flooding. Duval and Clay county are high flood risk areas with one or more occurrences each year (Florida Division of Emergency Management, 2018). As seen in Table 49, the direct economic losses for buildings in Clay and Duval county are predicted to be as high as between $42M and $114M (Florida Division of Emergency Management, Appendix E, 2018). With this information in mind, it is evident that flooding in Duval and Clay county are predicted to be highly devastating not only to the economy but to communities and individuals. Therefore, the need for accurate flood modeling is crucial to the prediction of flood magnitudes – which ultimately defines the damages that communities should expect to foresee in the worst of scenarios.

Table 49. Direct Flood-Related Economic Losses in Clay and Duval County (FDEM, 2018)

Direct Economic Loss for Buildings, by County, by Return Period (in dollars)		
County	100-Year Flood	500-Year Flood
Clay	$25,311,000.00	$42,068,000.00
Duval	$59,076,000.00	$114,236,000.00

The modification of the SJRWMD's HSPF model produced mostly solid flood frequency estimates in the sub-basins of interest. The resulting peak flood flows in each model run typically occurred one to two days after the Target Date that was modified. However, the resulting peak flow occurred directly on the Target Date in several model runs. It is believed that when the peak flow occurred on the Target Date, the daily timestep of the model was potentially smoothing the peak to some degree. Since the original HSPF models were created by various individuals at the SJRWMD, there is a possibility that there are slight differences in modeling approaches between sub-basins. The Black Creek sub-basin naturally produces higher flow rates compared to the other basins that were studied. Because the Black Creek sub-basin contains naturally higher flow rates, the simulation of additional precipitation frequency values resulted in the model crashing consistently. An attempt at expanding the HSPF model capacity was made. However, it was unsuccessful. Suggestions by the SJRWMD were also taken into consideration to expand the model capacity but those were also unsuccessful. Like the observation made by Gebremariam et al. (2014), source-code modification for the HSPF model was challenging primarily because of lack of documentation related to code structure and subroutines. The most complete set of flood estimates obtained in the Black Creek sub-basin were the 10- to 50-year flood estimates using the 1995 land-use condition, median precipitation frequency values, uniform rainfall distribution, and antecedent moisture conditions. Simply attempting to simulate the 90^{th} percentile precipitation frequency values crashed the model on the 25-year flood frequency run. An attempt at running the 2030 land-use with additional precipitation values was not even executed because of the prior model crashes.

Additionally, the HSPF model runs were generally lower than the FEMA FIS estimates. Therefore, there is potential for additional research to be conducted regarding the expansion of the HSPF model's capability to simulate higher flood flows.

The model runs in the Julington Creek, Durbin Creek, and Big Davis Creek sub-basins produced satisfactory results. These land-use variation, variation of precipitation frequency values, and variation of rainfall distribution was assessed. Overall, the 2030 land-use paired with the 90th percentile precipitation frequency, uniform rainfall distribution, and antecedent moisture conditions produced the highest flood flows; however, these relatively high flood flow values were still lower than the adjusted FEMA FIS estimates for those locations. Although the 2030 land-use runs were successfully simulated in these basins and produced relatively high flood flows, because of the complications involved in running the 2030 land-use runs in the Black Creek sub-basin, the 1995 land-use became the default for the remainder of the sub-basins. It is also important to note that the mouth of Julington Creek is more strongly tidally influenced and could even be influenced by storm surge, which makes hydrologic modeling in those locations more challenging.

The Ortega River and Pablo Creek sub-basin HSPF models ran well. The 1995 land-use, 90th percentile precipitation frequency values, uniform distribution, and antecedent moisture conditions were considered in the model runs. However, it would be beneficial to assess the 2030 land-use condition paired with the 90th percentile precipitation frequency values and Type II Modified rainfall distribution for all sub-basins where it was not assessed. This combination of parameters yields the highest flood flows. Additionally, it is important to note that the ten chosen target dates, which received the simulation of precipitation frequency values, were selected from various seasons. The consideration of ten target dates from the wet season alone may have produced higher average flood flows due to the wetter starting conditions. Ortega River and Pablo Creek are also

more heavily tidally influenced at the mouth and could experience a greater deal of storm surge, which poses additional challenges to the hydrologic modeling process. Additionally, it was previously observed that the FEMA FIS drainage areas were usually larger than the drainage areas in the HSPF models. A possible reason for the difference in area is the consideration of tidal influence. The hydrologic HSPF models do not consider the tidal areas of each sub-basin. The tidal areas of the project locations were instead modeled in the hydrodynamic portion of the model (mentioned earlier in this thesis), which is not part of this research.

In a case study conducted by Ninov et al. (2008), the results of their HSPF modeling for flood assessment yielded flood flows that were 130% higher than the historical flood flows, while the modeled annual, seasonal, and low flows were approximately 25% to 33% less than the observed respectively. This case study provides a perspective on the variety of results that can be obtained with the use of the HSPF model. This is an interesting perspective to consider. The research of Ninov et al. (2008) produced flood flows that were too high while the results of the HSPF flood modeling presented in this research appears to be too low compared to FEMA FIS estimates. However, the results of the HSPF model simulations cannot be concretely proven and serve only as estimates.

The Log-Pearson Type III (LP3) statistical computations were successful. There trends found in the data were conclusive and expected. This was the expected outcome of the LP3 results as it is a common method for flood frequency estimation.

The Power Law (PL) statistical computations were mostly successful. The PL derived flood estimates were typically much higher than the LP3 results and the HSPF modeled results. The PL derived flood estimates were even higher than the adjusted FEMA FIS estimates at times. The PL distributions produced more reasonable estimates for the 10- and 25-year flood estimates. The PL

distribution seemed to massively overestimate the 50- and 100-year flood flows. The PL was selected because of the praise it received in various research studies for being a simple and effective method. However, there was certainly a caveat that the PL performs best with a larger data set (Kidson and Richards, 2005). Therefore, it can be deduced that the 34- to 44-year data sets obtained from the HSPF model were not adequately large enough. Although there were two data sets (USGS North Fork Gage and USGS South Fork Gage) that contained 88 and 79 years of real data, the PL distribution seemed to overestimate the flood flows at those locations in comparison to the FEMA FIS. The difference in computing the PL distribution regression coefficients using the Linear Regression model and Nonlinear Regression model also produced varying results. It was evident that the data sets were better suited for one method over the other in certain cases.

The use of the FEMA FIS estimates proved to be an asset as the estimates were derived by qualified professionals. There is a degree of validity in comparing the methodologies assessed in this research to the FEMA FIS estimates. However, it has also been established that the FEMA FIS estimates were all obtained using varying methods. This raises a question regarding the consistency of the FEMA FIS estimates. It was evident in this research that different methodologies can at times produce widely varying flood flows. As previously established, the FEMA FIS estimates are either based on hydrologic modeling or statistical estimates. Research conducted by Okoli et al. (2019), compared statistical and hydrological methods for the estimation of design floods based on 10,000 years of synthetically generated weather and discharge data. Although their hydrologic modeling did not reflect any real applications and was intended as a baseline for discussion for comparison of results, their ultimate findings suggest that more than one flood estimate should be obtained and the maximum value (within reason) should be selected to minimize the likelihood of underestimating the design flood (Okoli, 2019). These findings are

in line with conclusions presented in this research thesis. The establishment of extreme flood estimates based on one methodology is outdated and involves higher risk in the development of planning measures for flood protection.

In addition to the several HSPF modeling recommendations proposed above, there are two more recommendations for further research. Firstly, it may be beneficial to consider a third statistical distribution in addition to the LP3 and PL distributions. This would aid in gaining additional understanding of the variety of flood estimates that may be obtained using different statistical distributions. As discussed in the previous section, normal distribution bell curves were created to understand the mean and standard deviation of the results of all the methods assessed in this research at each location of interest. A second recommendation for further research involves the implementation of a different statistical distribution to effectively compare the results of this research. Although the implementation of the normal distribution resulted in a mostly reasonable set of bell curves, several bell curves depicted negative flood flows. Negative flood flows are physically impossible; however, they were present when computing ±3 standard deviations (a foundational step of the normal distribution) from the mean in certain locations. Therefore, it is recommended that a different distribution is assessed to compare the flood estimates obtained from the different flood flow estimation methods presented in this research. In a survey conducted by the World Meteorological Organization (1989), the Extreme Value Type 1 (EV1) and log-normal distributions are the most used for the analysis of extreme floods. The selection of the most appropriate statistical distribution for flood frequency analysis is frequently a challenging task and the decision is frequently subjective or historical (World Meteorological Organization, 1989). Therefore, it can be concluded that there is no true correct distribution. There is only the best fitting distribution that is often discovered through trial and error.

In conclusion, this research has developed a new methodology for producing flood estimates. The modification of the St. Johns River Water Management District's HSPF model to estimate flood estimates is a brand-new methodology. Several of the HSPF models need to be expanded for sub-basins where the extreme flood flows exceed the model flow capacity. However, reasonable flood estimates can still be obtained from this new methodology in every sub-basin belonging to the St. Johns River. Current existing flood flow estimates are typically established as a one-value estimate per return frequency as seen in the FEMA Flood Insurance Studies. Additionally, the selected methodologies from which their (FEMA FIS) estimates were obtained are not always consistent. It is suggested that future extreme flood estimation procedures include the assessment of multiple methodologies to minimize the risk of underestimating design floods. This research is unique in producing a set of estimates for the 10-, 25-, 50-, and 100-year floods for the Black Creek, Julington Creek, Durbin Creek, Big Davis Creek, Ortega River, and Pablo Creek sub-basins based on hydrologic modeling, statistical analysis, and comparison to existing flood estimates.

FIGURES

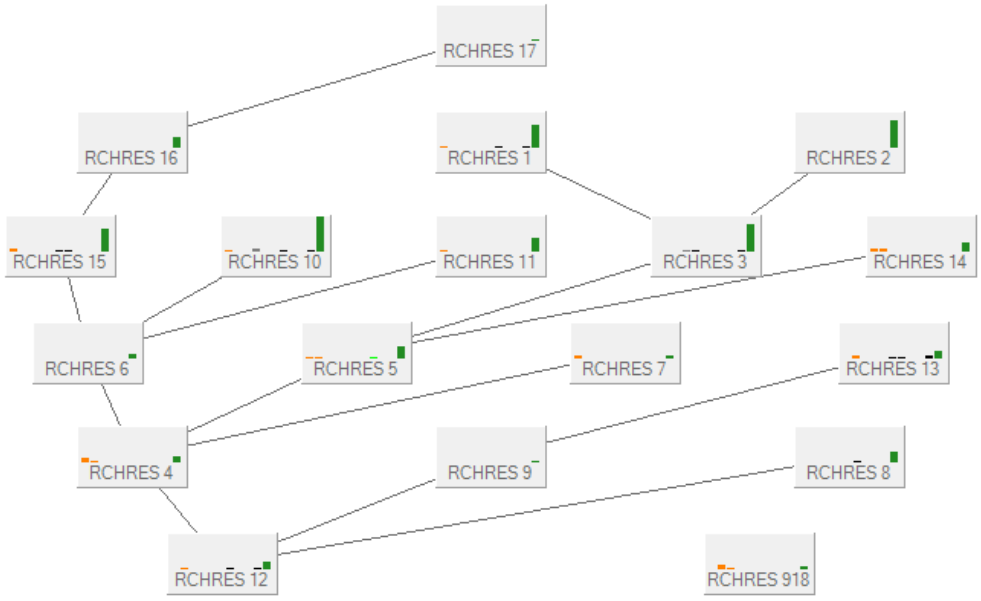

Figure 1. Black Creek HSPF Model View (USGS and EPA, 2012)

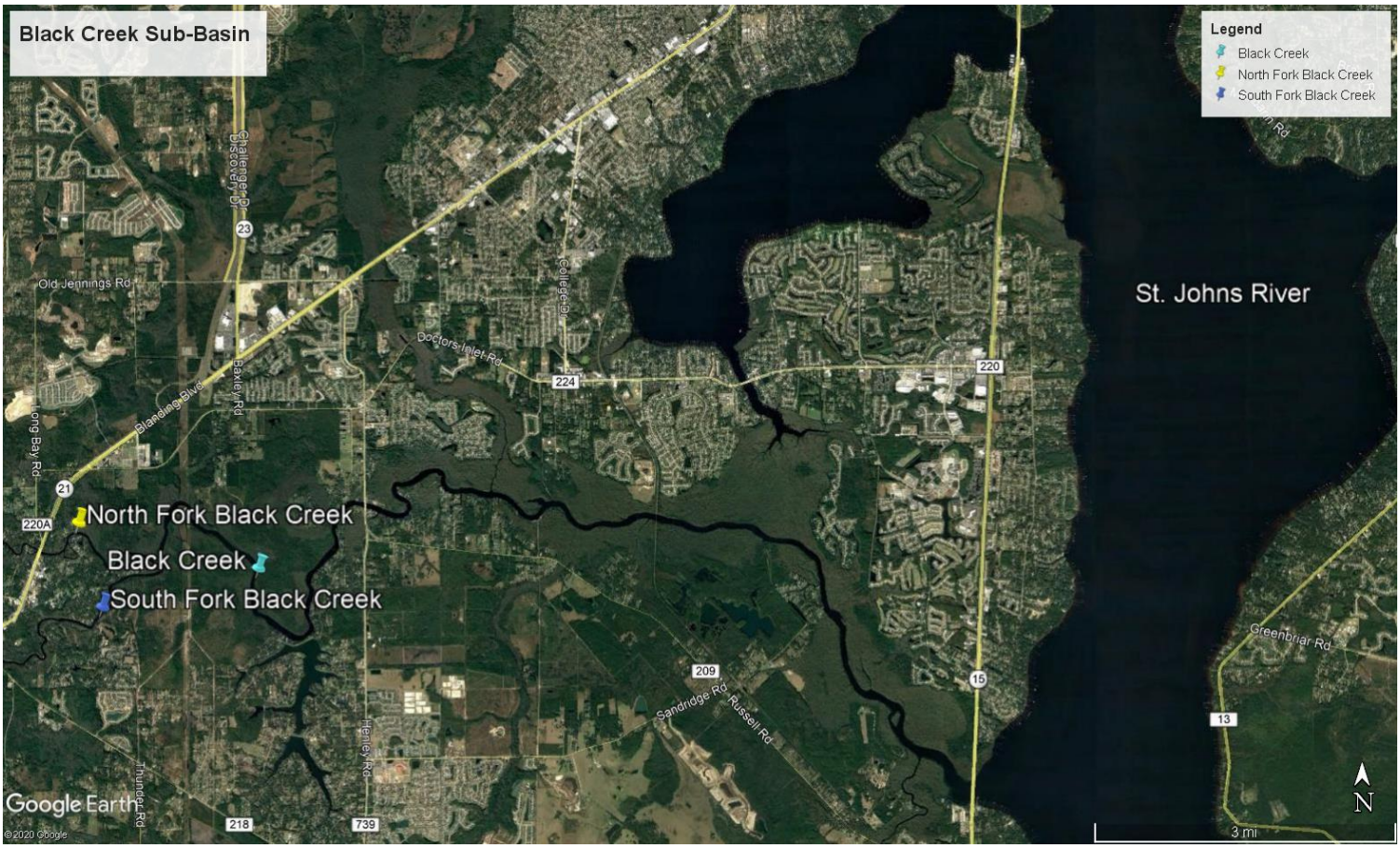

Figure 2. Black Creek Aerial Photo (Google Earth Pro, 2020)

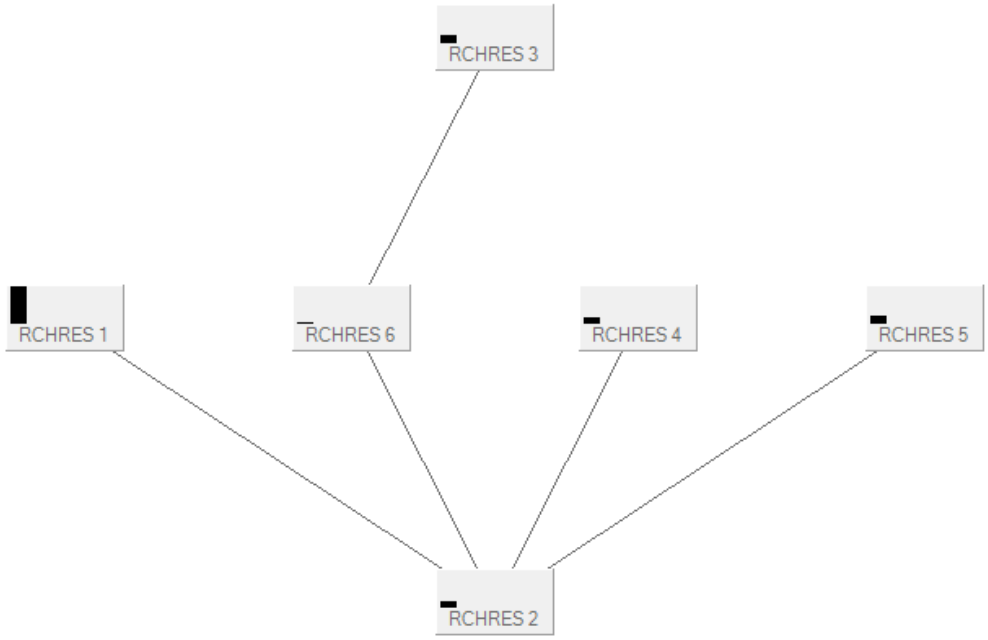

Figure 3. Julington Creek HSPF Model View (USGS and EPA, 2012)

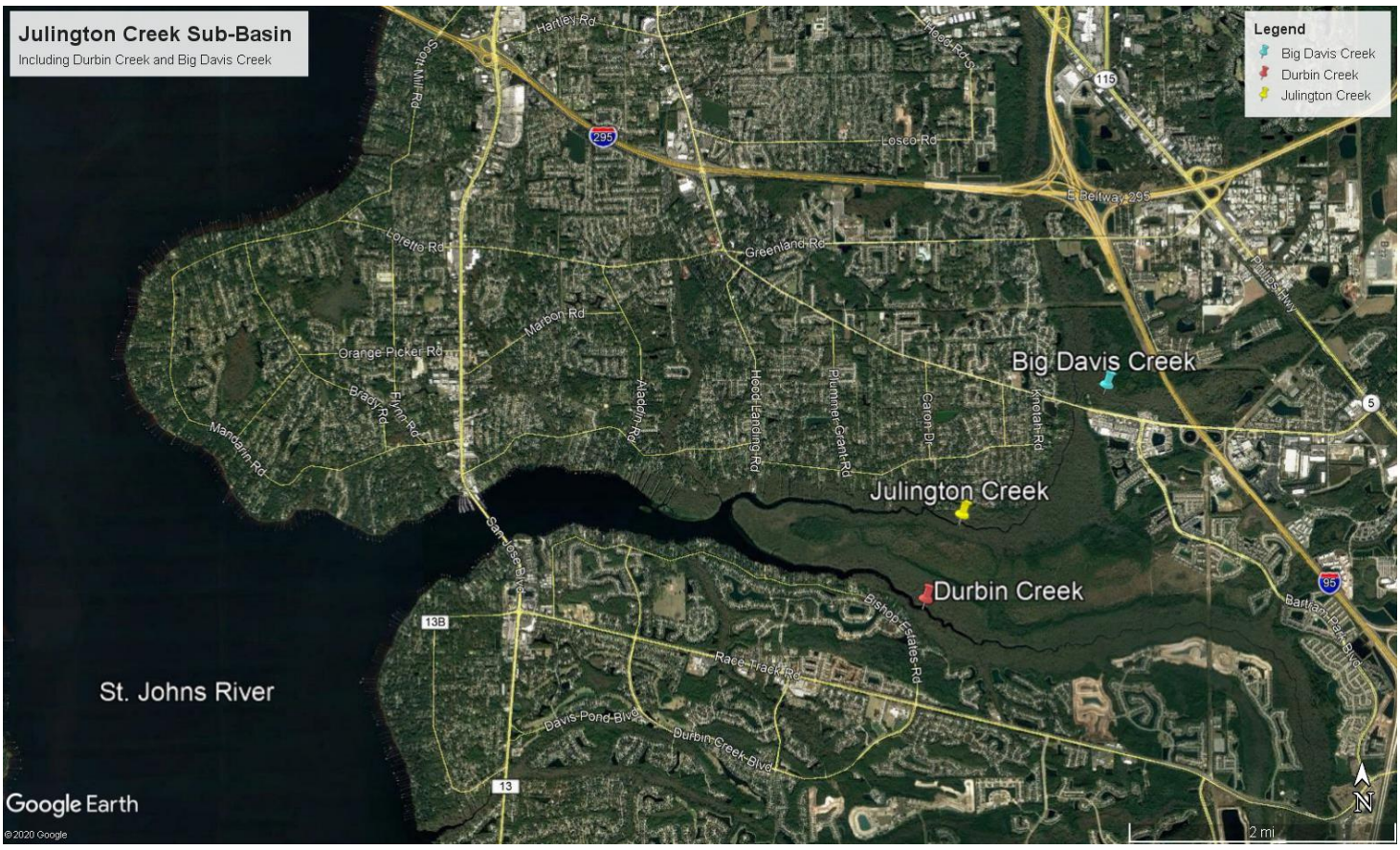

Figure 4. Julington Creek, Dubin Creek, Big Davis Creek Aerial Photo (Google Earth Pro, 2020)

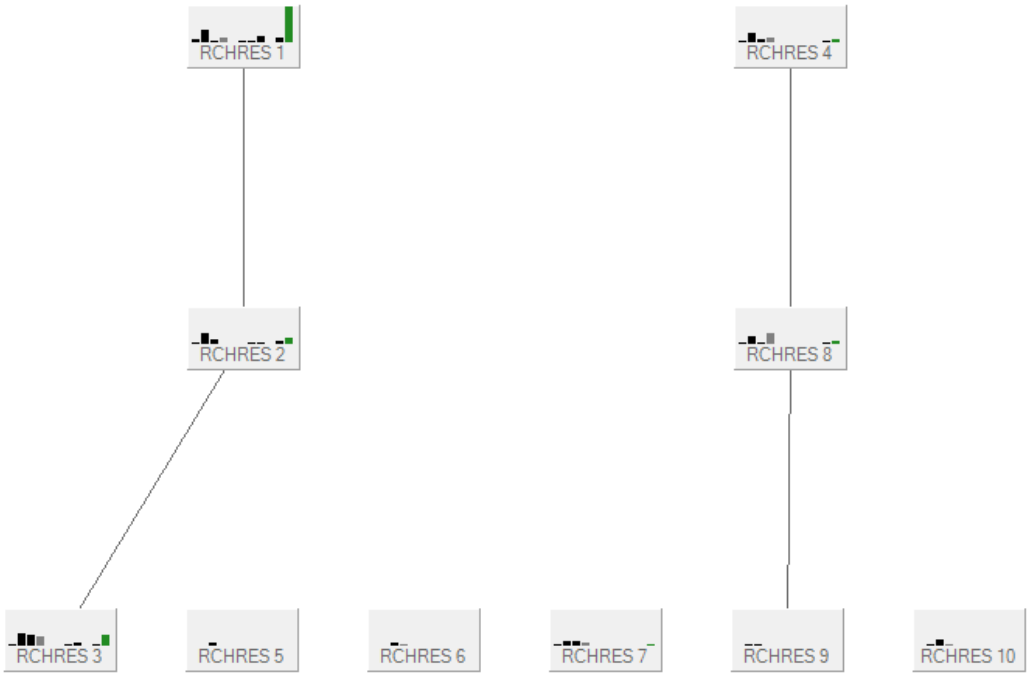

Figure 5. Ortega River HSPF Model View (USGS and EPA, 2012)

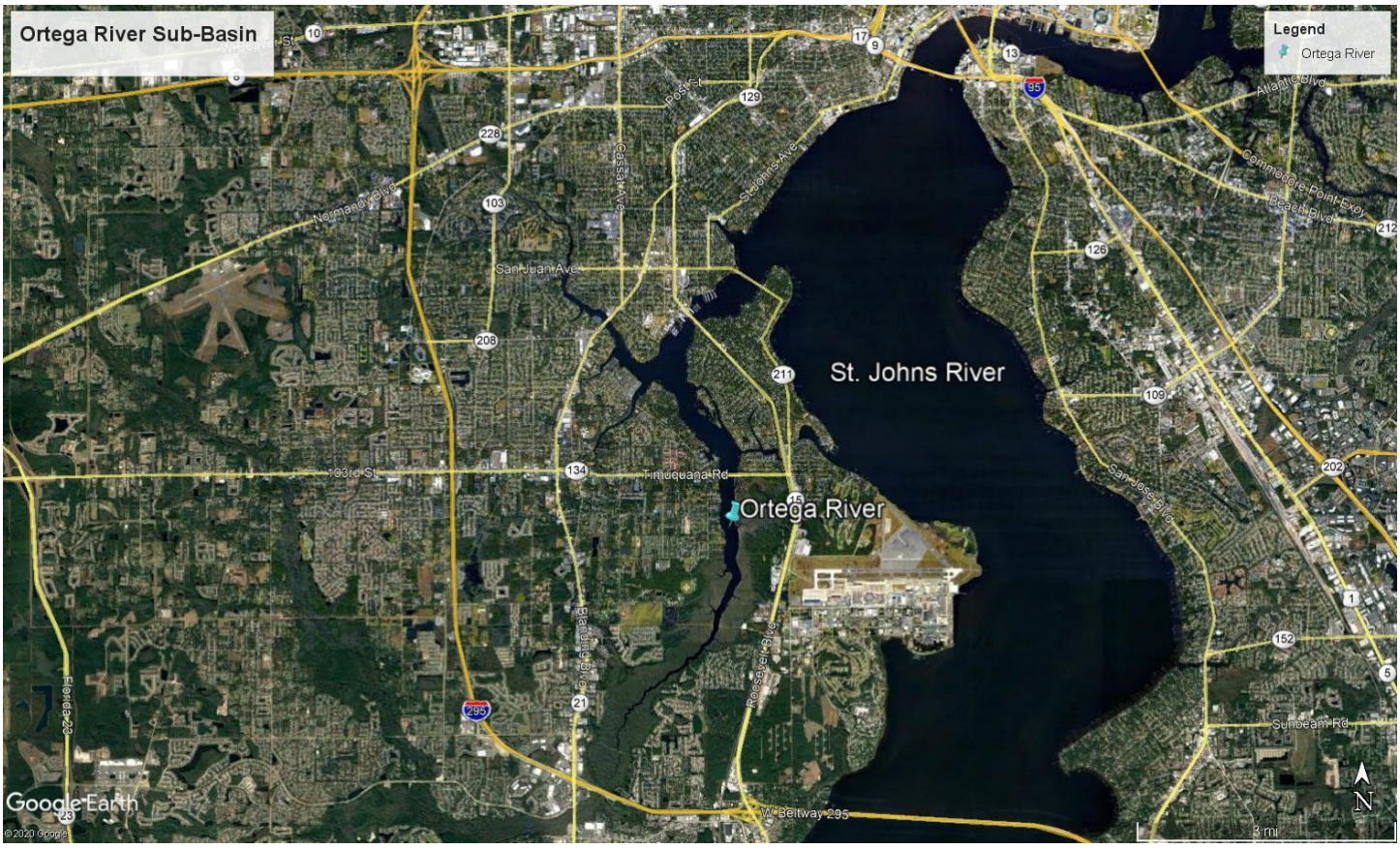

Figure 6. Ortega River Aerial Photo (Google Earth Pro, 2020)

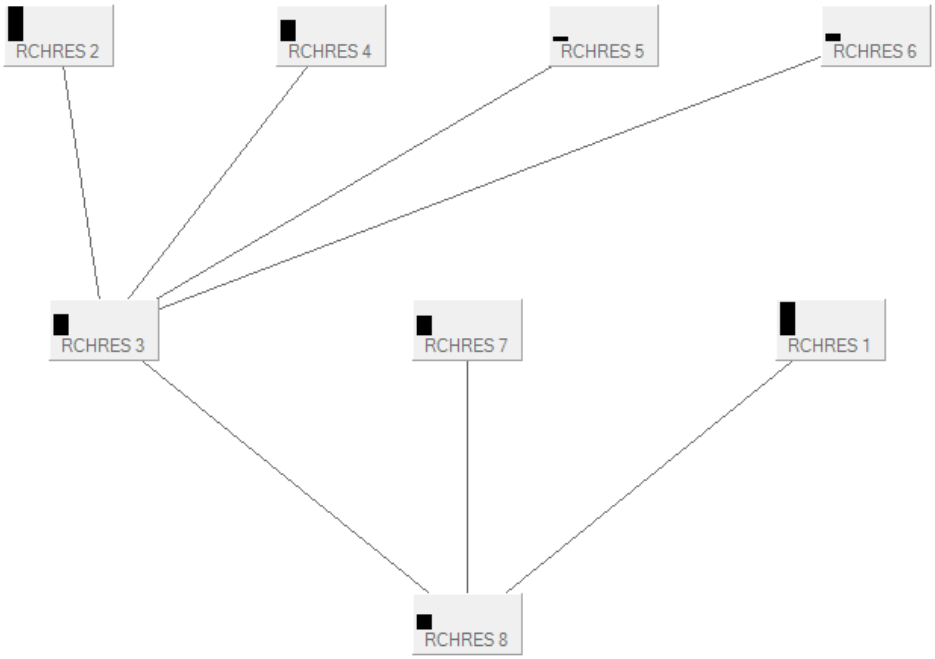

Figure 7. Pablo Creek HSPF Model View (USGS and EPA, 2012)

Figure 8. Pablo Creek Aerial Photo (Google Earth Pro, 2020)

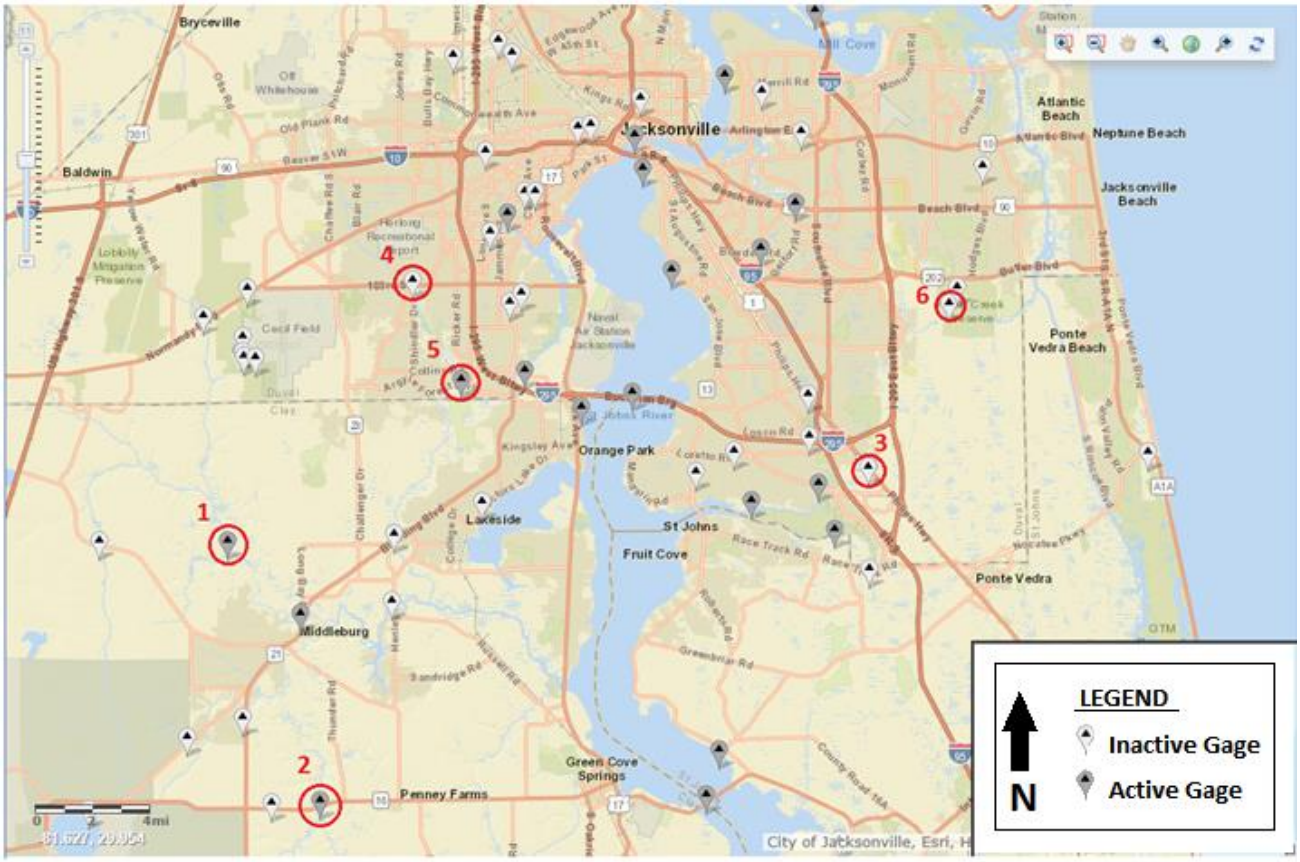

Figure 9. Real USGS Gage Locations (USGS, National Water Information System: Mapper, 2020)

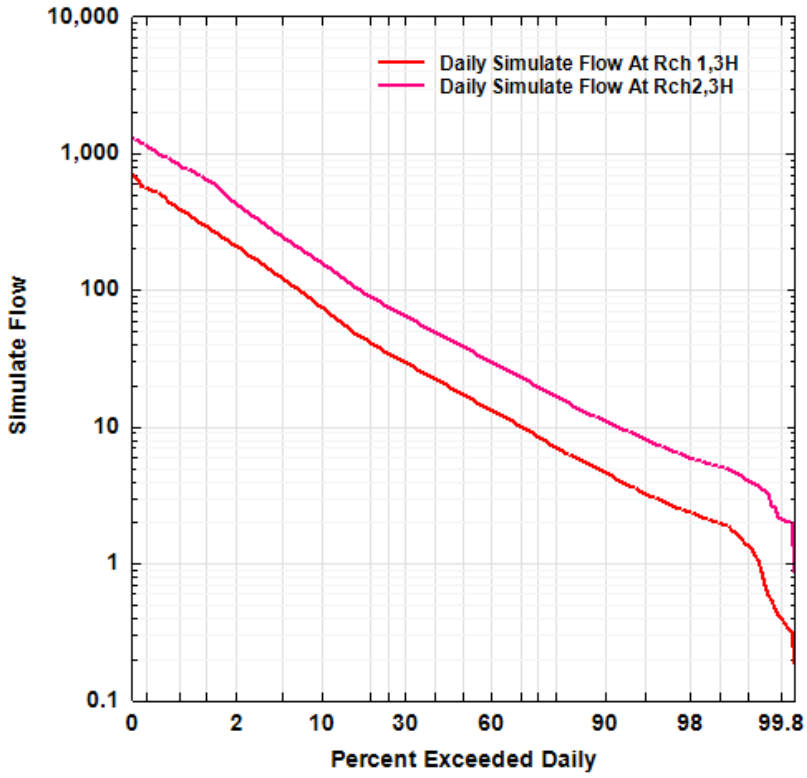

Figure 10. HSPF Return Frequency Curve (USGS and EPA, 2012)

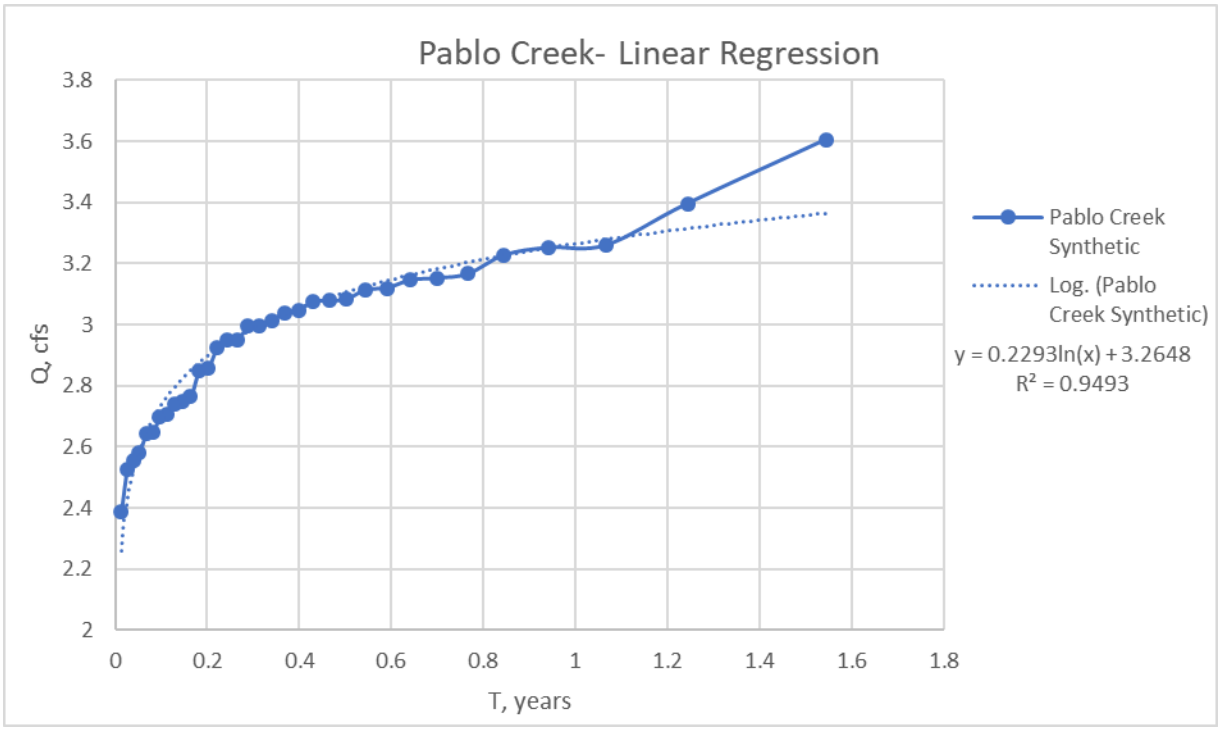

Figure 11. Pablo Creek Power Law Linear Regression

APPENDIX A

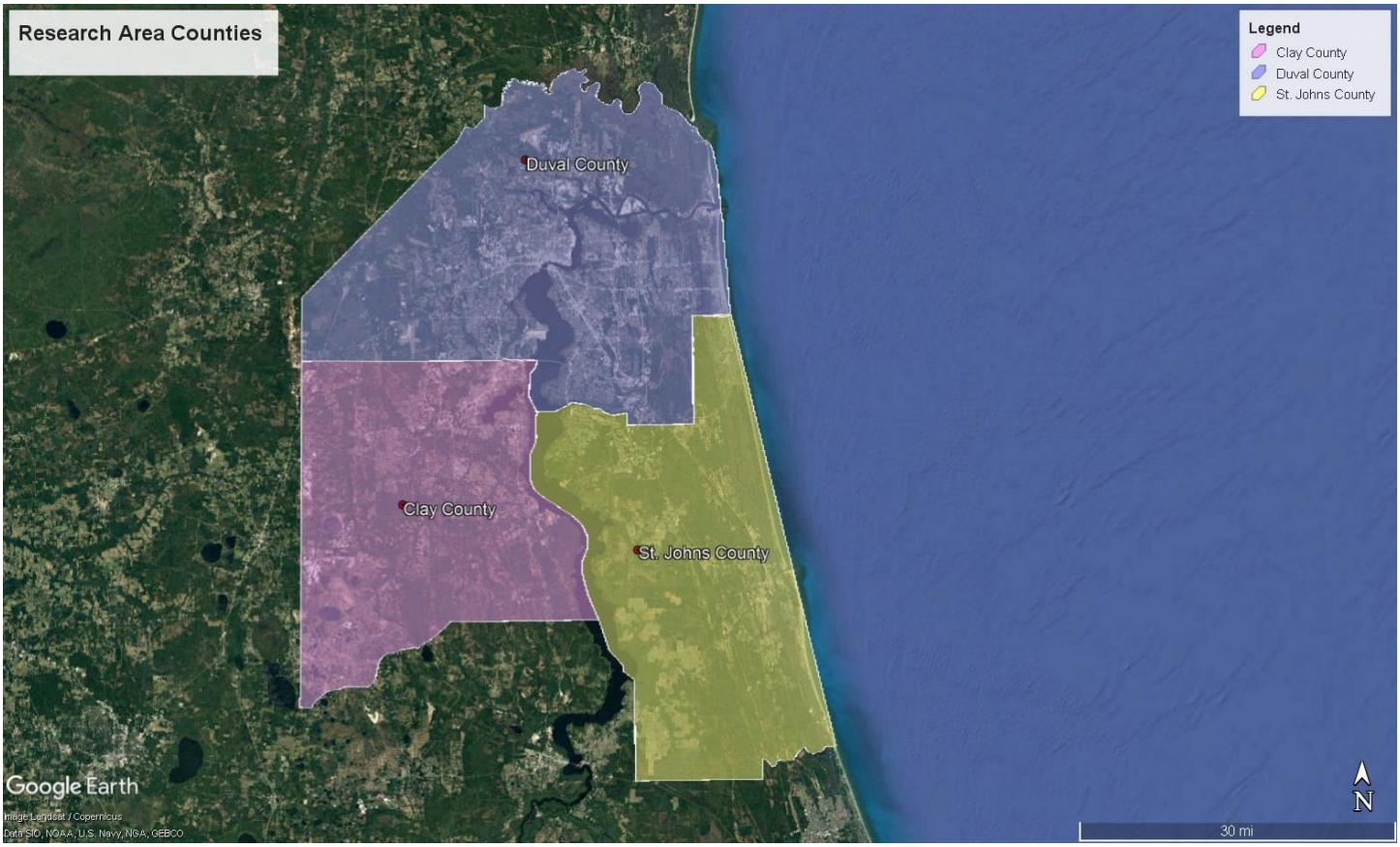

Source: Google Earth Pro (2020)

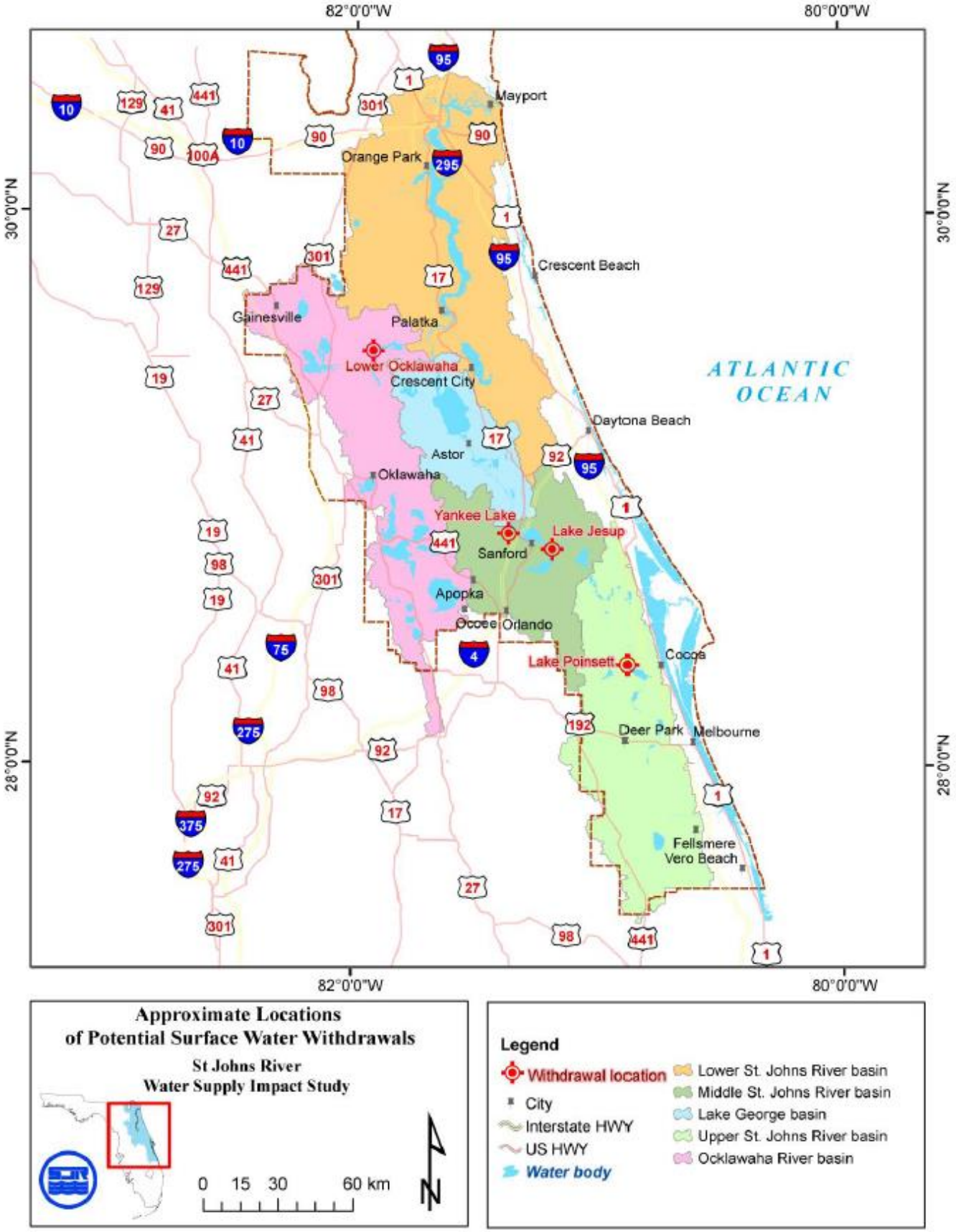

Source: Water Supply Impact Study (2012)

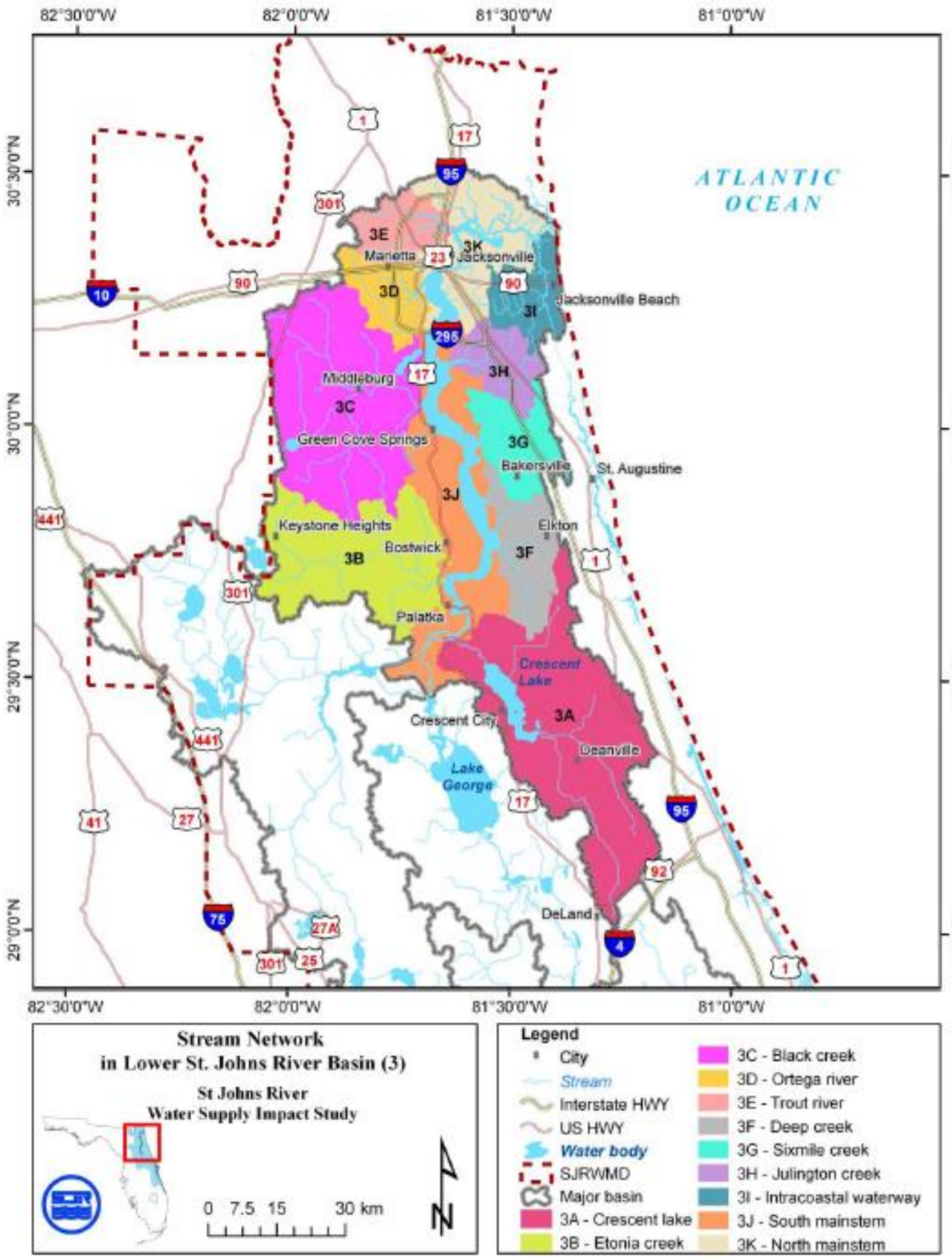

Source: Water Supply Impact Study (2012)

APPENDIX D

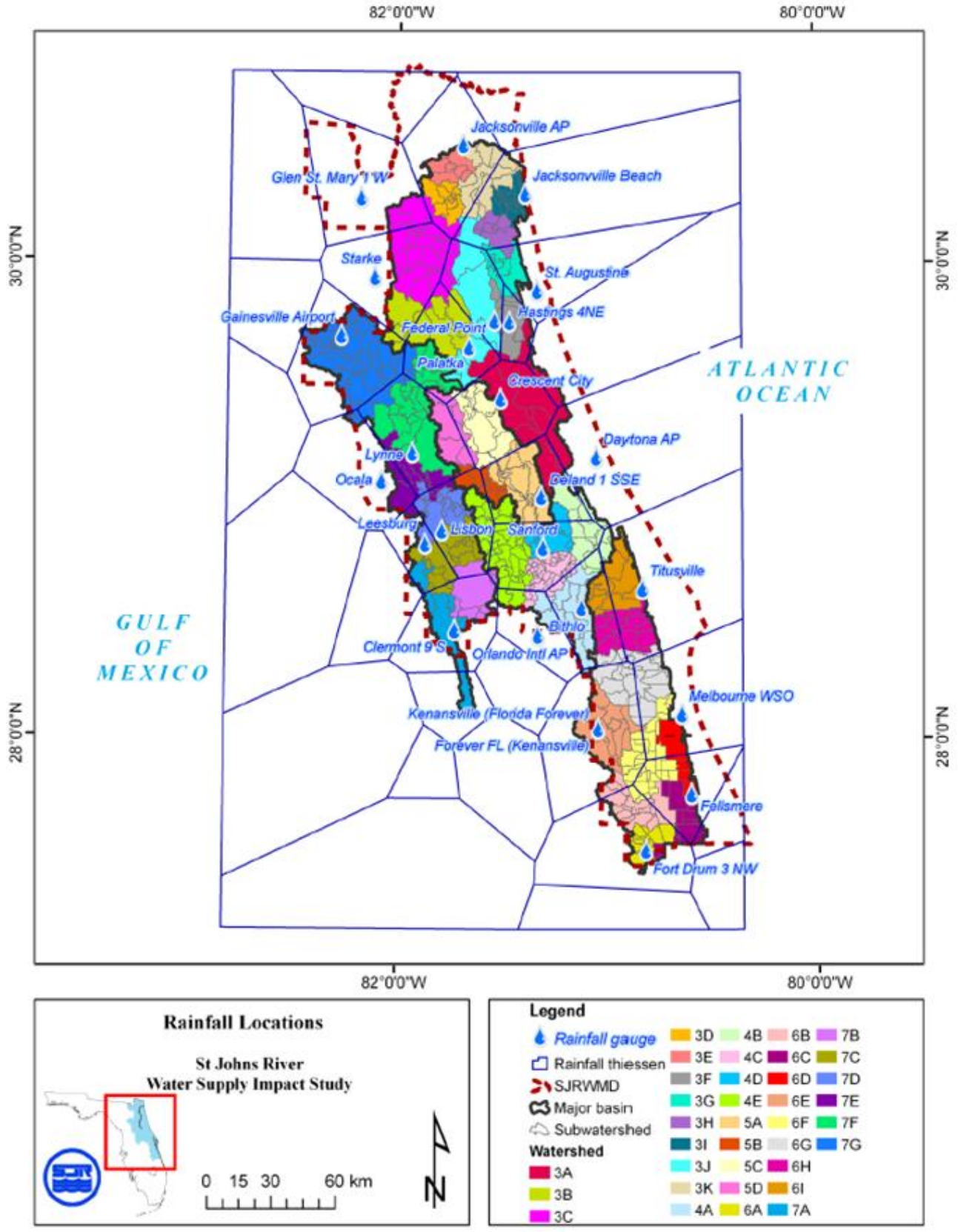

Source: Water Supply Impact Study (2012)

APPENDIX E

Time	Rainfall Ratio (Accumulated Total/ 24-hour Total)		
(Hours)	Type I (in.)	Type II (in.)	Modified Type II (in.)
0	0	0	0
0.5	0.008	0.005	0.006
1	0.017	0.011	0.012
1.5	0.026	0.017	0.018
2	0.035	0.022	0.025
2.5	0.045	0.029	0.032
3	0.055	0.035	0.039
3.5	0.065	0.042	0.046
4	0.076	0.048	0.054
4.5	0.087	0.056	0.062
5	0.099	0.064	0.071
5.5	0.122	0.072	0.08
6	0.125	0.08	0.089
6.5	0.14	0.09	0.099
7	0.156	0.1	0.11
7.5	0.174	0.11	0.122
8	0.194	0.12	0.135
8.5	0.219	0.134	0.149
9	0.254	0.147	0.164
9.5	0.303	0.163	0.181
10	0.515	0.181	0.201
10.5	0.583	0.204	0.226
11	0.624	0.235	0.258
11.5	0.654	0.283	0.307
12	0.682	0.663	0.606
12.5	0.705	0.735	0.718
13	0.727	0.772	0.757
13.5	0.748	0.799	0.785
14	0.767	0.82	0.807
14.5	0.784	0.835	0.826
15	0.8	0.85	0.842
15.5	0.816	0.865	0.857
16	0.83	0.88	0.87
16.5	0.844	0.889	0.882
17	0.857	0.898	0.893
17.5	0.87	0.907	0.903
18	0.882	0.916	0.913
18.5	0.893	0.925	0.922
19	0.905	0.934	0.931
19.5	0.916	0.943	0.939
20	0.926	0.952	0.947
20.5	0.936	0.958	0.955
21	0.946	0.964	0.962
21.5	0.955	0.97	0.969
22	0.965	0.976	0.976
22.5	0.974	0.982	0.983
23	0.983	0.988	0.989
23.5	0.992	0.994	0.995
24	1	1	1

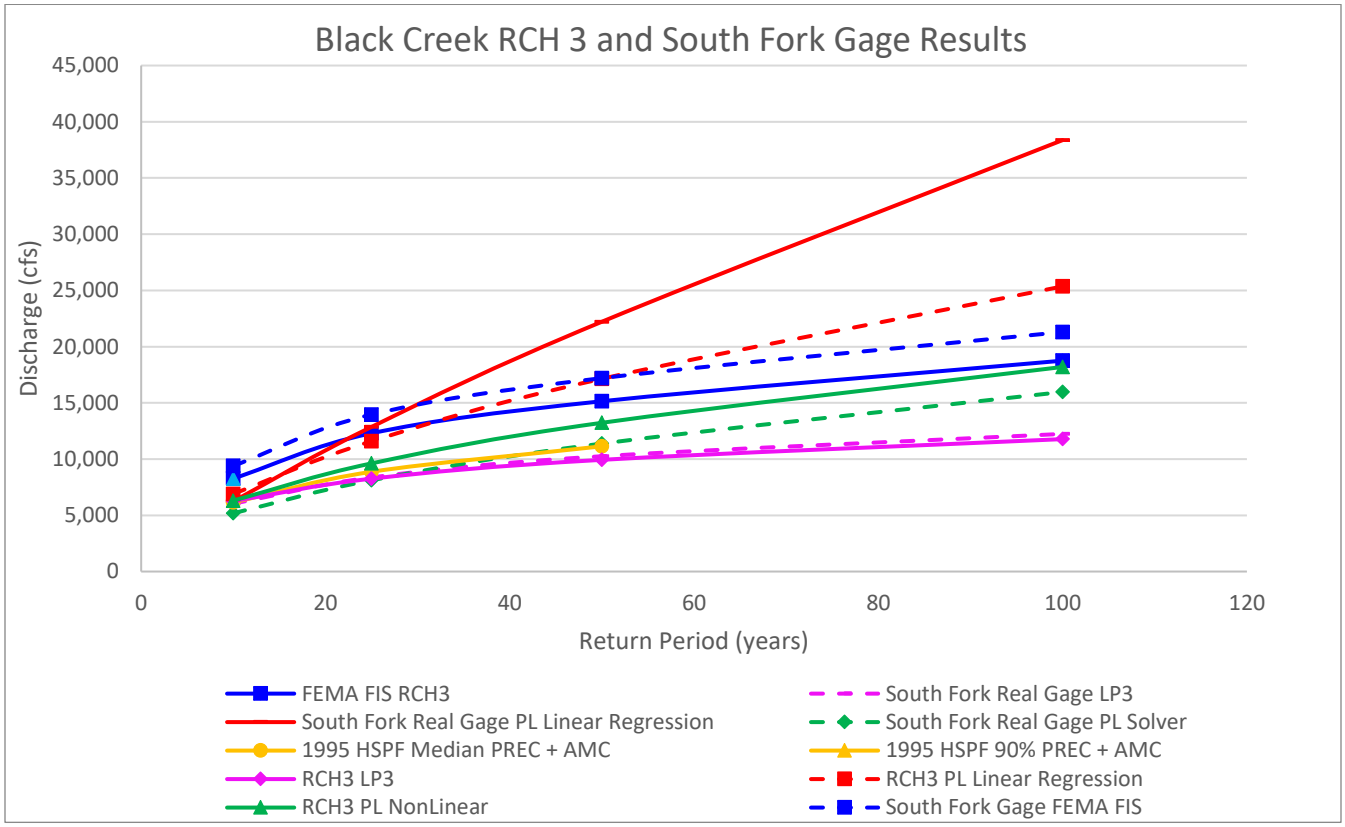
Black Creek RCH 3 and South Fork Gage Results
Discharge (cfs)
45,000
40,000
35,000
30,000
25,000
20,000
15,000
10,000
5,000
0
0
20
40
60
80
100
120
Return Period (years)
FEMA FIS RCH3
South Fork Real Gage LP3
South Fork Real Gage PL Linear Regression
South Fork Real Gage PL Solver
1995 HSPF Median PREC + AMC
1995 HSPF 90% PREC + AMC
RCH3 LP3
RCH3 PL Linear Regression
RCH3 PL NonLinear
South Fork Gage FEMA FIS

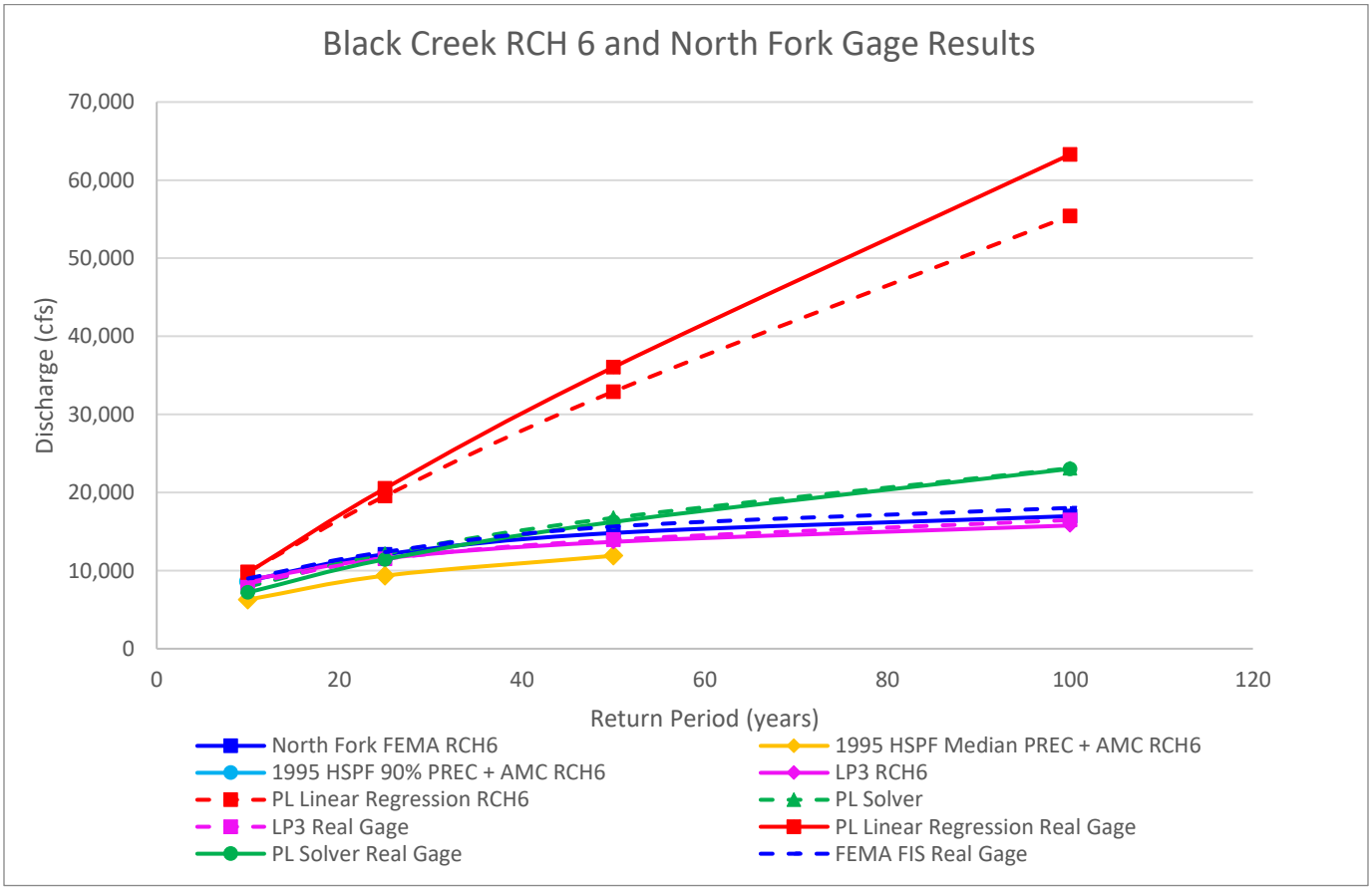
Black Creek RCH 6 and North Fork Gage Results
Discharge (cfs)
70,000
60,000
50,000
40,000
30,000
20,000
10,000
0
0
20
40
60
80
100
120
Return Period (years)
North Fork FEMA RCH6
1995 HSPF Median PREC + AMC RCH6
1995 HSPF 90% PREC + AMC RCH6
LP3 RCH6
PL Linear Regression RCH6
PL Solver
LP3 Real Gage
PL Linear Regression Real Gage
PL Solver Real Gage
FEMA FIS Real Gage

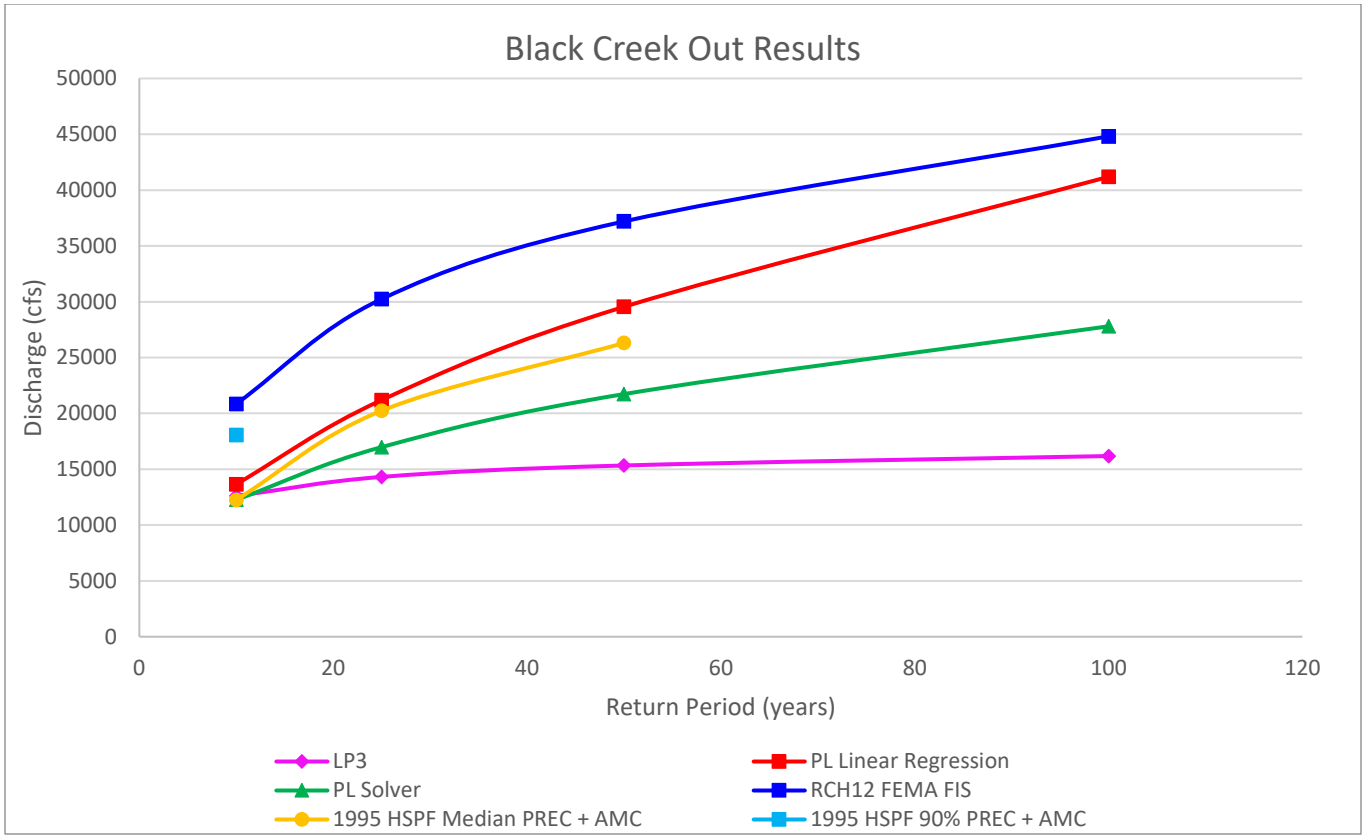
Black Creek Out Results
Discharge (cfs)
50000
45000
40000
35000
30000
25000
20000
15000
10000
5000
0
0
20
40
60
80
100
120
Return Period (years)
LP3
PL Linear Regression
PL Solver
RCH12 FEMA FIS
1995 HSPF Median PREC + AMC
1995 HSPF 90% PREC + AMC

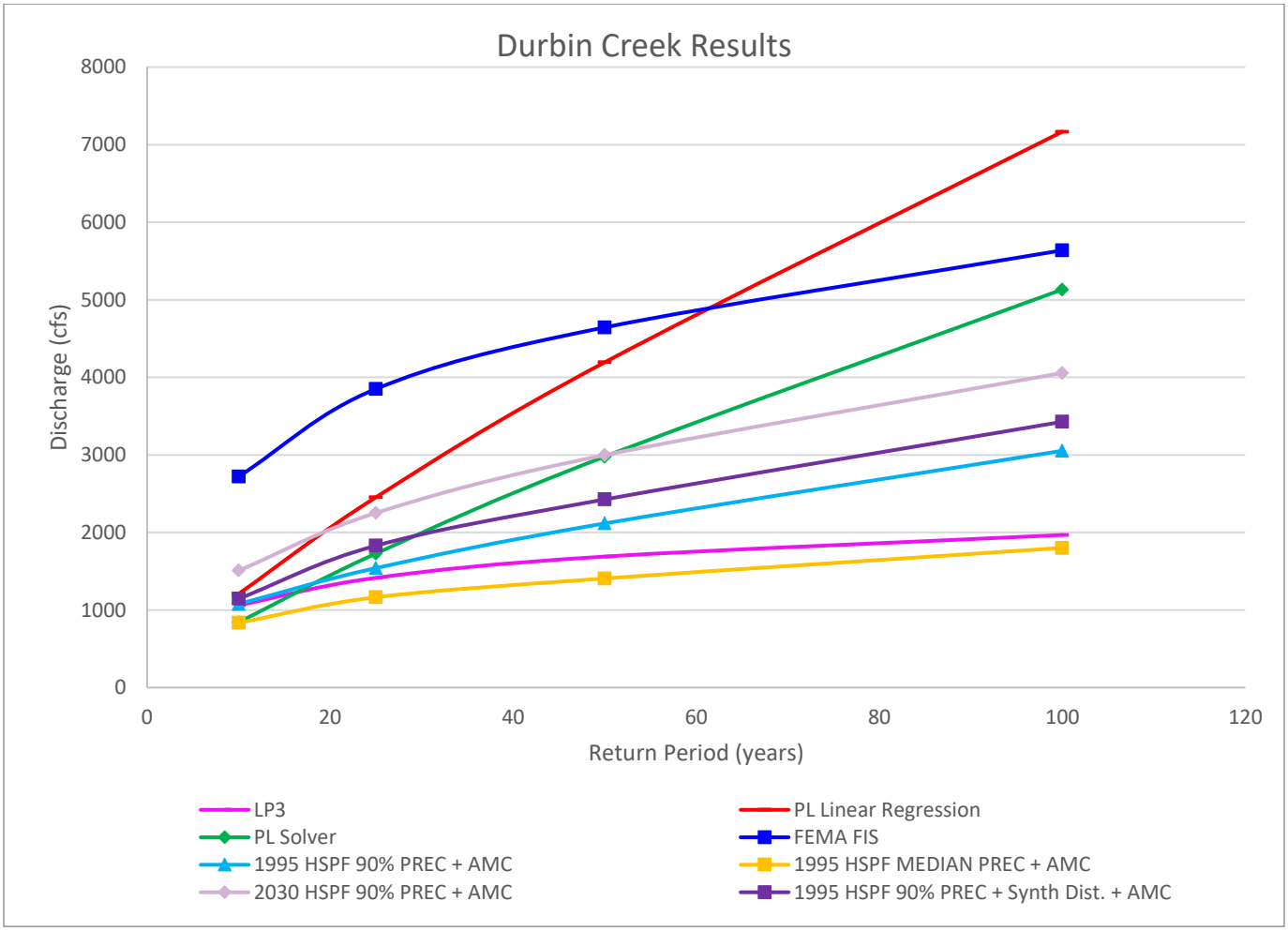
Durbin Creek Results
Discharge (cfs)
8000
7000
6000
5000
4000
3000
2000
1000
0
0
20
40
60
80
100
120
Return Period (years)
LP3
PL Linear Regression
PL Solver
FEMA FIS
1995 HSPF 90% PREC + AMC
1995 HSPF MEDIAN PREC + AMC
2030 HSPF 90% PREC + AMC
1995 HSPF 90% PREC + Synth Dist. + AMC

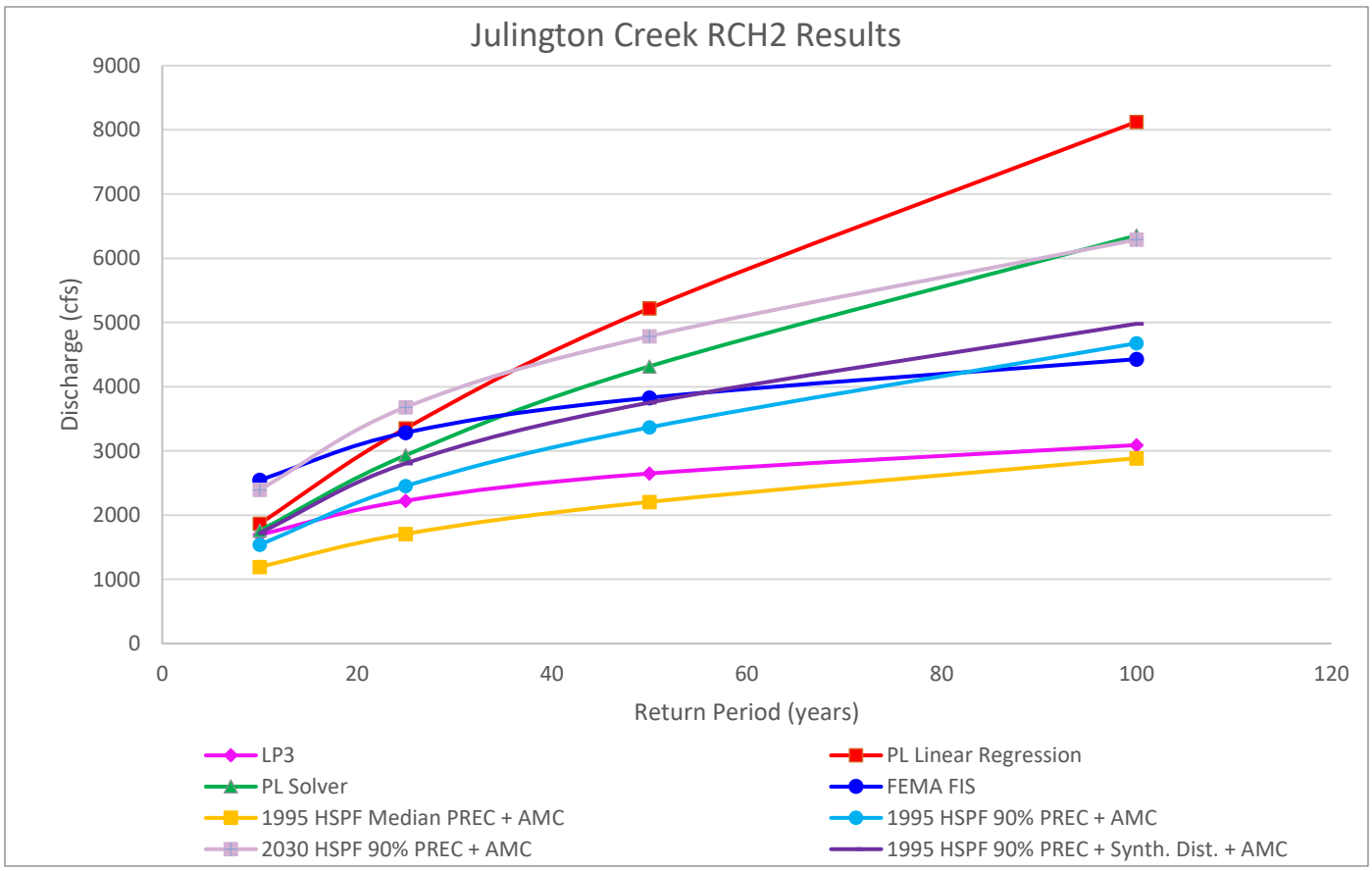
Julington Creek RCH2 Results
Discharge (cfs)
Return Period (years)
LP3
PL Linear Regression
PL Solver
FEMA FIS
1995 HSPF Median PREC + AMC
1995 HSPF 90% PREC + AMC
2030 HSPF 90% PREC + AMC
1995 HSPF 90% PREC + Synth. Dist. + AMC

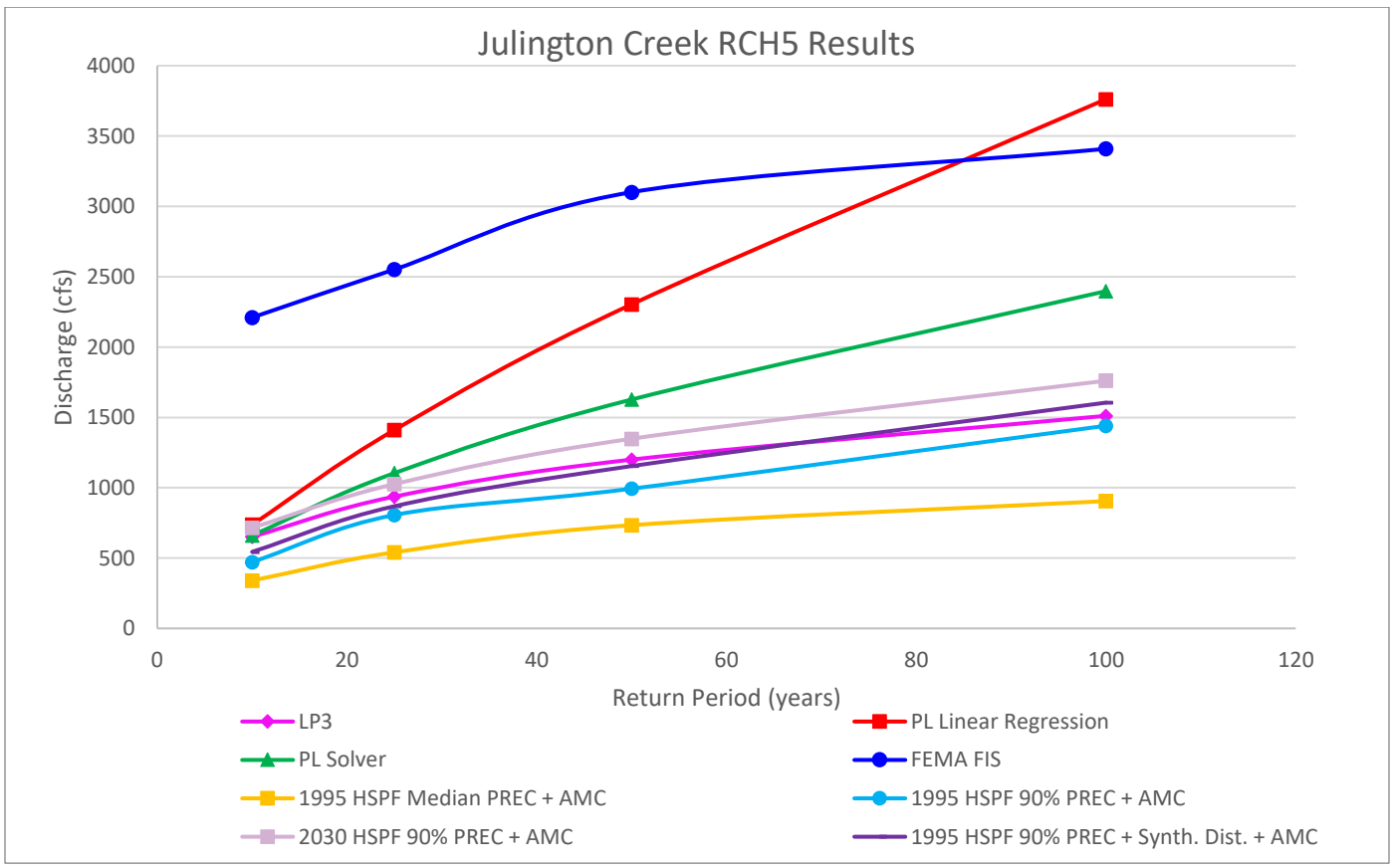
Julington Creek RCH5 Results
Discharge (cfs)
Return Period (years)
LP3
PL Linear Regression
PL Solver
FEMA FIS
1995 HSPF Median PREC + AMC
1995 HSPF 90% PREC + AMC
2030 HSPF 90% PREC + AMC
1995 HSPF 90% PREC + Synth. Dist. + AMC

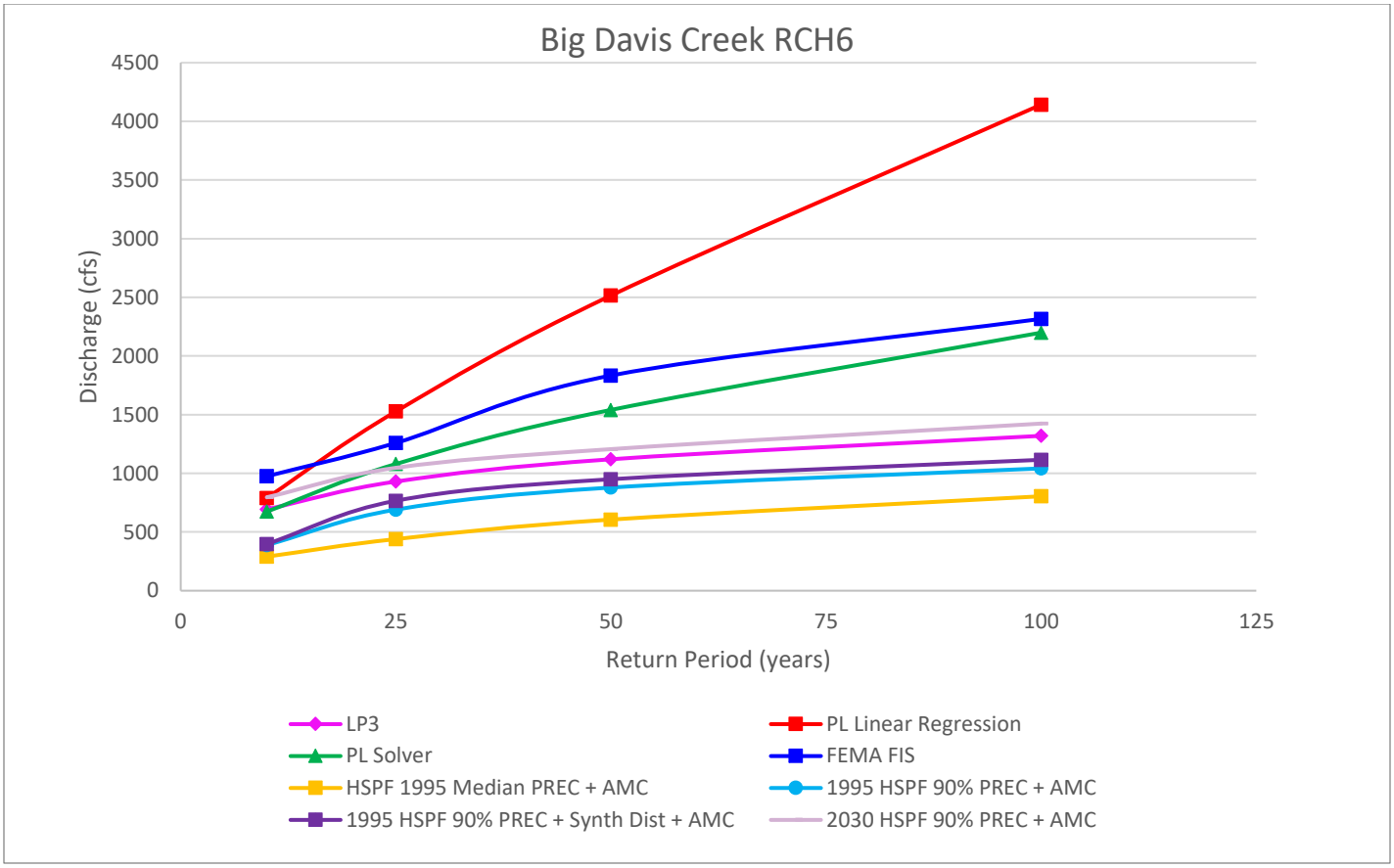
Big Davis Creek RCH6
Discharge (cfs)
4500
4000
3500
3000
2500
2000
1500
1000
500
0
0
25
50
75
100
125
Return Period (years)
LP3
PL Linear Regression
PL Solver
FEMA FIS
HSPF 1995 Median PREC + AMC
1995 HSPF 90% PREC + AMC
1995 HSPF 90% PREC + Synth Dist + AMC
2030 HSPF 90% PREC + AMC

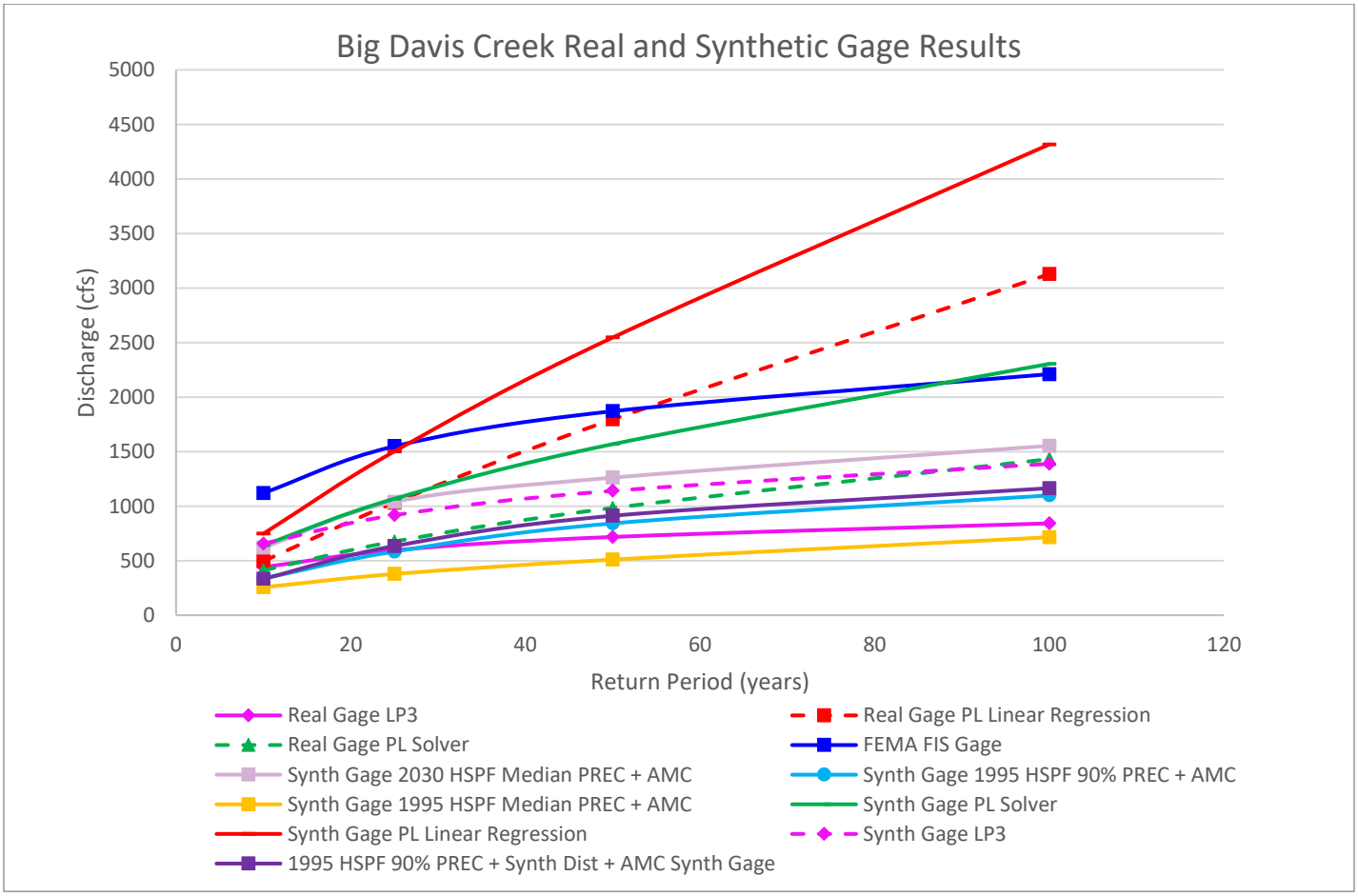
Big Davis Creek Real and Synthetic Gage Results
Discharge (cfs)
5000
4500
4000
3500
3000
2500
2000
1500
1000
500
0
0
20
40
60
80
100
120
Return Period (years)
Real Gage LP3
Real Gage PL Linear Regression
Real Gage PL Solver
FEMA FIS Gage
Synth Gage 2030 HSPF Median PREC + AMC
Synth Gage 1995 HSPF 90% PREC + AMC
Synth Gage 1995 HSPF Median PREC + AMC
Synth Gage PL Solver
Synth Gage PL Linear Regression
Synth Gage LP3
1995 HSPF 90% PREC + Synth Dist + AMC Synth Gage

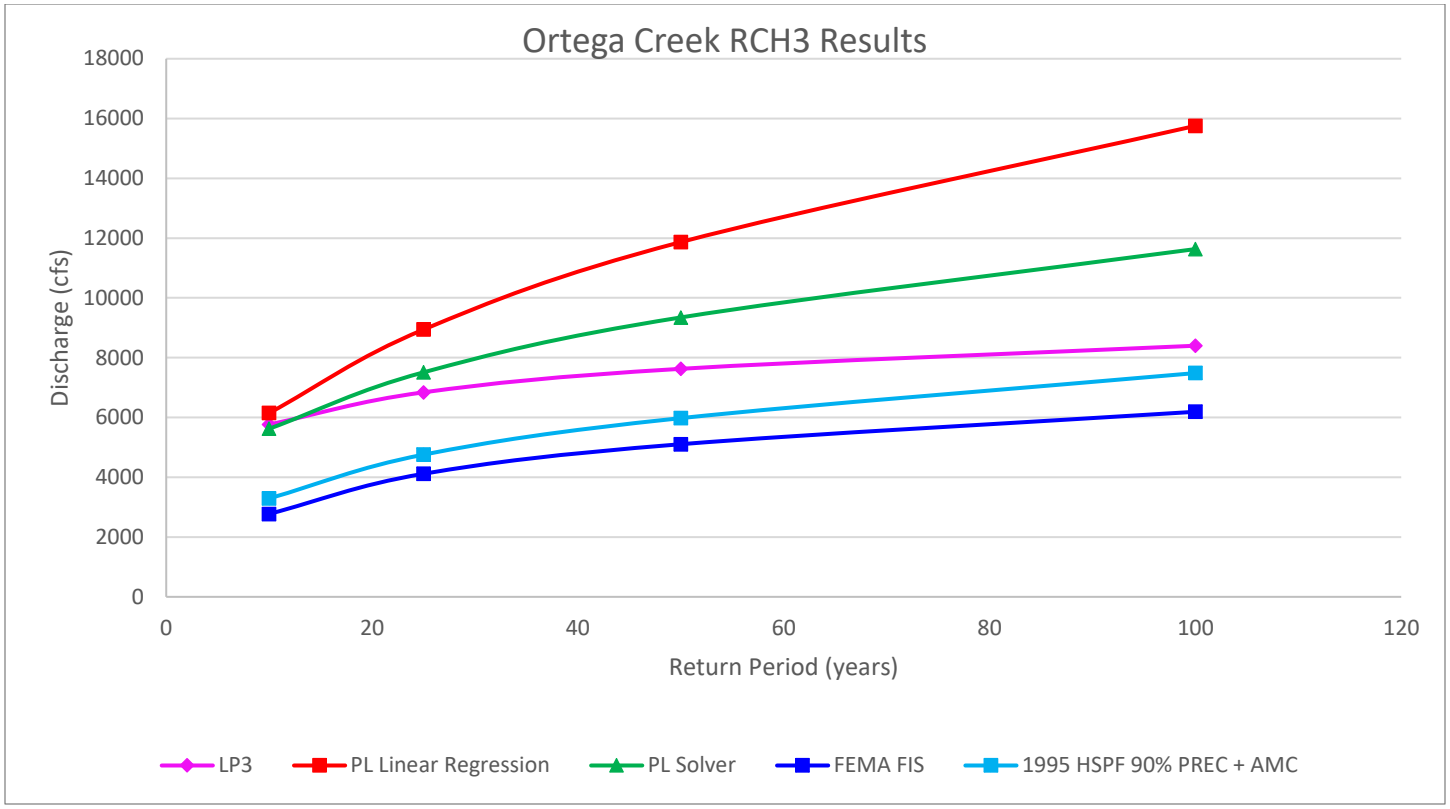
Ortega Creek RCH3 Results
Discharge (cfs)
18000
16000
14000
12000
10000
8000
6000
4000
2000
0
0
20
40
60
80
100
120
Return Period (years)
LP3
PL Linear Regression
PL Solver
FEMA FIS
1995 HSPF 90% PREC + AMC

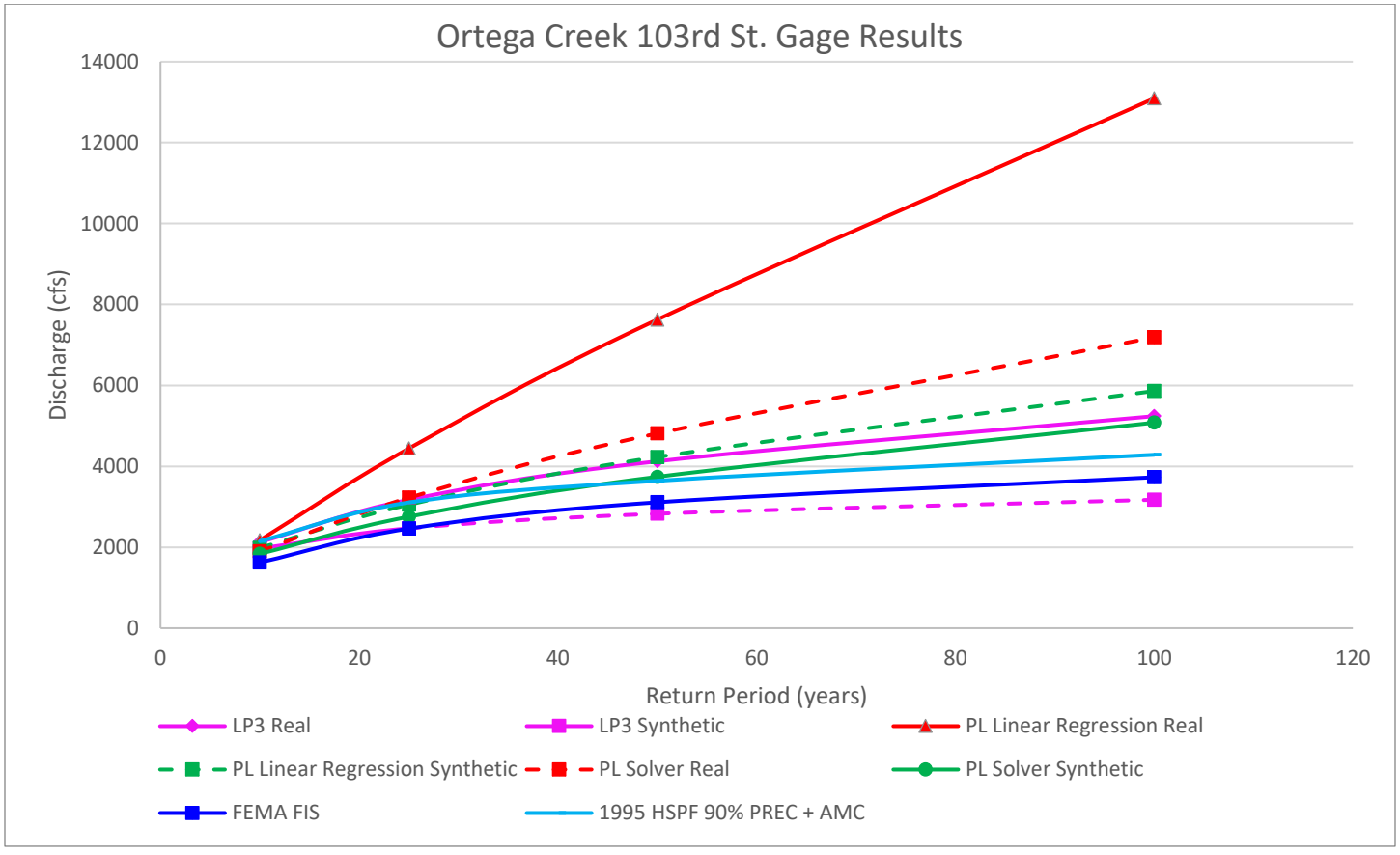
Ortega Creek 103rd St. Gage Results
Discharge (cfs)
14000
12000
10000
8000
6000
4000
2000
0
0
20
40
60
80
100
120
Return Period (years)
LP3 Real
LP3 Synthetic
PL Linear Regression Real
PL Linear Regression Synthetic
PL Solver Real
PL Solver Synthetic
FEMA FIS
1995 HSPF 90% PREC + AMC

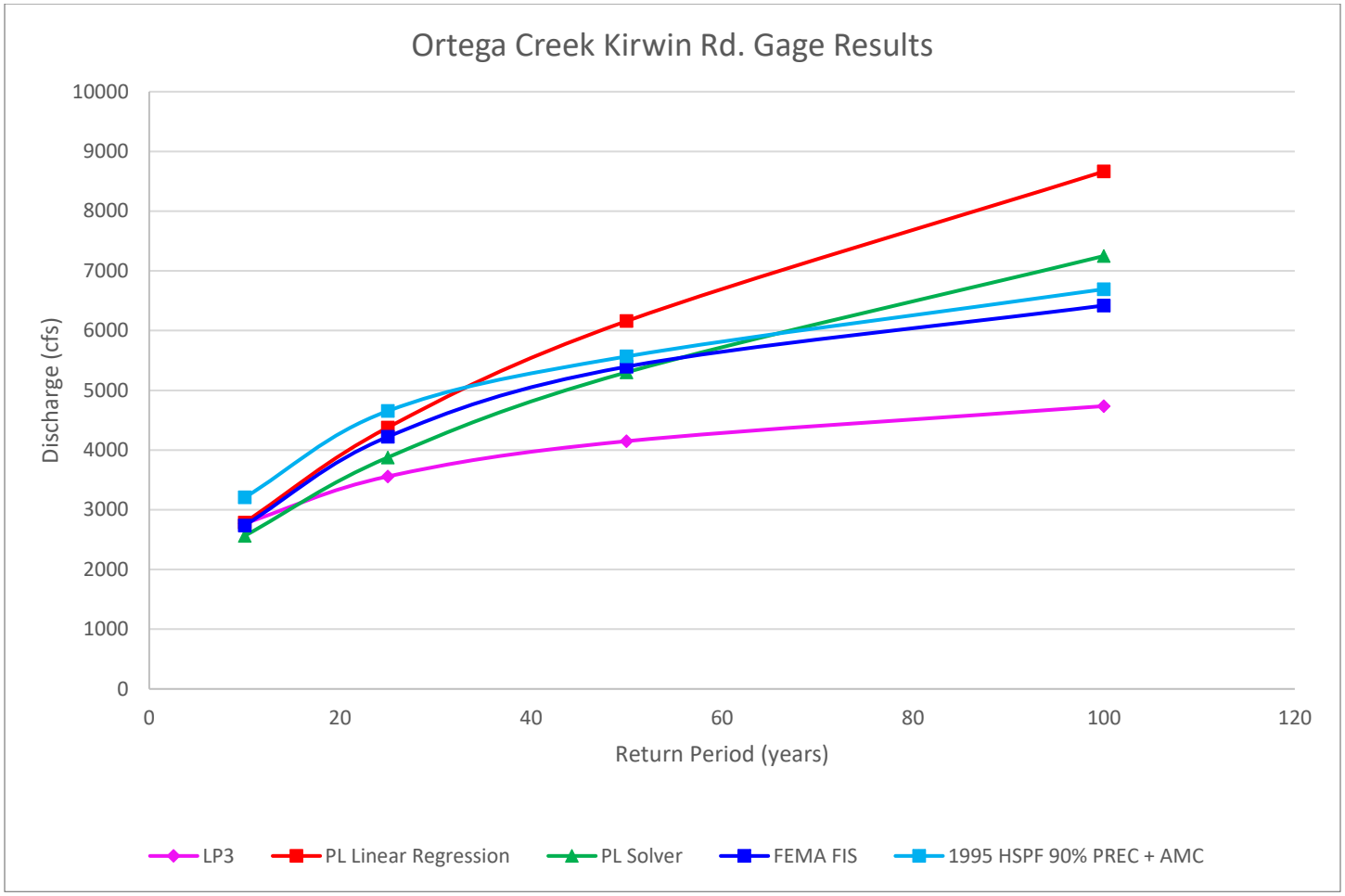
Ortega Creek Kirwin Rd. Gage Results
Discharge (cfs)
10000
9000
8000
7000
6000
5000
4000
3000
2000
1000
0
0
20
40
60
80
100
120
Return Period (years)
LP3
PL Linear Regression
PL Solver
FEMA FIS
1995 HSPF 90% PREC + AMC

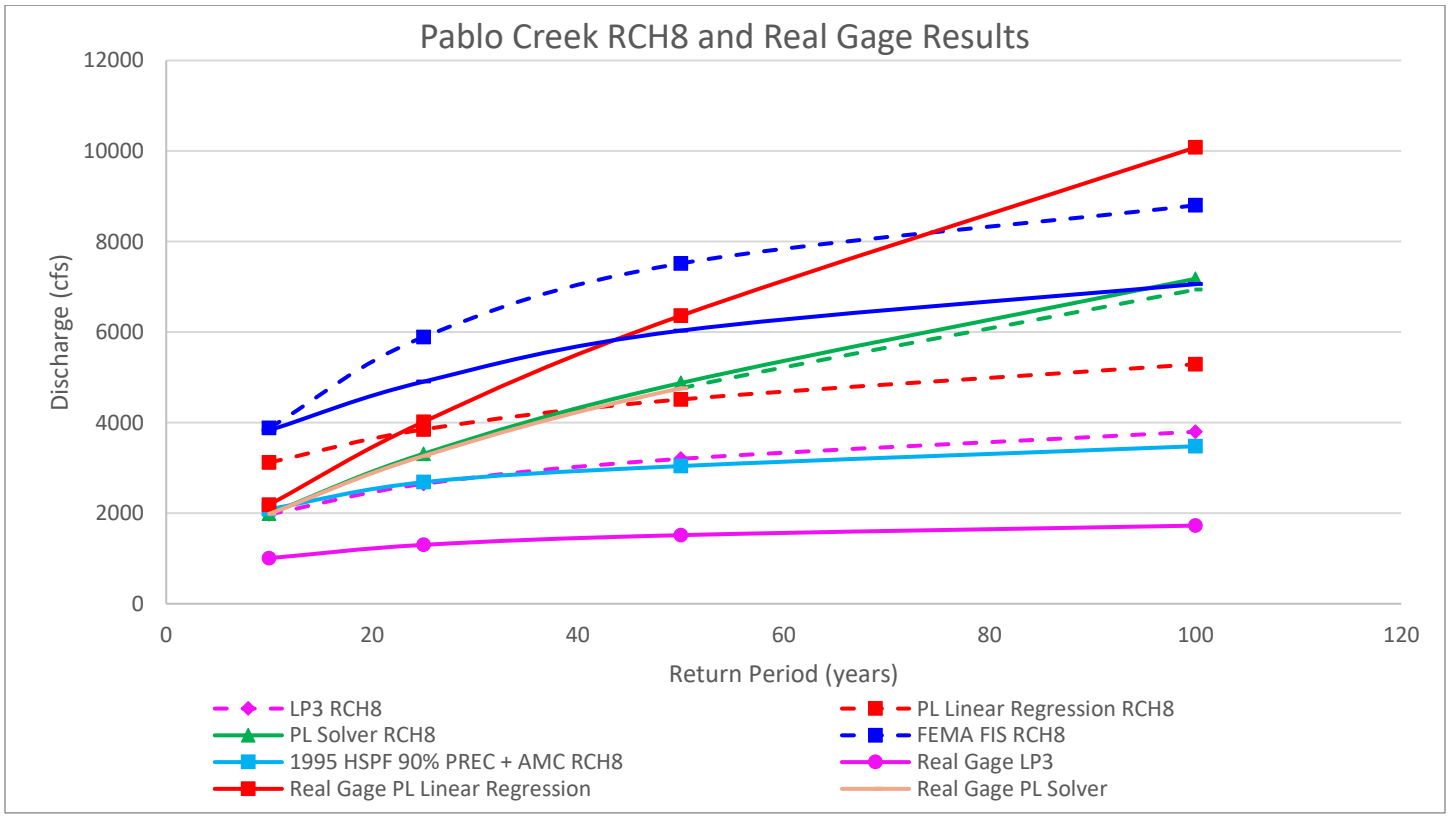
Pablo Creek RCH8 and Real Gage Results
Discharge (cfs)
12000
10000
8000
6000
4000
2000
0
0
20
40
60
80
100
120
Return Period (years)
LP3 RCH8
PL Linear Regression RCH8
PL Solver RCH8
FEMA FIS RCH8
1995 HSPF 90% PREC + AMC RCH8
Real Gage LP3
Real Gage PL Linear Regression
Real Gage PL Solver

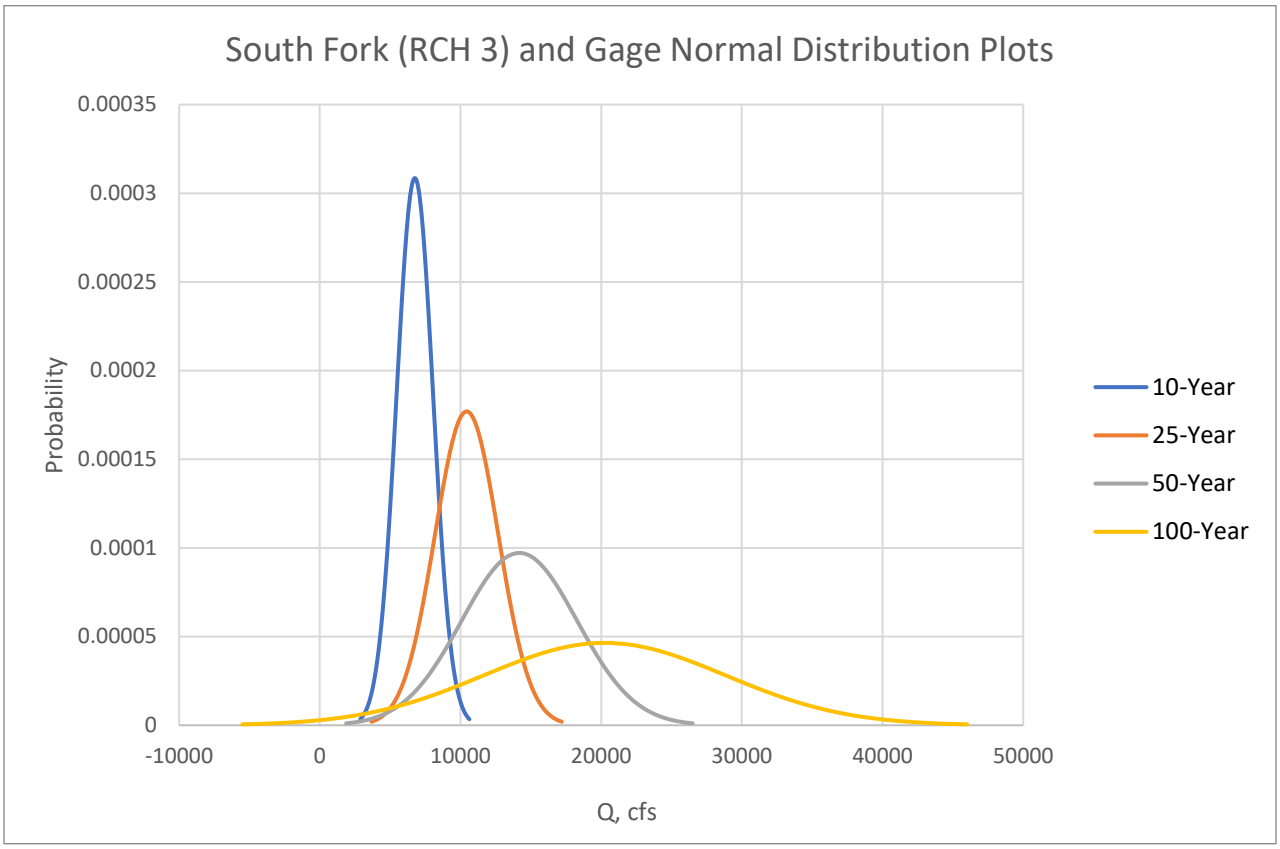
South Fork (RCH 3) and Gage Normal Distribution Plots
Probability
0.00035
0.0003
0.00025
0.0002
0.00015
0.0001
0.00005
0
-10000
0
10000
20000
30000
40000
50000
Q, cfs
10-Year
25-Year
50-Year
100-Year

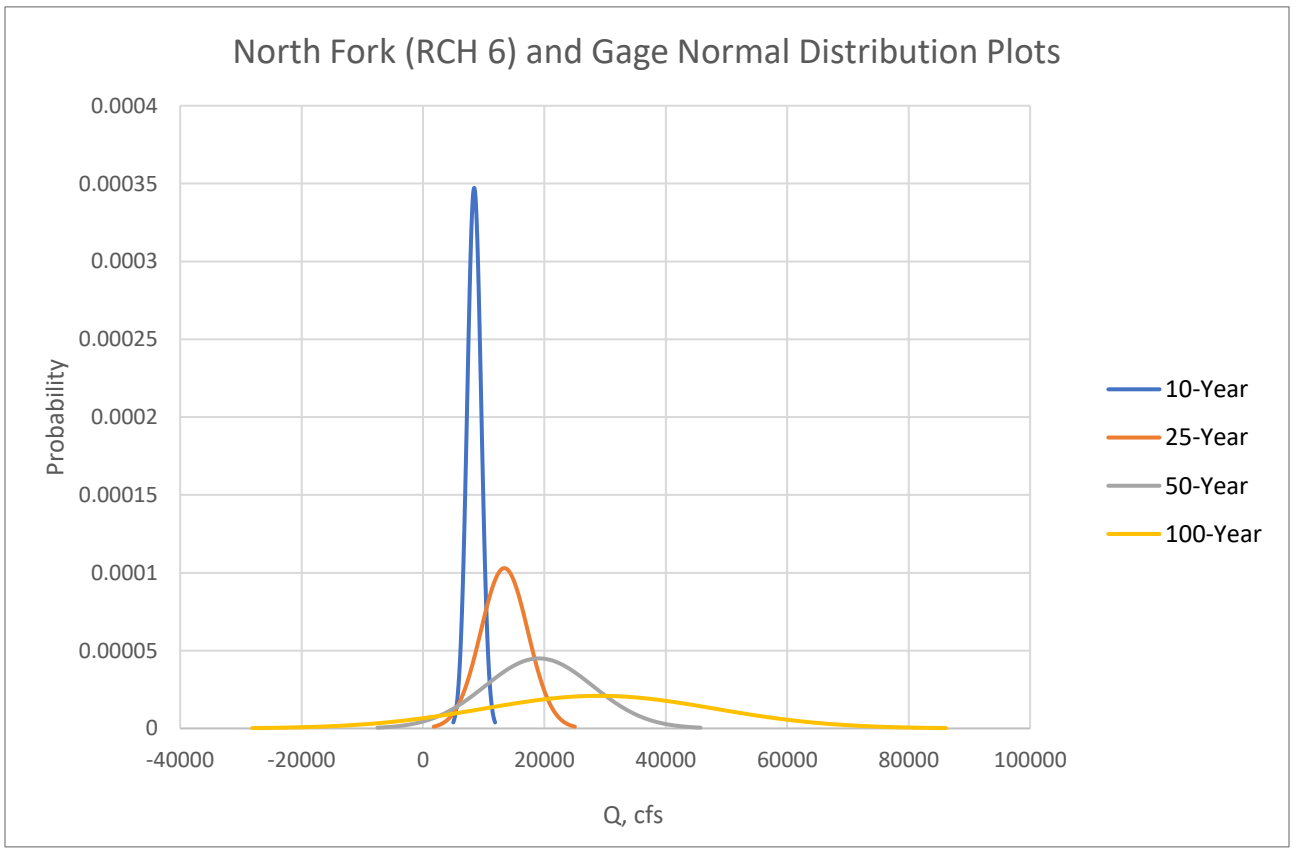
North Fork (RCH 6) and Gage Normal Distribution Plots
Probability
0.0004
0.00035
0.0003
0.00025
0.0002
0.00015
0.0001
0.00005
0
-40000
-20000
0
20000
40000
60000
80000
100000
Q, cfs
10-Year
25-Year
50-Year
100-Year

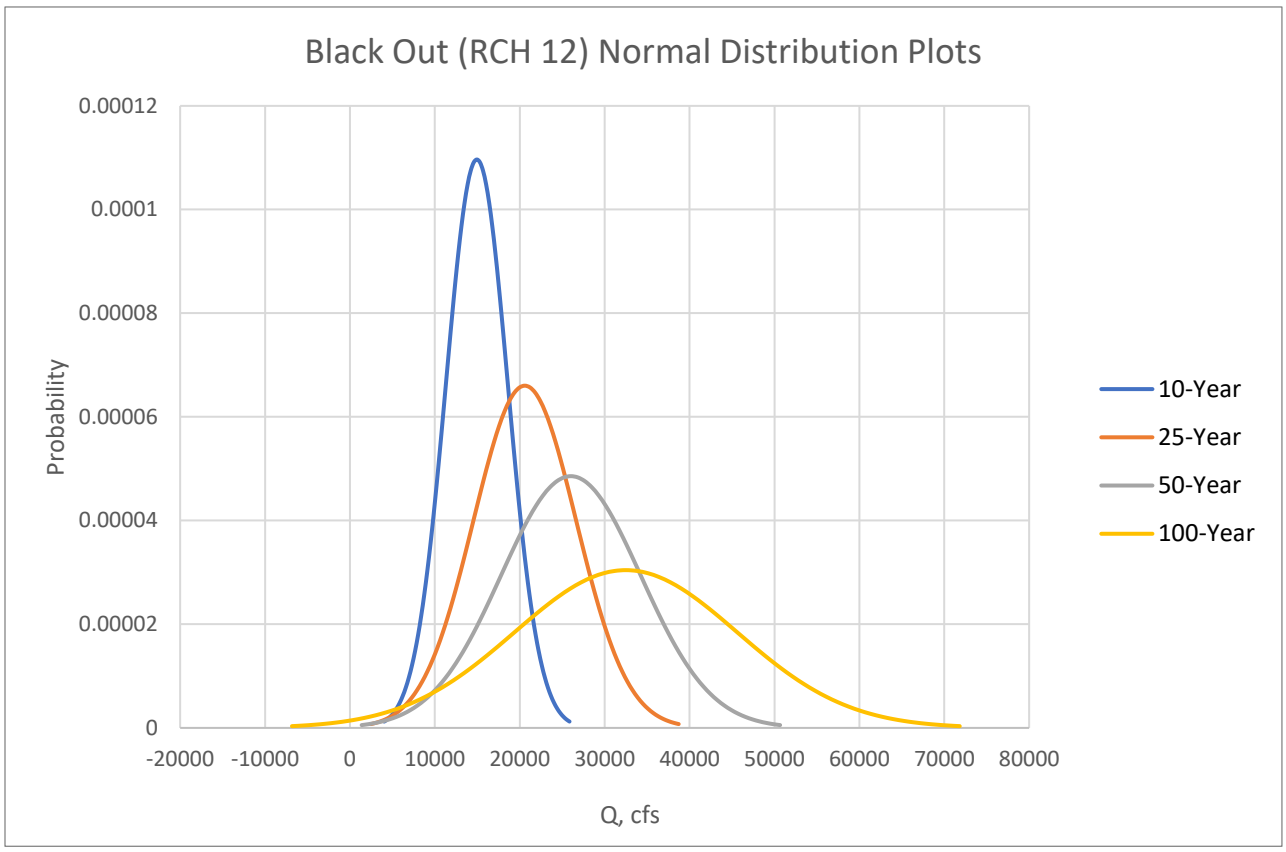
Black Out (RCH 12) Normal Distribution Plots
0.00012
0.0001
0.00008
0.00006
0.00004
0.00002
0
Probability
-20000
-10000
0
10000
20000
30000
40000
50000
60000
70000
80000
Q, cfs
10-Year
25-Year
50-Year
100-Year

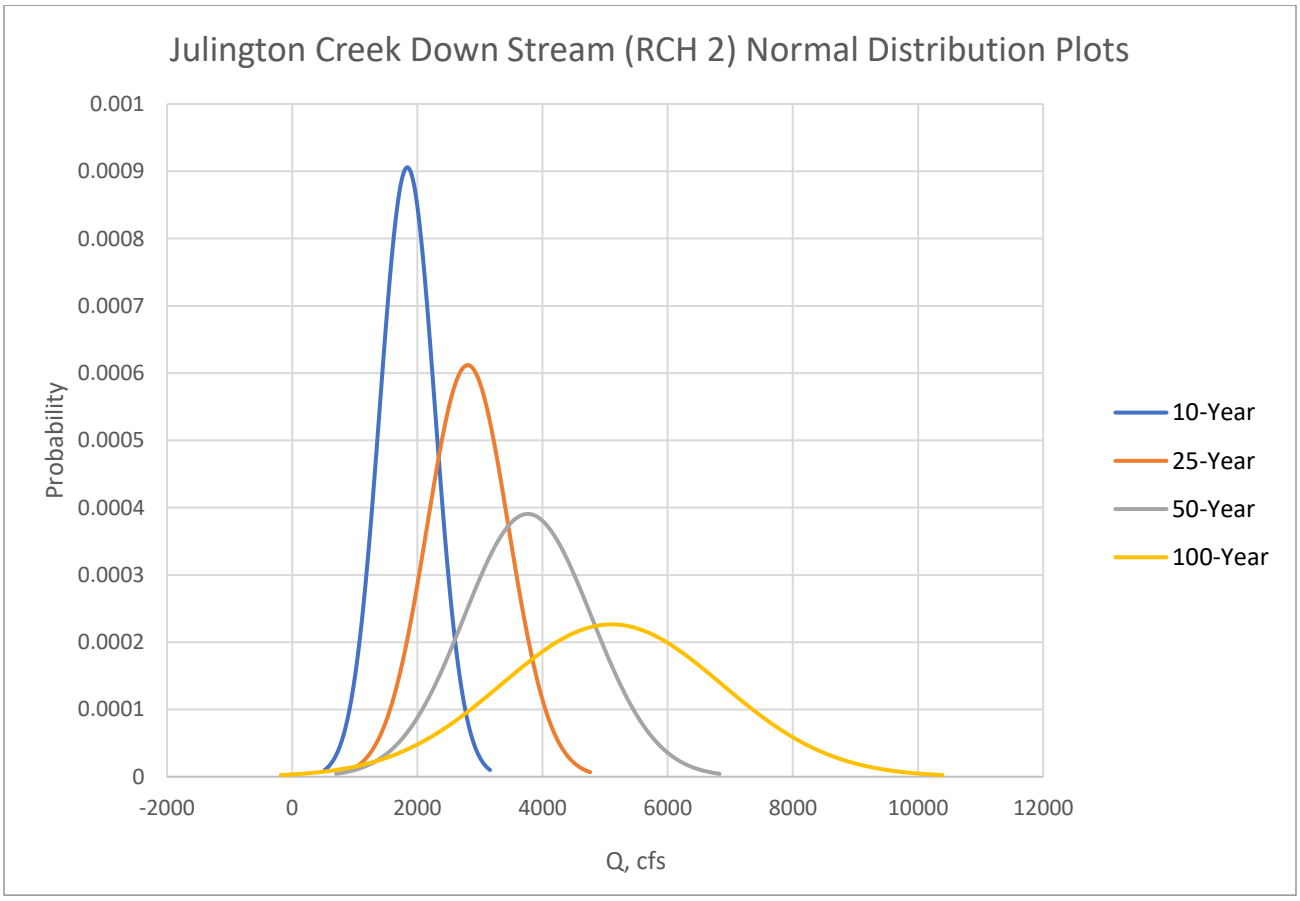
Julington Creek Down Stream (RCH 2) Normal Distribution Plots
0.001
0.0009
0.0008
0.0007
0.0006
0.0005
0.0004
0.0003
0.0002
0.0001
0
Probability
-2000
0
2000
4000
6000
8000
10000
12000
Q, cfs
10-Year
25-Year
50-Year
100-Year

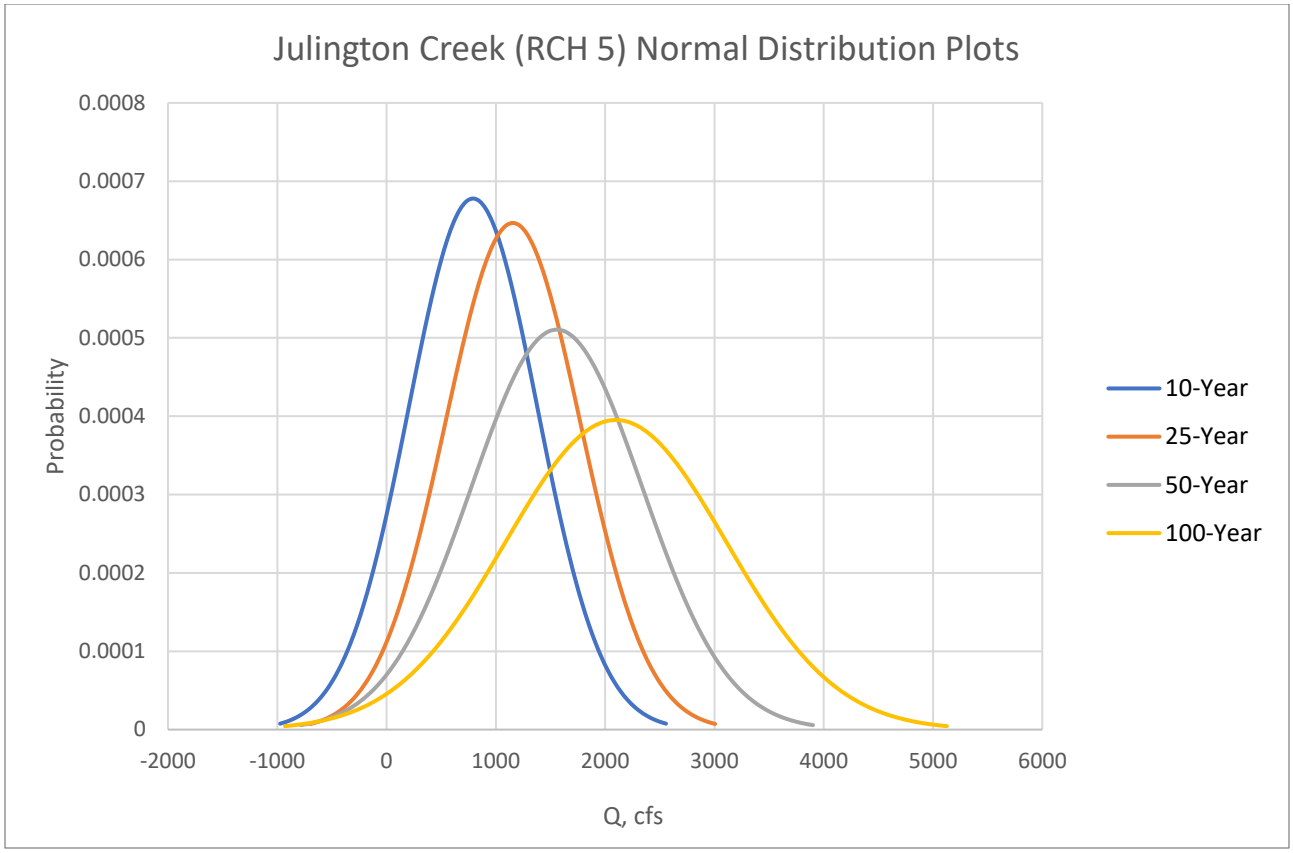
Julington Creek (RCH 5) Normal Distribution Plots
Probability
0.0008
0.0007
0.0006
0.0005
0.0004
0.0003
0.0002
0.0001
0
-2000
-1000
0
1000
2000
3000
4000
5000
6000
Q, cfs
10-Year
25-Year
50-Year
100-Year

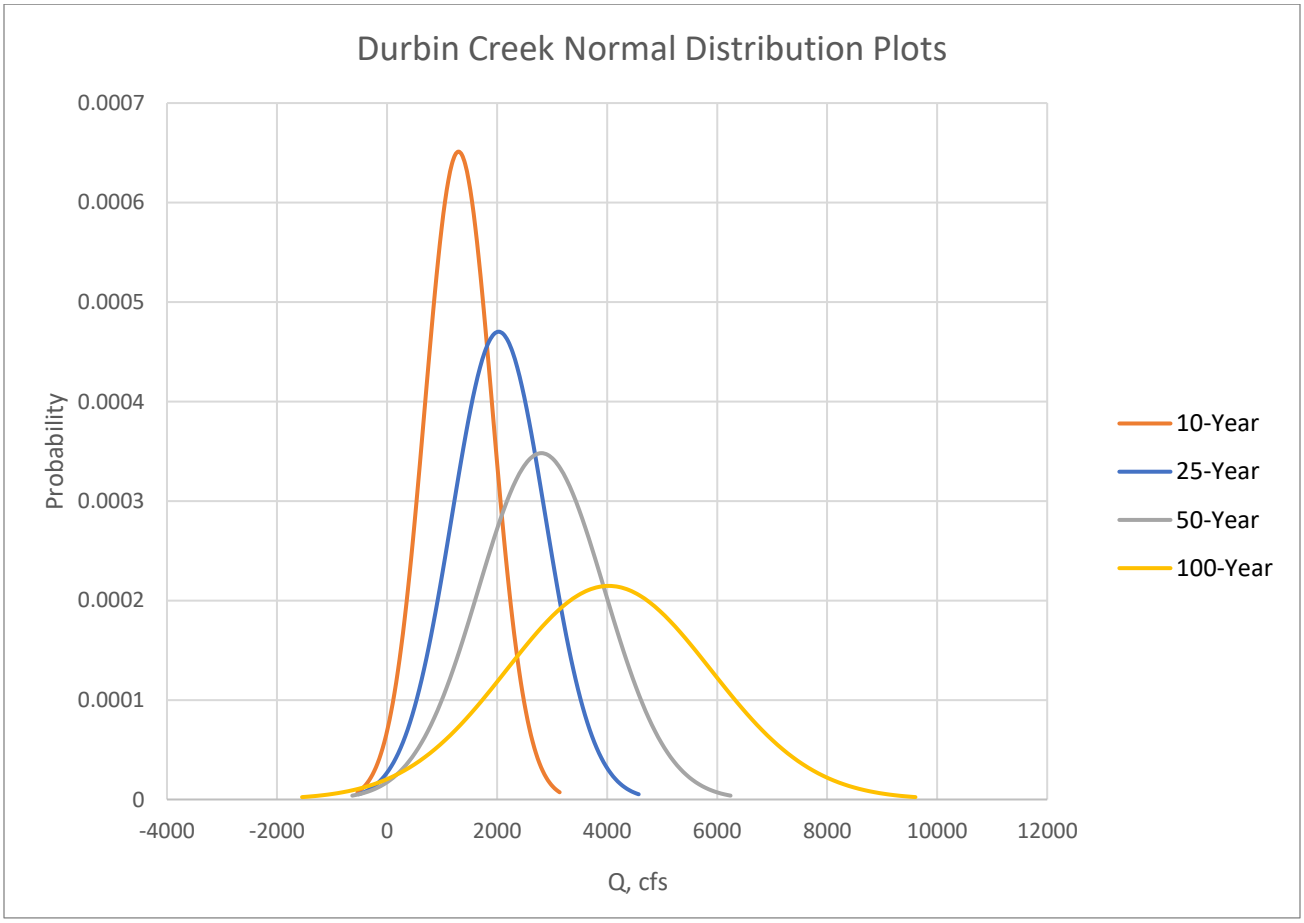
Durbin Creek Normal Distribution Plots
Probability
0.0007
0.0006
0.0005
0.0004
0.0003
0.0002
0.0001
0
-4000
-2000
0
2000
4000
6000
8000
10000
12000
Q, cfs
10-Year
25-Year
50-Year
100-Year

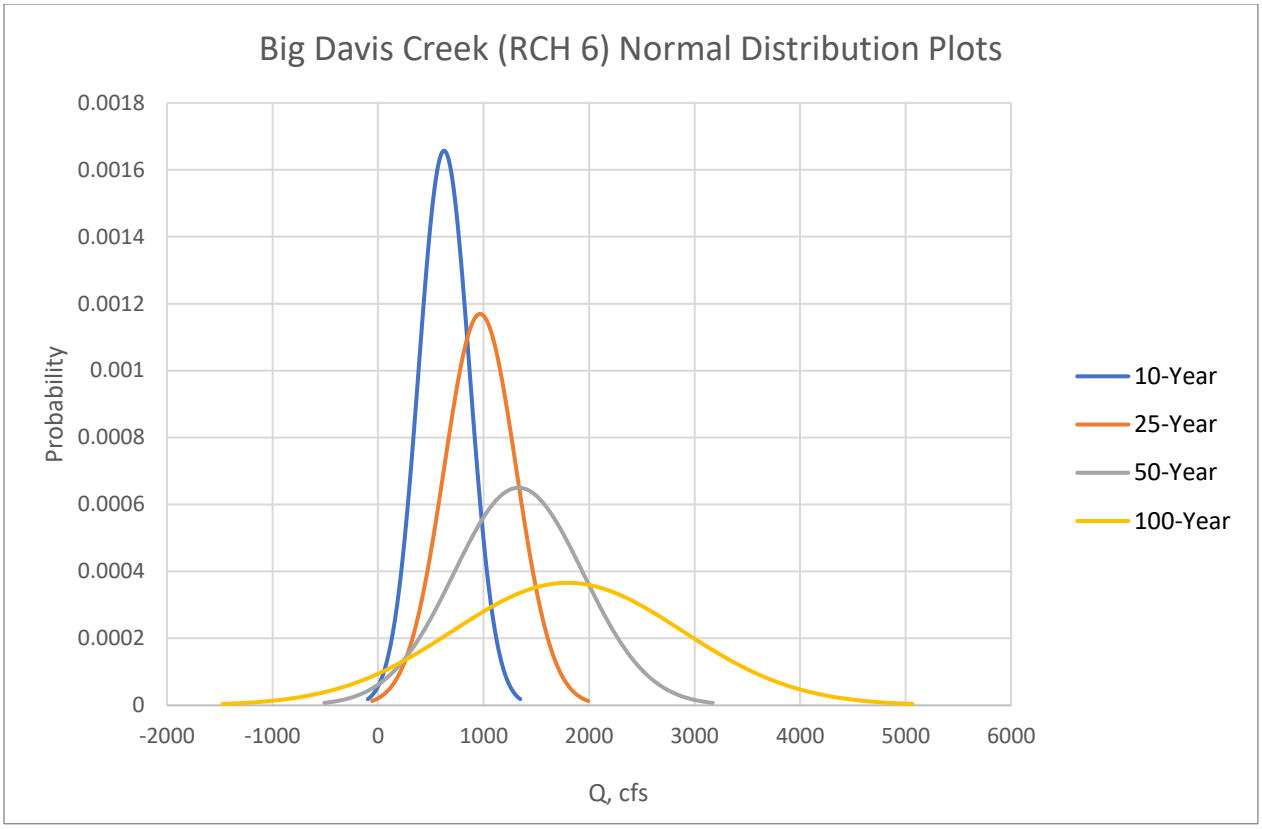
Big Davis Creek (RCH 6) Normal Distribution Plots
0.0018
0.0016
0.0014
0.0012
0.001
0.0008
0.0006
0.0004
0.0002
0
Probability
-2000
-1000
0
1000
2000
3000
4000
5000
6000
Q, cfs
10-Year
25-Year
50-Year
100-Year

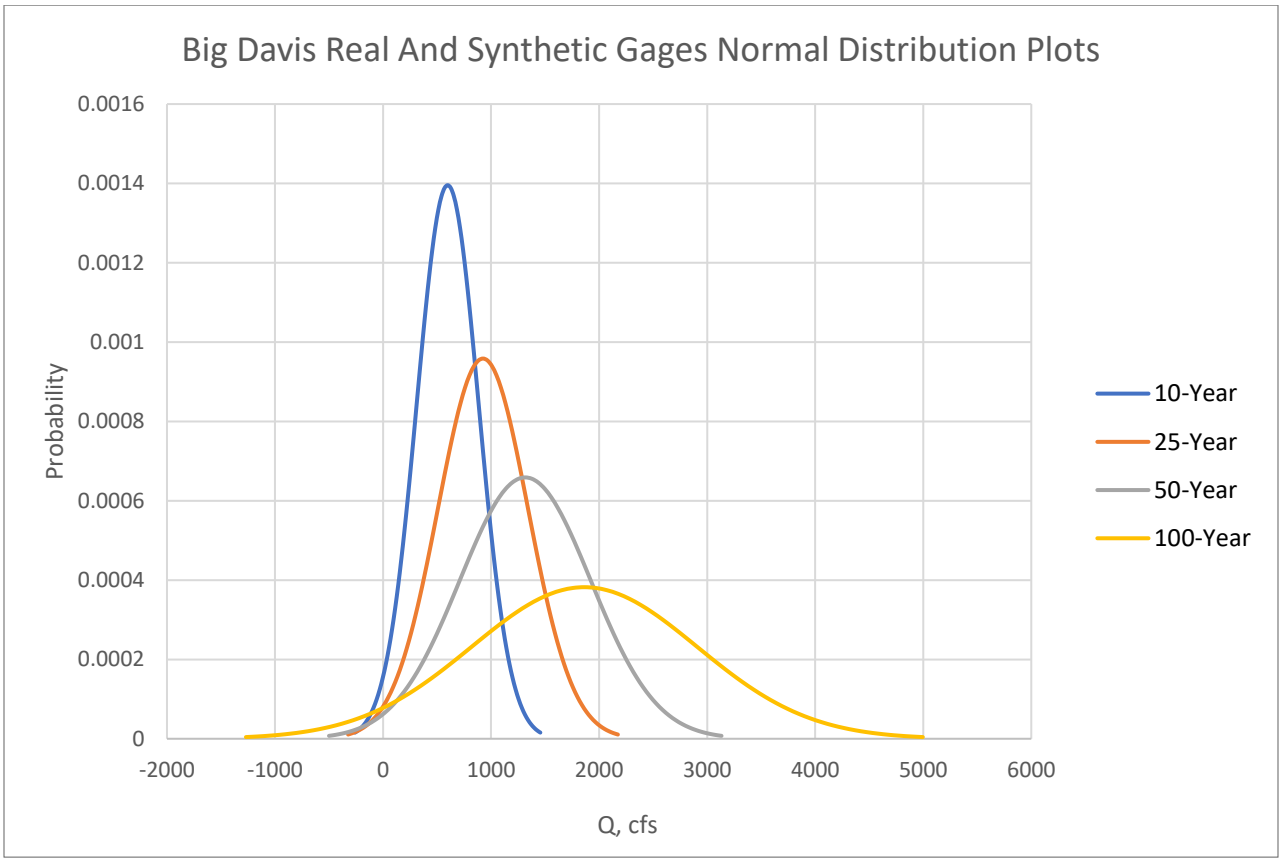
Big Davis Real And Synthetic Gages Normal Distribution Plots
0.0016
0.0014
0.0012
0.001
0.0008
0.0006
0.0004
0.0002
0
Probability
-2000
-1000
0
1000
2000
3000
4000
5000
6000
Q, cfs
10-Year
25-Year
50-Year
100-Year

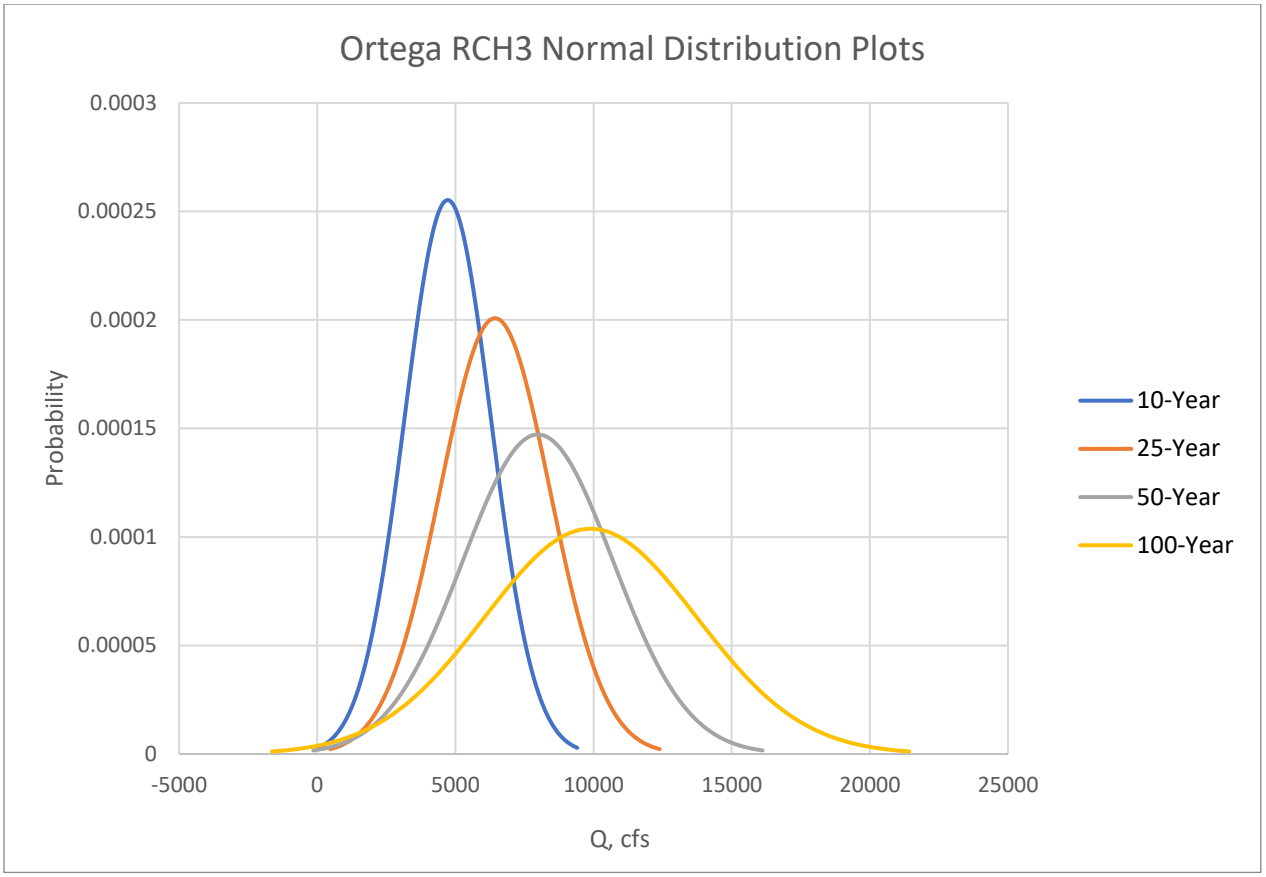
Ortega RCH3 Normal Distribution Plots
0.0003
0.00025
0.0002
0.00015
0.0001
0.00005
0
Probability
-5000
0
5000
10000
15000
20000
25000
Q, cfs
10-Year
25-Year
50-Year
100-Year

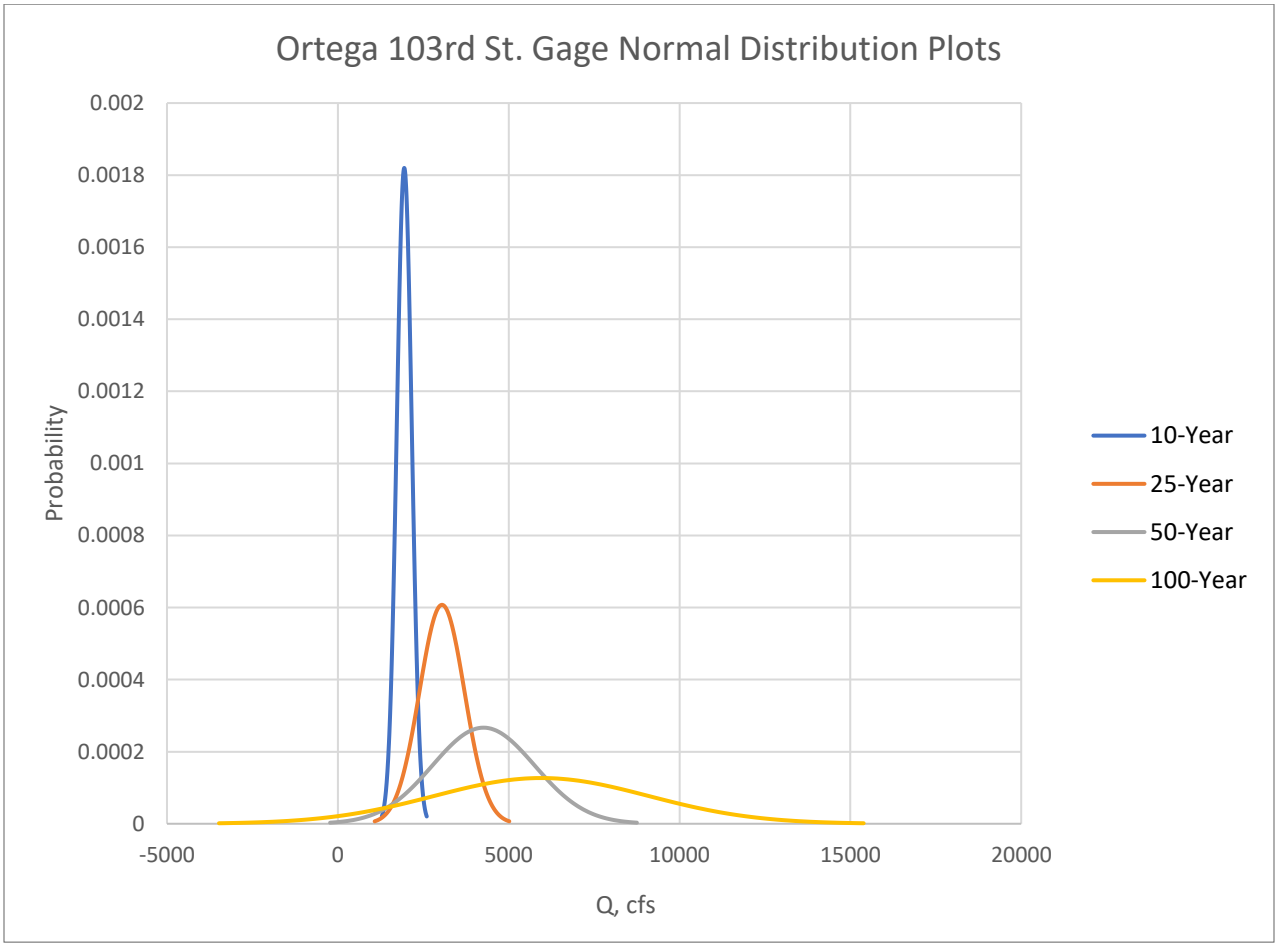
Ortega 103rd St. Gage Normal Distribution Plots
0.002
0.0018
0.0016
0.0014
0.0012
0.001
0.0008
0.0006
0.0004
0.0002
0
Probability
-5000
0
5000
10000
15000
20000
Q, cfs
10-Year
25-Year
50-Year
100-Year

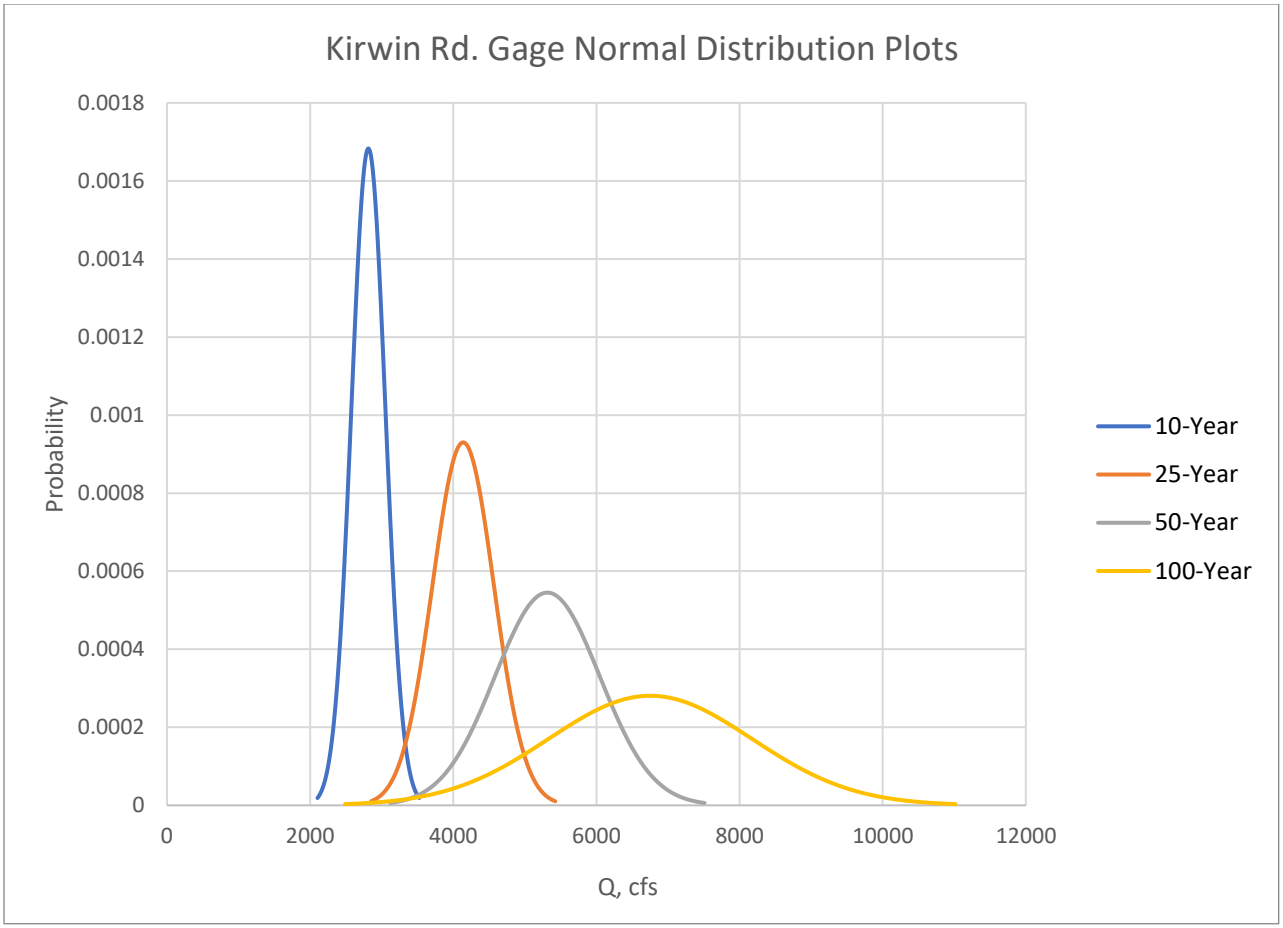
Kirwin Rd. Gage Normal Distribution Plots
Probability
0.0018
0.0016
0.0014
0.0012
0.001
0.0008
0.0006
0.0004
0.0002
0
0
2000
4000
6000
8000
10000
12000
Q, cfs
10-Year
25-Year
50-Year
100-Year

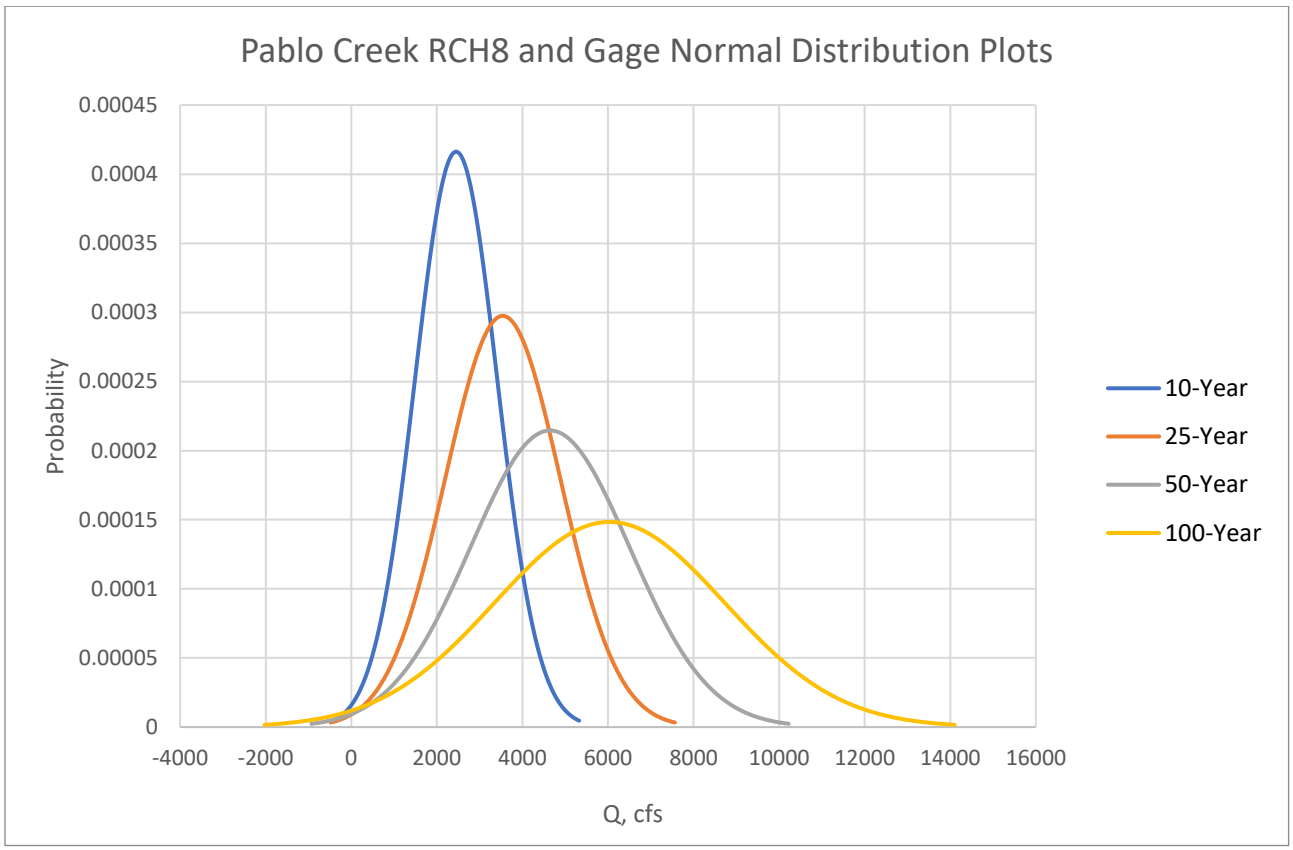
Pablo Creek RCH8 and Gage Normal Distribution Plots
Probability
0.00045
0.0004
0.00035
0.0003
0.00025
0.0002
0.00015
0.0001
0.00005
0
-4000
-2000
0
2000
4000
6000
8000
10000
12000
14000
16000
Q, cfs
10-Year
25-Year
50-Year
100-Year

REFERENCES

Alipour, M., Rezakhani, A., & Shamsai, A. (2016). Seasonal fractal-scaling of floods in two U.S. water resources regions. Journal of Hydrology, 540, 232–239. doi: 10.1016/j.jhydrol.2016.06.016

Andriani P. & McKelvey B. (2009). From Gaussian to Paretian Thinking: Causes and Implications of Power Laws in Organizations. *Organization Science*, Vol. 20, No. 6 (Nov. - Dec., 2009), pp. 1053-1071. Retrieved from http://leeds-faculty.colorado.edu/dahe7472/Adriani%2025614715.pdf

Brody, S. D., Zahran, S., Maghelal, P., Grover, H., & Highfield, W. E. (2007). The Rising Costs of Floods: Examining the Impact of Planning and Development Decisions on Property Damage in Florida. *Journal of the American Planning Association*, *73*(3), 330–345. doi: 10.1080/01944360708977981

Federal Emergency Management Agency (2013). *Flood Insurance Study: Duval County, Florida.* (12031CV001A). Retrieved from https://fris.nc.gov/fris/

Federal Emergency Management Agency (2014). *Flood Insurance Study: Clay County, Florida.* (12019CV001A). Retrieved from https://fris.nc.gov/fris/

Florida Division of Emergency Management (2018). Enhanced state hazard mitigation plan, State of Florida. Retrieved from https://www.fema.gov/hazard-mitigation-plan-status.

Florida Division of Emergency Management (2018). Enhanced state hazard mitigation plan, *Appendix E: Risk Assessment Data*, State of Florida. Retrieved from https://www.fema.gov/hazard-mitigation-plan-status.

Gebremariam, S. Y., Martin, J. F., Demarchi, C., Bosch, N. S., Confesor, R., & Ludsin, S. A. (2014). A comprehensive approach to evaluating watershed models for predicting river flow regimes critical to downstream ecosystem services. Environmental Modelling & Software, 61, 121–134. doi: 10.1016/j.envsoft.2014.07.004

Google Earth Pro. (2020). Version 7.3.3.7786. [Computer Software]. Retrieved from https://www.google.com/earth/versions/

Haan, C. T. (1977). *Statistical methods in hydrology*. Ames: Iowa State Univ. Pr.

Kidson, R. & Richards, K. (2005, July 1). Flood frequency analysis: assumptions and alternatives. *Progress in Physical Geography,* 29(392). Retrieved from https://journals.sagepub.com/doi/abs/10.1191/0309133305pp454ra

Kumar, R. (2019). Flood Frequency Analysis of the Rapti River Basin using Log Pearson Type-III and Gumbel Extreme Value-1 Methods. Journal of the Geological Society of India, 94(5), 480–484. doi: 10.1007/s12594-019-1344-0

Kyd C. (2006). An Introduction to Excel's Normal Distribution Functions. Retrieved from https://exceluser.com/

Malamud, B. & Turcotte D. (2006). The applicability of power-law frequency statistics to floods. *Journal of Hydrology.* 322(2006). Retrieved from https://www.researchgate.net/publication/222655854_The_applicability_of_power-law_frequency_statistics_to_floods

Microsoft Corporation (2016). Microsoft Excel (Solver plug-in). Retrieved from https://office.microsoft.com/excel

National Oceanic and Atmospheric Administration Atlas 14 (2017). Retrieved from https://hdsc.nws.noaa.gov/hdsc/pfds/pfds_map_cont.html

Ninov P., Ribarova I. Kalinkov P., & Dimova G. (2008). Application of the HSPF Model for Flood Simulation with Analysis of the Results in Terms of Monitoring Uncertainties/Case Study of the Lesnovska River, Bulgaria. International Congress on Environmental Modelling Software. Retrieved from https://scholarsarchive.byu.edu/cgi/viewcontent.cgi?article=2858&context=iemssconference

Okoli K., Mazzoleni M., Breinl K., & Baldassarre G. (2019). A systematic comparison of statistical and hydrological methods for design flood estimation. Hydrology Research.. 50(6): 1665-16678. Retrieved from https://iwaponline.com/hr/article/50/6/1665/69899/A-systematic-comparison-of-statistical-and

Oregon State University (2005). Analysis Techniques: Flood Frequency Analysis. Retrieved from https://streamflow.engr.oregonstate.edu/analysis/floodfreq/#log

Oregon State University (2005). Analysis Techniques: Flood Frequency Example with Daily Data (Log-Pearson Type III Distribution). Retrieved from https://streamflow.engr.oregonstate.edu/analysis/floodfreq/meandaily_example.htm

Rao. D. (1986). Technical Publication SJ 86-2. Magnitude and Frequency of Flood Discharges in Northeast Florida. Retrieved from https://www.sjrwmd.com/documents/technical-reports/

Saf, B., Dikbas, F. , Yasar, M. (2007). Determination of regional frequency distributions of floods in West Mediterranean river basins in Turkey. Fresenius Environmental Bulletin. 16. 1300-1308.

Samantaray S., Sahoo A. (2020). Estimation of flood frequency using statistical method: Mahanadi River basin, India. H2Open Journal. 3(1): 189-207. Retrieved from https://doi.org/10.2166/h2oj.2020.004

Schiariti, P., P.E., CPESC (n.d.). Basic Hydrology – Runoff Curve Numbers. Retrieved from http://njscdea.ncdea.org/

St. Johns River Water Management District (1985). *A Guide to SCS Runoff Procedures.* (SJ85-5). Retrieved from https://www.sjrwmd.com/documents/technical-reports_/

St. Johns River Water Management District (1990). *Rainfall Analysis for Northeast Florida Part V: Frequency Analysis of Wet Season and Dry Season Rainfall.* (Project No. 10 200 02)

St. Johns River Water Management District (2012). *St. Johns River Water Supply Impact Study* (SJ20120-1). Retrieved from https://www.sjrwmd.com/documents/water-supply/#wsis-final-report

St. Johns River Water Management District (2012). *Appendix M of St. Johns River Water Supply Impact Study* (SJ20120-1). Retrieved from https://www.sjrwmd.com/documents/water-supply/#wsis-final-report

Suphunvorranop, T. (1985). *A Guide to SCS Runoff Procedures*. United States Department of Water Resources Technical Publication No. 85-5.

US Army Corps of Engineers (1994). *Engineering and Design: Flood Runoff Analysis* (Engineer Manual 110-2-1417).

United States Environmental Protection Survey (2013). *BASINS – Better Assessment Science Integrating Point and Non-point Sources* (Version 4.5) [Computer Software]. Retrieved from https://www.epa.gov/ceam/basins-download-and-installation

United States Geologic Survey (2020). *National Water Information System: Mapper.* Retrieved from https://maps.waterdata.usgs.gov/mapper/index.html

United States Geologic Survey and Environmental Protection Agency (2012). *HSPF - Hydrologic Simulation Program - FORTRAN* (Version 4.5) [Computer Software]. https://www.epa.gov/ceam/hydrological-simulation-program-fortran-hspf

World Meteorological Organization (1989). Operational Hydrology Report No. 33. *Statistical Distributions for Flood Frequency Analysis.* Retrieved from https://library.wmo.int/index.php?lvl=notice_display&id=8845#.X58LZ4hKiUk

Yazdi, M. N., Ketabchy, M., Sample, D. J., Scott, D., & Liao, H. (2019). An evaluation of HSPF and SWMM for simulating streamflow regimes in an urban watershed. Environmental Modelling & Software, 118, 211–225. doi: 10.1016/j.envsoft.2019.05.008

VITA

Samantha Kovalenko, the author, began studying Civil Engineering at the University of North Florida through a dual enrollment program when she was a high school senior. Since then, she received her Bachelor of Science in Civil Engineering in 2018. Samantha completed many internships during her undergraduate career and went on to work with Arcadis in Portland, Oregon after graduating in 2018. Samantha decided to return to Florida in 2019 to pursue a Master of Science at the University of North Florida. While completing her Master of Science, Samantha began working full-time with the U.S. Army Corps of Engineers as a Civil Engineer in 2020. She works in the Waterways Section of the Engineering Design Branch. She anticipates graduating from the University of North Florida with a Master of Science in April 2021.